UNIVERSITÀ DEGLI STUDI DI PADOVA

School of Engineering

Department of Civil, Architectural and Environmental Engineering ICEA

Course of Civil Engineering

Master's Thesis

SLIT NET DAMS IN A SMALL SCALE MODEL: DEBRIS FLOW CONTROL WITH DIFFERENT BASAL OPENINGS

Student: Andrea Ragazzi

Supervisors: Prof. Eng. Simonetta Cola (Unipd, Padova)

Prof. Eng. Roland Kaitna (Boku, Vienna)

Prof. Eng. Johannes Hübl (Boku, Vienna)

Academic Year 2013-2014

PREFACE

The present thesis was carried out at the Institute of Mountain Risk Engineering, University of Natural Resources and Life Sciences, Vienna (IAN-BOKU) in partial fulfillment of the requirements for acquiring the M.Sc. degree in Civil Engineering (30 ECTS). It contains the work conducted from March 2014 to August 2014 under the supervision of Prof. Roland Kaitna and Prof. Johannes Hübl from IAN-BOKU and Prof. Simonetta Cola from the Department of Civil, Architectural and Environmental Engineering of the University of Padua. The thesis was part of an applied research project, which is described in the IAN-Report 157 (Hübl *et al.*, 2014).

Vienna, August 2014

ABSTRACT

Debris flows – mixtures of sediment and water transiting steep channels – are natural phenomena which regularly occur in mountain regions. Since they represent a serious hazard for human lives and civil infrastructures, scientific investigations are carried out in order to better understand their behaviours.

The aim of this work was to analyze the response of a new type of barrier, here defined as slit net dam, towards debris flow phenomena. Sixteen experiments were carried out in a small-scale model at the BOKU University of Vienna (Institute of Mountain Risk Engineering – IAN) testing different barrier configurations; in particular the research focused on the study of five different basal openings, i.e. the distance from the barrier bottom to the lowermost net element. To test the barrier behaviour, a material volume ranging from 0.40 to 0.47 m^3 was released from a reservoir; the debris flow material was composed by a mixture of gravel, sand and loam and with different water contents. Parameters such as total volume retained by the barrier, front velocity of the flow and force values within the cables were systematically measured.

The barriers tested showed and proved that the basal opening has a relevant role on debris flow dynamics. In particular, it was observed that smaller basal openings provide major retention of the released material, whereas larger basal openings allow the passage of a greater percentage of material. Observations of the flow behaviour showed the development of a reflected wave nearby the barrier, revealing that in a first moment the net element acts as a solid barrier. The barrier is thus capable to reduce the debris flow wave and, if the basal opening is larger enough, it provides a successive release of the incoming material.

The research also highlighted the problems which can occur when small-scale experiments are carried out, suggesting that force values must be evaluated with caution; further investigations are required in order to clarify the possibility to extend small-scale results to the reality.

RIASSUNTO

I debris flow (o colate detritiche) – miscele di sedimenti e acqua in transito lungo canali ripidi – sono fenomeni naturali che si verificano regolarmente nelle regioni di montagna. Poichè essi rappresentano un grave pericolo per vite umane e infrastrutture civili, sono auspicabili indagini scientifiche al fine di comprendere meglio i loro comportamenti.

Lo scopo di questo lavoro è stato analizzare la risposta di un nuovo tipo di barriera, qui definito come slit net dam, nei confronti di fenomeni di debris flow. Sedici esperimenti sono stati condotti in un modello in scala ridotta presso l'Università BOKU di Vienna (Institute of Mountain Risk Engineering - IAN) testando diverse configurazioni per la barriera; la ricerca si è focalizzata in particolare sullo studio di cinque diverse aperture basali, definite come la distanza tra la base della barriera e il primo elemento della rete. Per valutare il comportamento della barriera, un volume di materiale variabile da 0.40 a 0.47 m^3 è stato rilasciato da un serbatoio; il materiale dei debris flow è stato riprodotto con una miscela di ghiaia, sabbia e terra argillosa, con diversi contenuti di acqua. Parametri quali volume totale trattenuto dalla barriera, velocità anteriore del flusso e valori di forza lungo i cavi sono stati sistematicamente misurati.

Le barriere testate hanno rivelato e dimostrato che l'apertura basale svolge un ruolo di rilievo nei confronti delle dinamiche dei flussi di detriti. In particolare, è stato osservato che piccole aperture basali forniscono una maggiore ritenzione del materiale rilasciato, mentre grandi aperture basali permettono il passaggio di una maggiore percentuale di materiale. Osservazioni sul comportamento del flusso hanno mostrato lo sviluppo di un'onda riflessa vicino alla barriera, rivelando che l'elemento di rete agisce in un primo momento come una barriera solida. La barriera è quindi in grado di ridurre l'onda di debris flow e, se l'apertura basale è abbastanza grande, è in grado di fornire un successivo rilascio del materiale in arrivo.

La ricerca ha inoltre messo in evidenza i problemi che possono verificarsi quando si conducono gli esperimenti su piccola scala, suggerendo che i valori di forza devono essere valutati con cautela; ulteriori indagini sono necessarie per chiarire la possibilità di estendere alla realtà i risultati ottenuti sul modello sperimentale.

TABLE OF CONTENTS

1 INTRODUCTION

Debris flow phenomena are a relevant problem in Alpine regions. These kinds of rapid mass movements are responsible for serious damages and even human losses every year. The study and the design of structural mitigation measures to protect infrastructures and settlements are of fundamental importance and represent a big challenge for scientists and engineers. In order to stop, retain, dissipate or deflect debris flow events, different mitigation structures can be built; within this context, large or small scale experimental tests are particularly useful to better understand the behaviour of barriers against the debris flows.

This thesis focuses on design and evaluation of a new type of open barrier, a slit dam with its opening covered by a flexible net: this barrier can hence be defined as "slit net dam".

The effect of different configurations for such a slit net dam on the flow of laboratory debris flows by changing the basal opening (i.e. the distance from the river bottom to the lowermost cable) was investigated.

This chapter introduces the debris flow background, starting with the scientific definitions and passing to the classifications and descriptions of the mitigation measures existing nowadays. Additionally, small and large scale experiments led by different authors are presented, together with a description of the experimental approaches used to model scaled tests. The description of the materials used and the methods adopted are given in Chapter 2. The experimental results are summarized in Chapter 3 and then discussed in Chapter 4. Finally, conclusions and suggestions are presented in Chapter 5.

1.1 DEBRIS FLOWS DEFINITIONS

A debris flow is a natural phenomenon which occurs in Alpine regions, mostly due to intensive rainfall. More generally, a debris flow is a movement of a soil mass that is mobilized due to gravitational forces. There are several ways to classify debris flows, either depending on type of material involved (presence or not of water, dimension of particles), or based on triggering mechanisms, velocity and discharge characteristics, shear strengths and shear rate, duration, bed slope (Cruden and Varnes, 1996; Coussot and Meunier, 1996; Hungr et al., 2001).

During motion, the solid and fluid stresses, as well as the interaction between them, influence the flow and this fact distinguishes debris flows from similar phenomena, such as rock avalanches and sediment-laden water floods (Iverson, 1997).

Pierson and Costa (1987) subdivided different types of flows on the basis of the sediment concentration and on the flow mean velocity of the landslide mass; their rheological classification is shown in Figure 1.

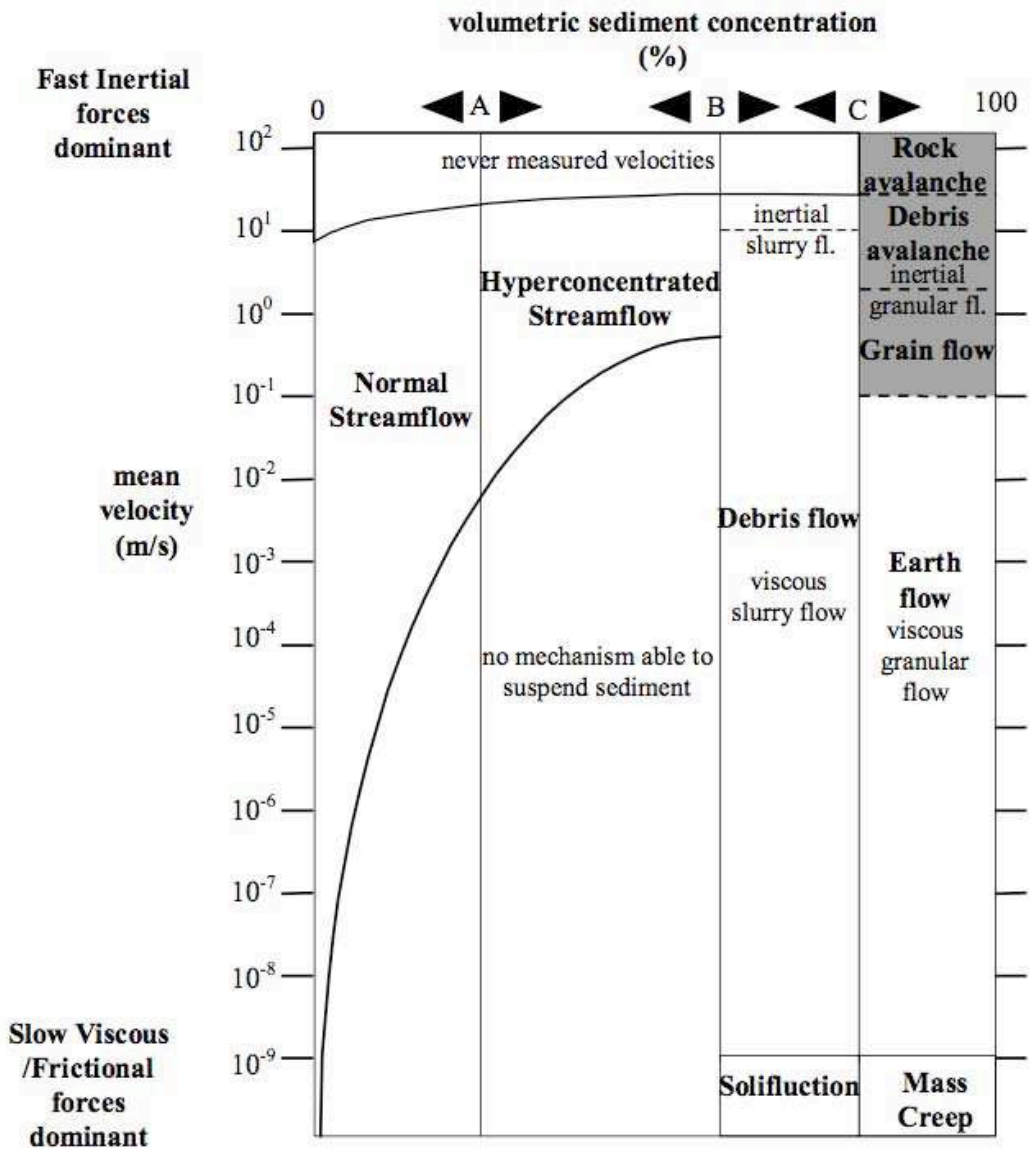

Figure 1. Flow rheological classification (taken form Pierson and Costa, 1987).

Cruden and Varnes (1996) proposed a classification according to the velocity assumed by the landslide phenomenon: they suggested seven velocity classes as shown in Table 1. According to them, a debris flow could be classified as an extremely rapid landslide with high values of velocity. In order to quantify the destructive potential, they also related the velocity class with a description of the possible damage effects (Table 2) and noted that landslides with high velocity would cause more damages and more loss of lives than the slow landslides.

Table 1. Landslide velocity scale (Cruden and Varnes, 1996).

Velocity Class	Description	Velocity [mm/s]	Typical Velocity
7	Extremely Rapid		
		$5x10^{3}$	5 m/s
6	Very Rapid		
		$5x10^{1}$	3 m/min
5	Rapid		
		$5x10^{-1}$	1.8 m/h
4	Moderate		
		$5x10^{-3}$	13 m/month
3	Slow		
		$5x10^{-5}$	1.6 m/year
2	Very Slow		
		$5x10^{-7}$	16 mm/year
1	Extremely Slow		

Table 2. Probable Destructive Significance of Landslides of Different Velocity Classes (Cruden and Varnes, 1996).

Velocity Class	Probable Destructive Significance
7	Catastrophe of major violence; buildings destroyed by impact of displaced material; many deaths; escape unlikely
6	Some lives lost; velocity too great to permit all persons to escape
5	Escape evacuation possible; structures, possessions, and equipment destroyed
4	Some temporary and insensitive structures can be temporarily maintained
3	Remedial construction can be undertaken during movement; insensitive structures can be maintained with frequent maintenance work if total movement is not large during a particular acceleration phase
2	Some permanent structures undamaged by movement
1	Imperceptible without instruments; construction possible with precautions

Coussot and Meunier (1996) proposed a classification of mass movements and flows existing in nature (Figure 2) by making a simple and synthetic summary. They separated the different phenomena according to two criteria. The first criterion considers the solid fraction type and recognizes fine, cohesive materials and coarse, cohesionless, granular materials, whereas the second criterion takes into account the sediment concentration which increases

moving from pure water flow to landslides or debris flow avalanches. It should be noted that the limits showed in Figure 2 are only conceptual and qualitative.

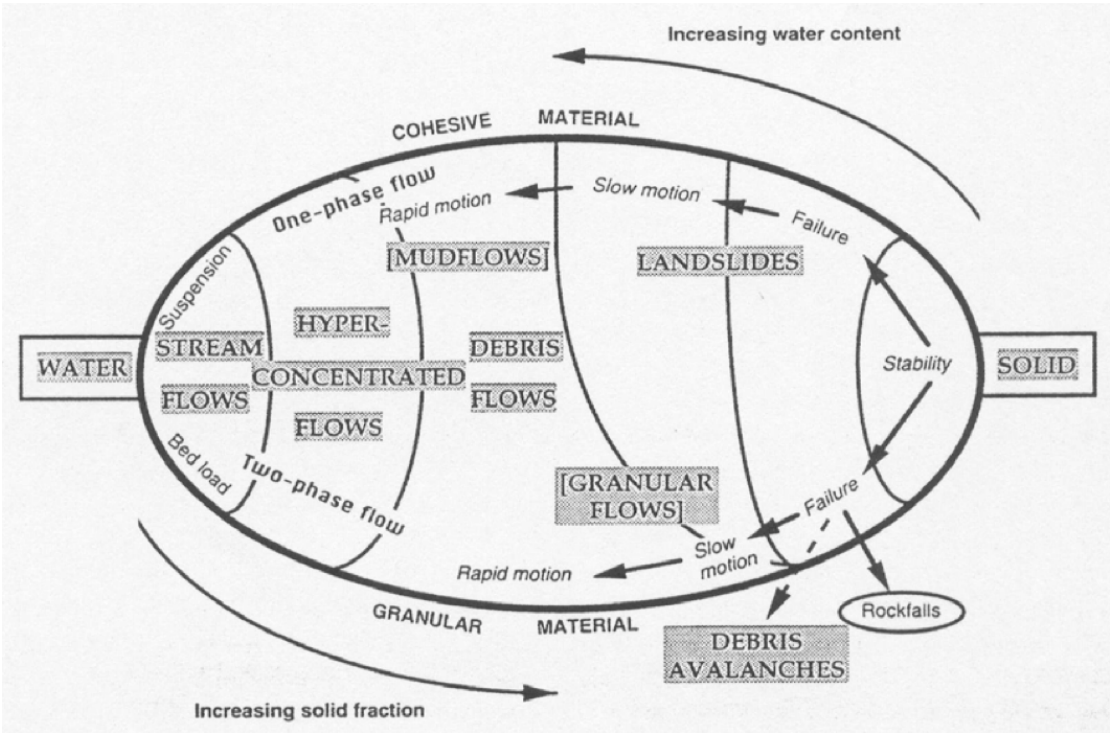

Figure 2. Classification of mass movements as a function of solid fraction and material type (taken from Coussot and Meunier, 1996).

Hungr et al. (2001) elaborated a classification of "landslides of the flow type" depending on the material typology, water content and velocity (Table 3). In particular they defined a debris flow as "a very rapid to extremely rapid flow of saturated non-plastic debris in a steep channel (Plasticity Index < 5 percent in sand and finer fractions)".

The typical debris flow mixture, as suggested by Hutchinson (1988), is often composed by high density materials with over 80% by weight solids (Figure 3). As a comparison, it is interesting to note that the debris flow density may be higher than the "wet concrete" density.

Another way to classify debris flow phenomena is to watch their path and in particular their topographic characteristic. As suggested by Cruden and Varnes (1996) it is possible to identify Hillslope (or Open Slope) debris flows and Channelized debris flows. The first type of flow moves along valley slopes and then is deposited on the final area (which have lower slope) or against natural or artificial barriers. The second type of flow occurs along existing channels and is characterized by flows with high density, 80% solids by weight.

Looking at the debris flow path, it is possible to recognize three different zones (Hungr, 2005): initiation, transportation and deposition. The initiation zone is usually characterized by steep slope with angles between 20° and 45°; in this zone a certain volume of soil starts to flow. Therefore the debris flow continues its run along the transportation zone and then finishes and stops on the deposition zone, when the slope angle decreases to low values.

Table 3. Classification of landslides of the flow type (Hungr et al., 2001).

Material	Water Content[1]	Special Condition	Velocity	Name
Silt, Sand, Gravel, Debris (talus)	dry, moist or saturated	- no excess pore-pressure, - limited volume	Various	Non-liquefied sand (silt, gravel, debris) flow
Silt, Sand, Debris, Weak rock[2]	saturated at rupture surface content	- liquefiable material[3], - constant water	Ex. Rapid	Sand (silt, debris, rock) flow slide
Sensitive clay	at or above liquid limit	- liquefaction in situ[3], - constant water content[4]	Ex. Rapid	Clay flow slide
Peat	saturated	- excess pore-pressure	Slow to very rapid	Peat flow
Clay or Earth	near plastic limit	- slow movements, - plug flow (sliding)	< Rapid	Earth flow
Debris	saturated	- established channel[5], - increased water content[4]	Ex. Rapid	Debris flow
Mud	at or above liquid limit	- fine-grained debris flow	> Very rapid	Mud flow
Debris	free water present	- flood[6]	Ex. Rapid	Debris flood
Debris	partly or fully saturated	- no established channel[5], - relatively shallow, steep source	Ex. Rapid	Debris avalanche
Fragmented Rock	various, mainly dry	- intact rock at source, - large volume[7]	Ex. Rapid	Rock avalanche

[1] Water content of material in the vicinity of the rupture surface at the time of failure.
[2] Highly porous, weak rock (examples: weak chalk, weathered tuff, pumice).
[3] The presence of full or partial in situ liquefaction of the source material of the flow slide may be observed or implied.
[4] Relative to in situ source material.
[5] Presence or absence of a defined channel over a large part of the path, and an established deposition landform (fan). Debris flow is a recurrent phenomenon within its path, while debris avalanche in not.
[6] Peak discharge of the same order as that of a major flood or an accidental flood. Significant tractive forces of free flowing water. Presence of floating debris.
[7] Volume greater than 10,000 m^3 approximately Mass flow, contrasting with fragmental rock fall.

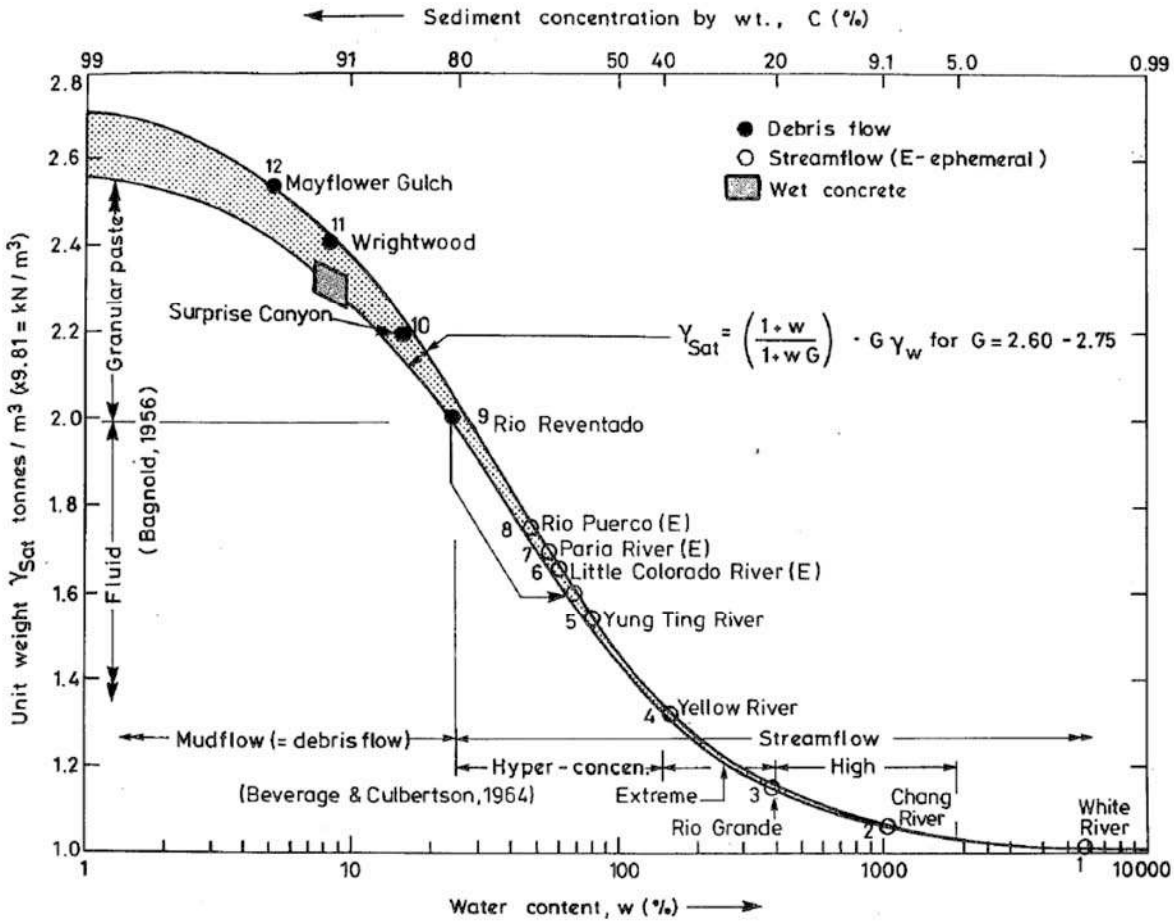

Figure 3. Continuous spectrum of sediment concentration, from sediment-laden rivers through ephemeral streams to debris flow (taken from Hutchinson, 1988).

1.2 DEBRIS FLOW MITIGATION MEASURES

Natural hazards are a serious problem in the Alpine regions which must be taken into account to avoid damages and loss of human life. In order to guarantee a certain level of safety, two types of preventive measures can be differentiated (Kienholz, 2003): active measures and passive measures. The first aims to make the hazard less effective, whereas the second aims to minimize the potential damage. Active measures are defense structures often located in "key points" which can stop or reduce the energy of a debris flow or more in general a particular landslide phenomenon. Passive measures aim to avoid the process in question, such as closing of a road, the evacuation of a particular area in danger, hazard maps and emergency planes, alarm systems. This study focuses only on active structural measures.

A first distinction can be done looking to the debris flow path: it is possible to recognize different areas where different countermeasures can be taken. As suggested by D'Agostino (2008), proceeding from the head of the basin towards the valley, it is possible to identify:

- transverse structures which aim for slope stabilization in trigger areas;
- transverse (and longitudinal) structures which aim to reduce steep channel gradients and to prevent stream bed erosion;
- structures which aim to reduce the energy impact of the flow and to retain boulders and trunks presenting large dimensions;
- deposition areas eventually closed by dams;
- channelized areas, at the end of the deposition basins, aimed at the disposal of residual materials which overflow from the lower dams;
- additional structures, such as dikes and walls, to protect important infrastructures or relevant areas.

According to Hübl and Suda (2008), the control of transportation and deposition processes of a debris flow phenomenon can be achieved with active structural mitigation measures such as: debris flow breakers, debris flow overfall barriers, deflection dams, retention basins and debris flow net barriers. These types of active measures have been developed to dissipate the kinetic energy of debris flows. Figure 4A shows schematically a retention basin located before a debris flow breaker: it works to decelerate and partially deposit the flow while the breaker subsequently further reduces the flow energy. As shown in Figure 4B, another way to reduce energy can be gained adopting a cascade of overfall barriers coupled with retention basins.

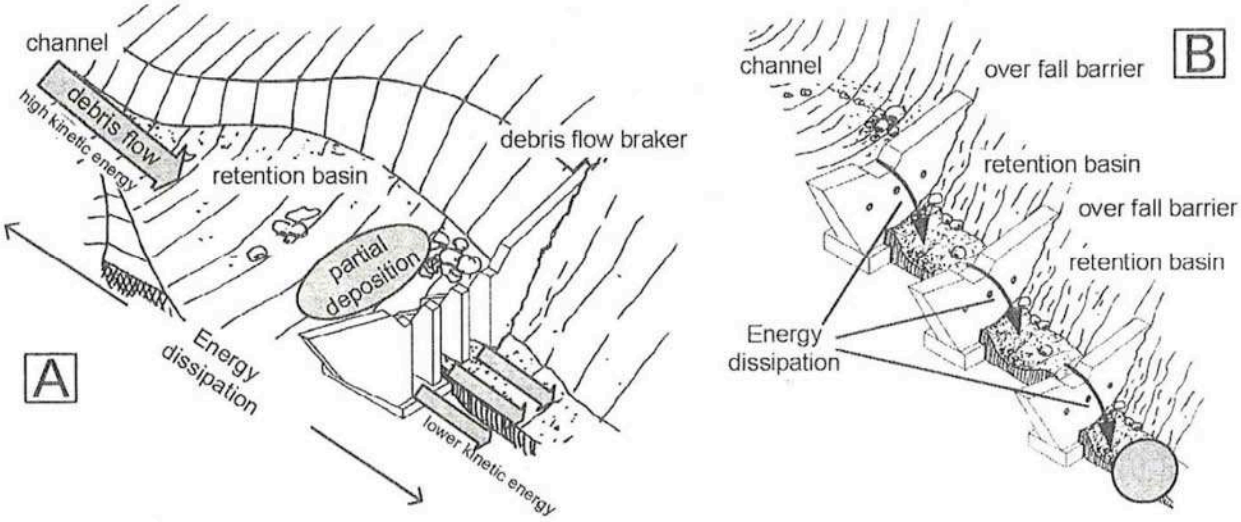

Figure 4. Debris flow breaker (A) and overfall barriers (B) coupled with retention basins (taken from Hübl and Suda, 2008).

Instead of a debris flow breaker, a net barrier can be used: it works mainly with the deformation of the steel material which composes the barrier (Figure 5B). Finally, if the purpose is to divert the flow, then it is appropriate to use deflection barriers, with the aim to change the direction and not to reduce the debris flow energy (Figure 5A).

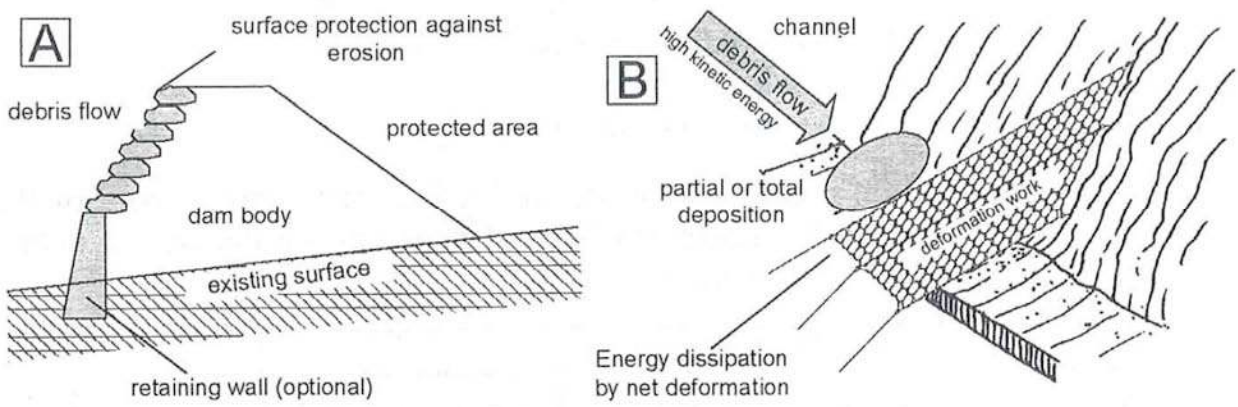

Figure 5. Deflection dam (A) and debris flow net barrier (B) (taken from Hübl and Suda, 2008).

Although different classification schemes of barriers can be made, it is common and easy to classify most of them in two main groups: Open Barriers and Solid Body Barriers.

An interesting classification of the different types of dams, based mainly on the shape of their functional parts, has been proposed by Wehrmann et al. (2006), suggesting also an organization into hierarchically ordered classes. The first distinction classifies Open Dams (which allow the passage of a part of sediment and water, thanks to functional openings) and

Solid Body Dams (which do not present openings but can have small weep holes on their body). Open Dams are then classified into a second hierarchical class according to the shape of the openings. Furthermore, the third and last class, is focused on the components which cover the openings. The authors provided a clear terminology to distinguish the different dams, thanks to a two-part nomenclature. The first part regards the shape of the openings, while the second part describes the cover components of the openings. Table 4 presents an overview of the final classification given by the authors.

Table 4. Classification of dams in torrential watersheds according to Wehrmann et al. (2006).

1. SOLID BODY DAMS	1.1 Single Solid Body Dams	
	1.2 Arched Solid Body Dams	
	1.3 Multiple Solid Body Dams	
2. OPEN DAMS	2.1 Slot Dams	Large Slot Dams Open Large Slot Dams Large Slot Rake Dams Large Slot Beam Dams Large Slot Grill Dams Closed Large Slot Dams Small Slot Dams Open Small Slot Dams Small Slot Rake Dams Small Slot Beam Dams Small Slot Grill Dams Closed Small Slot Dams
	2.2 Slit Dams	Open Slit Dams Slit Rake Dams Slit Beam Dams Slit Grill Dams Closed Slit Dams
	2.3 Compound Dams	Open Compound Dams Compound Rake Dams Compound Beam Dams Compound Grill Dams Closed Compound Dams
	2.4 Sectional Dams	Open Sectional Dams Sectional Rake Dams Sectional Beam Dams Sectional Grill Dams Closed Sectional Dams
	2.5 Lattice Dams	Plane Rake Dams Plane Beam Dams Plane Grill Dams Frame Dams
	2.6 Net Dams	

According to the classification given by Wehrmann et al. (2006), in the follow paragraphs Solid and Open dams are presented.

1.2.1 SOLID BODY DAMS

These barriers were probably the first types of dam used as an active measure against debris flow (a typical example is shown in Figure 6); they were built mainly until the end of 1960s (Hübl and Fiebiger, 2005). They work to stop the debris material behind the body dam and are effective until the storage capacity is ended. An evolution of these barriers is characterized by the presence of small slots which work as drains, with the aim to reduce the pressure behind the barrier (Figure 7).

Because solid body dams have a limited storage capacity, time compromises their effectiveness; once the basins are completely filled, removal of the deposited sediments is not easy and requires excavation machines with the consequent practical problems. For this and other reasons, different types of barriers (like open barriers) have been developed.

Figure 6. Solid body dam in Einachgraben, Austria (taken from Hübl and Fiebiger, 2005).

Figure 7. Solid body dam with drains in Koednitzbach, Austria (taken from Hübl and Fiebiger, 2005).

1.2.2 OPEN DAMS

As previously shown in Table 4, there are many types of open dams depending on the ultimate objective to be achieved. These dams are generally designed to allow the passage of sediment which does not create damage in downstream areas and to retain dangerous materials like big destructive boulders (Lien, 2003). An overview of the major types of open barriers is shown in Figure 8.

To fulfill the functions of sediment "sorting" and sediment "dosing", open barriers present openings on their body with the shape of slots or slits (Hübl and Fiebiger, 2005). Sediment sorting consists in a segregation of the particles: that means not all of the sediment can pass through the barrier. In addition, sediment dosing allows instead an unsorted sedimentation behind the dam. Open dams have usually an ability of self-emptying: as suggested by Fattorelli and D'Agostino (2008), it may be around 20% and almost never more than 50%. Therefore, a regular cleaning of sediments deposited should be carried out after medium and large events to maintain the functionality of the dam.

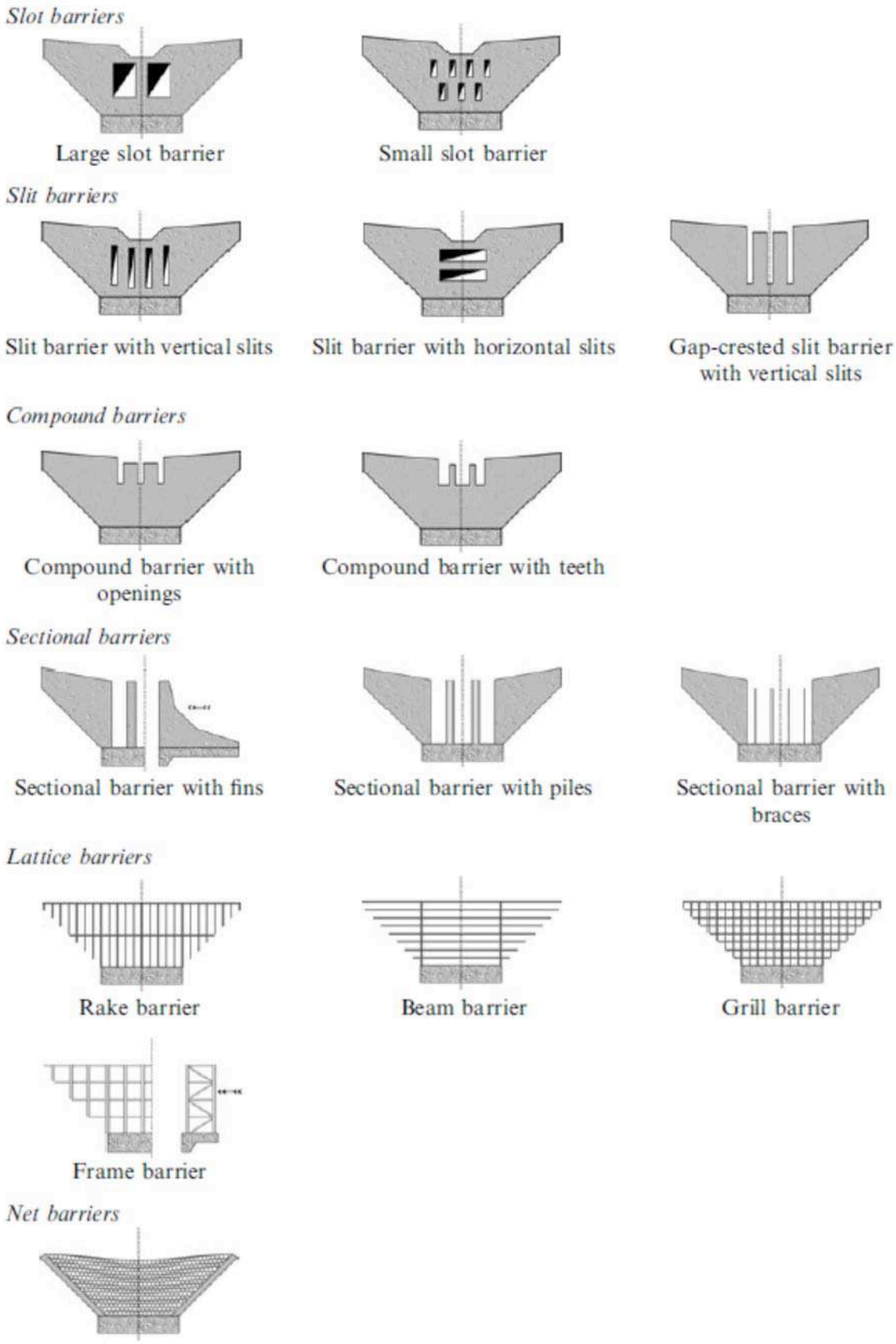

Figure 8. Different typologies of open barrier (taken from Hübl and Fiebiger, 2005).

Slit dams

As the name implies, slit dams are characterized by one or more vertical or horizontal slits. According to the classification proposed by Wehrmann et al. (2006), they may have:

a continuous overflow crest with long openings, which presents sides larger than half the height of the barrier;

or a gap-crested overflow area and openings with heights larger than half the height of the barrier.

Regarding the specific case of "gap-crested slit dams" they can be defined as slit dams only if their slits have widths opening smaller than the width of the solid element in between (Figure 9, Figure 10); otherwise, they are defined as "Sectional dams" (Figure 11, Figure 12, Figure 13). A further distinction can be done looking at the orientation of the slit; indeed it is possible to identify slit dams with n vertical long slits or slit dams with n horizontal long slits (Figure 14). Slit dams can be wholly covered by removable elements: in this case they are defined as "closed slit dam" (Figure 15). Otherwise, they are named "open slit dam" and are further subdivided according to the elements which cover the slit openings. Again following the classification proposed by Wehrmann et al. (2006), open slit dams (and open dams in general) are distinguished in:

rake dams, with chiefly vertical bars;

beam dams, with chiefly horizontal bars (Figure 16);

grill dams, with vertical and horizontal bars.

Another attribute is added depending on the inclination plane formed by the elements, and in this way they can be defined also as "perpendicular" or "inclined". Furthermore, perpendicular elements are generally integrated directly on the body dams whereas inclined elements are installed upstream with respect to the opening.

Figure 9. Slit barrier with one vertical slit (taken from Hübl et al., 2005).

Figure 10. Open slit dam with 2 vertical slits (taken from Wehrmann et al., 2006).

Figure 11. Open sectional dam with 2 fins (taken from Wehrmann et al., 2006).

Figure 12. Open sectional dam with fins and beams (taken from Hübl et al., 2005).

Figure 13. Open sectional dam with piles (taken from Hübl et al., 2005).

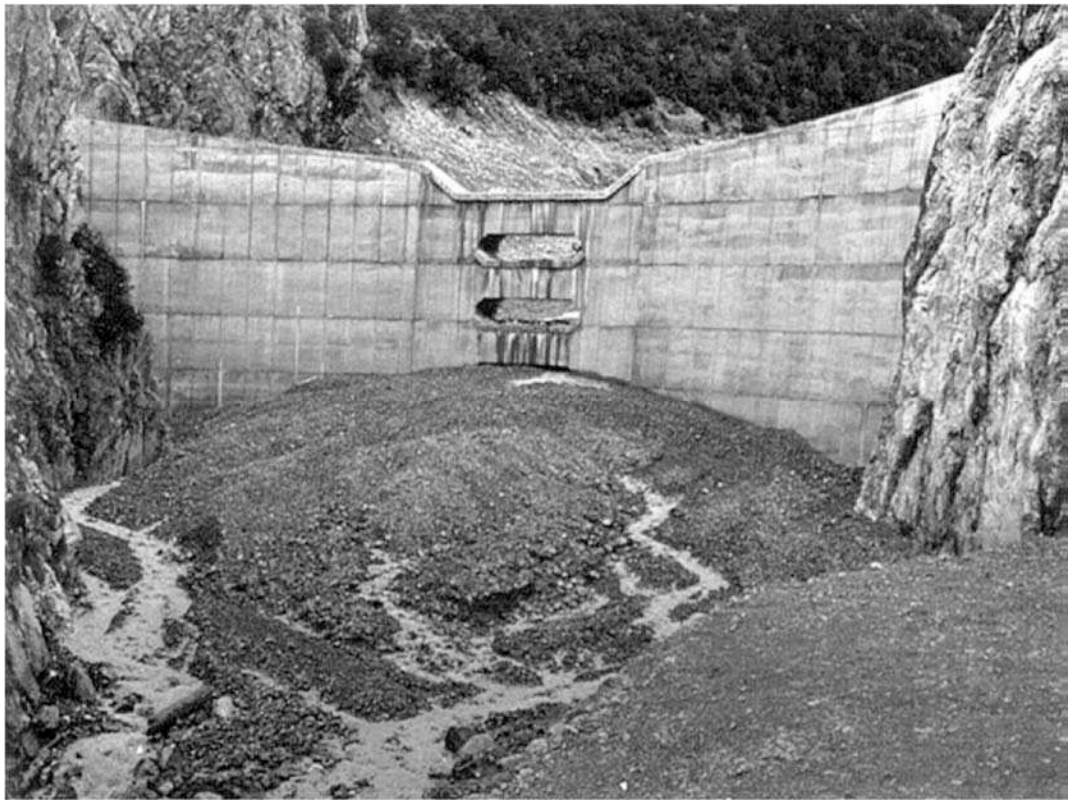

Figure 14. Slit dam with horizontal slits (taken from Hübl et al., 2005).

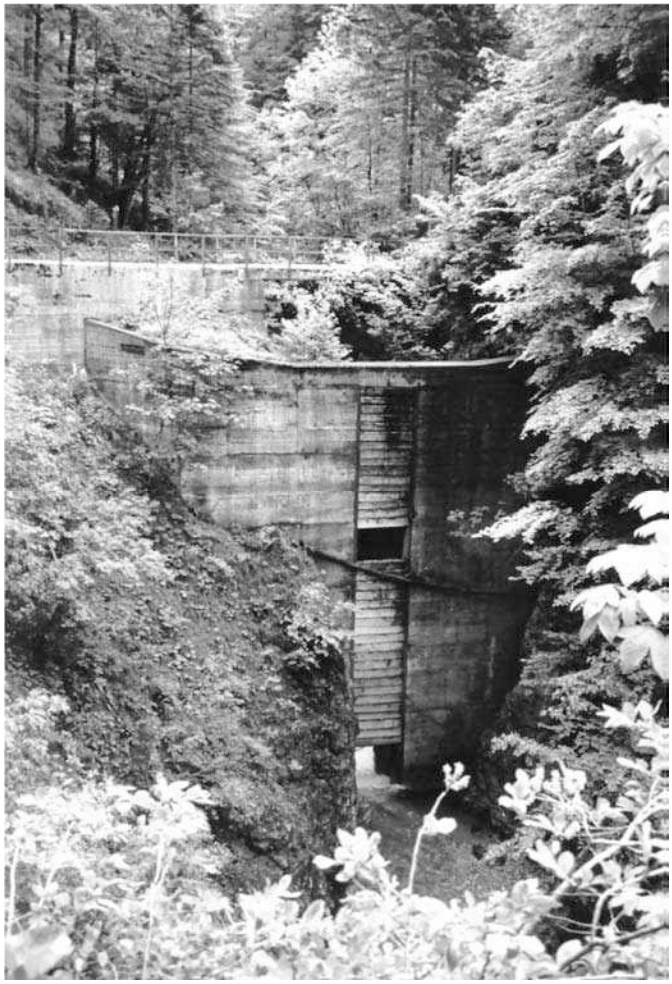

Figure 15. Closed slit dam (taken from Wehrmann et al., 2006).

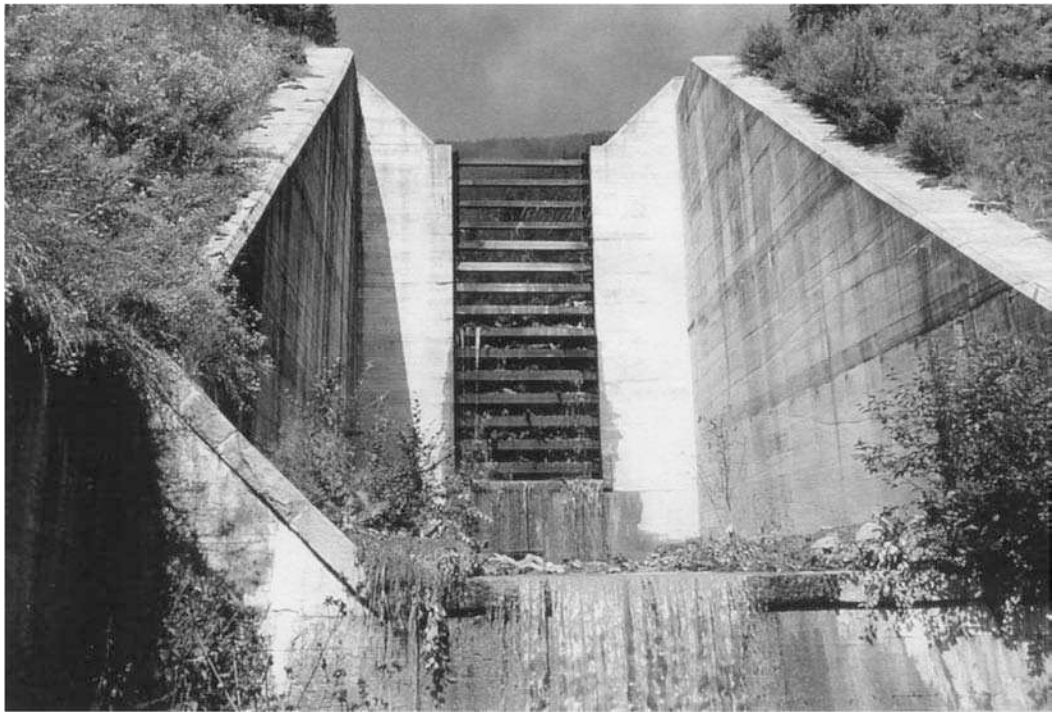

Figure 16. Slit beam dam (taken from Wehrmann et al., 2006).

Net dams

Flexible net barriers, originally designed as a rockfall barrier, were only recently adopted as a debris flow countermeasure. Several debris flow events which have accidentally hit these barriers, indicated high effectiveness and have consequently placed the focus on further researches (Roth et al., 2004). These barriers present some advantages in comparison with the classic concrete and steel dams: fast installations, lower costs, lower environmental impact, and easy reactivation of the initial conditions after an event.

Net barriers are usually placed in river channels typically with widths of 15 m (up to 25 m adding additional posts) and are anchored to the river banks by spiral rope anchors or self-drilling anchors. The nets are hold up by support and lateral steel ropes and may have some elements which allow dissipation of the energy developed by the events (Geobrugg, 2009). Even though the net crosses the entire river section, this does not mean that water, as well as fine particles, are not allowed to pass; indeed a basal opening between the river bed and the lower support rope is often present (this peculiarity can be noticed in Figure 17).

Figure 17. Net barrier placed on a river section (taken from Geobrugg, 2009).

Net mesh elements can have circular or square shape even if the former seems to work better, due to higher flexibility and higher energy absorption capacity (Roth et al., 2004). The net mesh size is usually about 30 cm and, in some cases, a second net with a smaller mesh size is coupled, in order to achieve a greater retaining capacity. With the aim to find the best mesh size, some authors have carried out small and large scale experiments. DeNatale et al. (1999) found that a mesh with ring wire of 30 cm had a better retention capacity than square

mesh wires with the same or smaller diameter (20 and 15 cm). Wendeler et al. (2008) suggested that ring diameter should be around 30-50 cm to be efficient; they also noted that this mesh size, as well as the dimension of the basal opening, should be equal to the d_{90} of the debris material (i.e. the 90% of the sediment mass or volume with that size is characterized by smaller grain size).

A great advantage of these types of barriers is that, once the net is completely filled up after an event (Figure 18), it can be quickly reactivated using excavating machines in order to carry away all the retained material. Normally it is not necessary to replace the net, but a careful inspection of it is requested, especially on the energy dissipation elements (Geobrugg, 2009).

Figure 18. A net barrier before and after a debris flow event (taken from Geobrugg, 2009).

1.3 DEBRIS FLOWS PHYSICAL MODELLING

Because of the difficulties to study debris flows phenomena directly in the field (unpredictability, high cost of the devices), laboratory studies have been often used, thanks to the easy realization and reproduction of scale problems. The physical modelling of debris flows has been studied and analyzed by several authors with different research questions. For example some authors have focused on the propagation (Hungr, 1995; Iverson, 1997; Rickenmann, 1999; Iverson et al., 2010), others on the rheological aspect (Pierson and Costa, 1987; Iverson, 2003), others on the behaviour against barriers (Hübl et al., 2009; Bugnion et al., 2012; Scheidl et al., 2012). In addition, large scale experiments can be carried out: they are obviously more difficult to realize (and also more expensive) but their results seem to be more representative of the real phenomena, as suggested by Iverson (1997).

A lot of experiments are presented in scientific literature; here I focus only on experiments and scaling issues in connection with the presence of obstacles or barriers. Among all these problems, some are called in literature as "impact pressure problems": they study the pressure exercised by the flow against a load cell. These problems, in conjunction with the studies that analyze the barrier response after a debris flow, are the most interesting for this thesis work and hence the problems presented below examine this particular field.

1.3.1 SMALL SCALE (LABORATORY) EXPERIMENTS

The laboratory experiments are typically carried out using an inclined flume with a deposition plane at the end. The debris flow start can be reproduced using for example a gate: with its opening the mixture goes down through the flume and ends on the deposition plane. During the experiments many measures about the incoming front can usually be taken: velocity, thickness, basal pore fluid pressure and basal normal stress, run-out shape (length and width) and eventually the impact pressure exercised by the flow against an obstacle. The variables are diverse; for example varying the mixture composition and the water content, different results can be obtained, analyzed and compared.

Canelli et al. (2012) carried out several tests on a flume in order to analyze the dynamical aspects of debris flows impacts on different type of barriers. Three different barriers were installed and tested: one was made of rigid steel with no holes, the second one was also made of rigid steel but with holes of 10 mm coupled with a finer polyester mesh (with 1 mm opening) and the third one was made of chicken wire with 1.5 cm opening (also with a polyester mesh). The barriers were located at the end of a flume 4 m long and 0.4 m wide with

a slope of 30°. They used saturated granular material, which was first filled and then released from a hopper at the top of the flume. Height and velocity of the debris front impacting the barriers were quantified using ultrasonic level measures. High definition cameras measured the effect of drainage due to the open barriers whereas four load cells determined the thrust applied on the top of the barrier. In each of the three barriers they noted the formation of a jet-like wave: in the rigid one that wave produced a first peak value of the thrust and then, due to the overpressure generated by the reflected wave, a greater thrust was measured against the barrier. Instead, in the filter barrier, thanks to the rapid drainage produced by the openings, the second thrust measured was never greater than the one produced by the impact front.

Zanuttigh and Lamberti (2006) studied the behaviour of two dry sandy mixtures impacting to four different types of obstacles placed at the end of a flume. The four obstacles were different in shape and orientation with respect to the flow direction and fixed on a lever system, connected to a force transducer, which allowed to measure the impact pressure. Furthermore, two laser systems revealed the flow depth, and a digital camera provided video recording with the aim to analyze the deposition extent and to verify the velocity values obtained with the laser measurements. The flume had a slope of 39°, with a reservoir at the top and a deposition plane at the end, the total length was 2.25 m and the width 0.10 m. The authors used the Froude similarity law and compared the relevant dimensions and parameters obtained with a hypothetical prototype with those found in a real situation (Rio Inferno, Verbania, North-Western Italy). For every type of barrier (shape and dimension) and position of them with respect to the flow direction, they carried out one test for each of the two mixtures. Final results were different in terms of both impact force and deposit shape and extent. They observed that the forces on the obstacles and the final deposits were very dependent on the obstacle type. Furthermore, they noted that the mixture with higher fraction of coarse particles produces higher force on the obstacles.

Another analysis was carried out by Scheidl et al. (2013) using a scale modelling approach in order to analyze the debris flow impact models. They fulfilled 16 experiments using a flume 6.5 m long, 0.45 m wide and with a 30% slope. At the end of the flume, a force panel with 24 aluminum devices (coaxially mounted with resistance strain gauges), was installed, in order to measure the pressure exerted by the incoming flow. From the reservoir positioned at the top, 400 kg of material were released for every experiment; the mixture consisted on 370 kg of solid particles (loam and bedload sediments) combined with different amount of water. In order to obtain flow height and velocity measurements, they used three ultrasonic devices positioned in three distinct sections along the flume. According to the

Froude scaling law, the data obtained from the load cells were used to estimate the pressure values. The authors noted that the type of signal processing adopted for the raw impact data strongly influence the final results and that the possible presence of large boulders could lead to uncertain results. They also concluded that dynamical impact models give more plausible results in comparison with hydrostatic models.

An interesting research was achieved by Armanini et al. (2004): they tested, in a small-scale flume, different typologies and different position configurations for mudflow breakers. These structures are aimed at reducing the energy of possible mudflows and debris flows in order to reduce the damages. The tests, carried out in order to satisfy simultaneously Froude and Reynold similarity, showed a possible best configuration for the breakers. The authors concluded that, for the general case of mudflow breakers positioned on a deposition basin, the most suitable solution consisted on two rows of breakers. In particular they noted that the second row of breakers has an important role on stopping the jets formed by the first row of breakers and that a configuration with more than two rows does not improve the situation.

1.3.2 LARGE-SCALE EXPERIMENTS

Even though small-scale experiments provide good description of the real debris flow phenomena with relative ease of construction, they often present some problems. These are mainly due to scale effects and can be avoided carrying out large-scale experiments. Indeed, in this case scaling considerations are not necessary and a better representation of the reality can be done. Although large-scale results are more representative for the real events, actually they present difficulties of realization due mostly to economic and practical factors (high costs and difficulties to find a good field test). In literature it is possible to find interesting experiments achieved by some authors in order to investigate better the real debris flow behaviours.

In June 1996, DeNatale et al. (1999) performed six experiments at the U.S. Geological Survey (USGS) Debris Flow Flume (in Oregon, USA) in order to test the behaviour of flexible barriers. The flume, made with reinforced concrete, was 95 m long, 2 m wide and 1.2 m deep with an inclination of 31° in the upper part and 3° in the lower part. The material used was composed by 10 m^3 of water-saturated sediment (gravelly sand) and was released from the top of the flume. In order to measure the total vertical stress and the pore fluid stress, a load cell and two piezometers were installed on the bottom, 1 m behind the flexible barrier; in the same position an ultrasonic depth sensor was set up in a support beam crossing the section. Load cells placed on two anchor cables and an extensometer in the front of the net,

were installed to measure tensile force and net deformation. In addition, a video camera provided the registration of each experiment. During the six tests, four different types of flexible barriers were tested; they had the same height of 2.4 m and the same length of 9.1 m, but different mesh openings. In detail, the first net had 30 cm square mesh openings, overlaid with chain link net panel liners in order to reduce the largest opening. The second one had 20 cm square mesh openings overlaid with chain link liner and an additional chicken wire liner arranged on the middle third of the net. The third one had 15 cm square mesh opening overlaid with full-width chain link and chicken wire liners. Furthermore, a fourth barrier made by 30 cm diameter rings with full-width chain link and a silt screen liner, was also tested. All the nets were supported by anchor cables along the perimeter and by two vertical steel columns on the extremities. The authors compared the results of the four different nets in terms of debris impact velocity, deflection of the net, volume of retained material. Every barrier showed a good performance in regard to the stopped material: in fact most of it was contained behind the net. In particular, the best net was the last one (the one with the silt screen and ring net mesh) with only 0.05% of passing material. The authors made also a comparison about the grain size distribution between the passed and the retained material. As expected by them, more sand passed with the chicken wire than with the finer-mesh silt screen. During each test, a diffuse spray of gravel was always observed before the debris wave arrival, but the entity of the final run-out of this was very contained (only few meters beyond the net). In conclusion the authors agreed that this research provided useful data and results that could be a good representative for small natural debris flows. A summary of the results acquired by the authors is shown in Table 5.

Table 5. Most relevant results obtained by DeNatale et al. (1999).

Characteristic	Test 1 (Barrier 1)	Test 2 (Barrier 2)	Test 3 (Barrier 2)	Test 4 (Barrier 3)	Test 5 (Barrier 3)	Test 6 (Barrier 4)
Debris Volume [m^3]	9.8	9.6	10.3	10.4	10.4	10.1
Debris Impact Velocity [m/s]	ND	9.0	6.5	8.0	6.0	5.0
Net panel Deflection [m]	ND	1.46	0.30	1.93	0.40	1.50
Volume passing the net [m^3]	SC	0.46	SC	0.12	0.046	0.0046
Percent Passing the net [%]	SC	4.8	SC	1.2	0.44	0.05

Note: The terms ND and SC mean respectively "no data" (due to problems of the acquisition system) and "system collapsed" (due to a collapse of the net after the debris flow impact).

Another large-scale experiment was carried out by Bugnion et al. (2012) in a disused quarry in Switzerland, where some hillslope debris flows were reproduced. In each experiment, 50 m^3 of satured material were released down to a steep channel 41 m long, 8 m wide and 30° inclined. In a control section placed 30 m from the top, front velocities, flow heights and impact pressures with two pressure plates were measured. Furthermore, at the end of the channel, a 15 m long and 3.5 m high flexible barrier was located; it was provided by load cells installed in the support ropes in order to measure the forces acting at the moment of the impact. In order to study the barrier dynamic behaviour, and to investigate its deformations, the authors modelled the flexible barrier with a finite element software called "FARO". A comparison between a simple one surge model (derived from a multi surge model) and the software "OpenFOAM", was also made to study the interaction between the flexible barrier and the undisturbed flow. This research has focused its attention on the importance of studying the flexible barriers behaviour on large-scale experiments, with the final aim to develop commercial software products which can be used by the engineers.

1.3.3 SCALING ISSUES

When large-scale engineering structures have to be designed, an accurate study is required. In the specific case of the debris flow hazards the study of the active measures behaviour towards debris flow phenomena is of fundamental importance. One option that the engineers can follow, is to develop a scaled model which represents the reality: in this case it is thus possible to recognize a prototype (which represents the real-full scale problem) and a model (which represents the prototype reduced on a suitable scale factor).

In a physical model, three types of similarity have to be considered:

GEOMETRIC: this similarity implies that the lengths of the prototype and the model must be the same. Thus all the dimensions must have the following ratio:

$$\frac{L_p}{L_m} \tag{1}$$

where L_p is the prototype length and L_m is the model length.

For geometric similarity, parameters having only length scales are involved (distance, area, volume).

KINEMATIC: this condition is applied on the velocities and a new ratio can be defined as:

$$_{V} \quad \frac{V_p}{V_m} \tag{2}$$

where V_p is the prototype velocity and V_m is the model velocity. This condition needs the respect of the geometric similarity.

DYNAMIC: in addition to the previous conditions, this similarity implies the ratio:

$$\frac{F_p}{F_m} \tag{3}$$

where F_p is the prototype force and F_m is the model force. To respect the dynamic similarity, Newton Second Law must be considered:

$$\sum_n F_n \quad m\frac{dV}{dt} \; ; \tag{4}$$

this formula can be rewritten as:

$$F_i \quad F_g \quad F \quad F \quad F_e \quad F_{Pr} \tag{5}$$

where the terms have the following meaning:

F_i are the inertial forces;

F_g are the gravitational forces;

F are the viscous forces;

F are the surface forces;

F_e are the elastic forces;

F_{Pr} are the pressure forces.

In terms of scale factors, it is possible to express a mechanics similarity:

$$\frac{F_{i,p}}{F_{i,m}} \quad \frac{F_{g,p}}{F_{g,m}} \quad \frac{F_{,p}}{F_{,m}} \quad \frac{F_{,p}}{F_{,m}} \quad \frac{F_{e,p}}{F_{e,m}} \quad \frac{F_{Pr,p}}{F_{Pr,m}} \tag{6}$$

where the subscripts p and m respectively indicate the prototype and the model forces. This similarity is never fully verified in practice; therefore the respect of similarity is required only for the most important forces (but at the same time evaluating the consequences of a failed respect of the other conditions). The idea is to simplify the problem following the hypothesis that two main forces are prevalent than the others, looking for the respect of the similarity only for these two main parameters.

In the physical modelling of a fluid flowing in an open channel, the main forces that govern the system are:

Inertial forces: $F_i \quad m\,a \quad (\ L^3)\ (V^2/L) \quad L^2V^2$ (7)

Gravitational forces: $F_g \quad m\,a_g \quad (\ L^3)\ g$ (8)

Viscous forces $F \quad (V/L)\ L^2 \quad VL$ (9)

Here, m denotes the mass, a is the acceleration, a_g is the acceleration of gravity (i.e. g), is the material's density, V is the velocity, is the dynamic viscosity, L is the length, L^2 is the area and L^3 is the volume.

Depending on the outweigh of gravitational or viscous forces, it will be possible to choose respectively the criteria of similarity of Froude or Reynolds.

Froude similarity consists in keeping constant the Froude Number Fr (which can be expressed by the ratio of the inertial and gravitational forces) moving from the prototype to the model. It is suitable to describe all phenomena in which the gravitational forces are predominant (this is the case of the most free surface flows). The Froude similarity is then expressed by this similitude:

$$Fr_p \quad Fr_m; \tag{10}$$

respecting this equality it is possible to scale free surface flows, open channels and other similar problems. To scale a problem, once the scale reduction is chosen, it is hence possible to define all the other parameters following the indication summarized in Table 6.

Table 6. Scaling ratio for Froude similarity.

Parameter	Dimension	Unit	Scale Ratio
Length	L	[m]	
Time	T	[s]	$T \quad \sqrt{\ }$
Velocity	L/T	[m/s]	$V \quad \sqrt{\ }$
Mass	M	[kg]	$M \quad {}^3$
Discharge	L^3/T	$[m^3/s]$	$Q \quad {}^{5/2}$
Force	$M\,V^2/L$	[N]	$F \quad {}^3$
Pressure	F/L^2	$[N/m^2]$	P

Note that in case of two identical materials, the scaling factor $_p/\ _m$ is equal to 1.

Reynolds similarity is instead used to describe all those phenomena in which the viscosity is predominant (that means viscous forces are more important than the gravitational forces). To perform a physical modelling in this case, equality of the Reynolds Numbers of the prototype and of the model is required:

$$Re_p \quad Re_m \tag{11}$$

Remembering that the Reynolds Number is the ratio between inertial and viscous forces, and if the same fluid is used in both the prototype and the model, the following relation can be derived:

$$_T \quad ^2 \tag{12}$$

For correctly modeling a viscous fluid in an open channel, the Froude and Reynolds scaling should be fulfilled, i.e. Froude and Reynolds numbers of the prototype flow and the model flow have to be the same. In case of modeling water flows, Reynolds scaling can be neglected because the viscous forces are expected to be very low compared to gravitational and inertial forces. Some authors have used this approach for their studies, but often with approximations and careful considerations about the choice applied. Zanuttigh and Lamberti (2006) observed that their experimental results, obtained with the Froude's law, are valid qualitatively and quantitatively for the forces, but appear only qualitatively valid for the deposits. Rickenmann (1999) derived empirical relationships for debris flows based on the assumption of Froude scaling. However, when following an equivalent fluid approach for debris flows (i.e. debris flows are considered as homogeneous mixtures of solid and fluid that can be represented by a fluid with a certain density and viscosity), it is to expect that viscous forces are relevant and therefore Reynold scaling should be fulfilled as well. For this reason the results of this study, especially measured values of forces within the cables, have to be interpreted with caution and can be used to compare experiments relatively. As Iverson's works demonstrated (Iverson, 1997), the scale effects have a great importance during the flow of debris flows and hence scaling with Froude's law is not always valid.

1.4 RESEARCH AIM

The present thesis work is connected to an existing applied research project at the Institute of Mountain Risk Engineering, University of Natural Resources and Life Sciences, Vienna (IAN-BOKU), which aims to investigate an optimization for an open barrier model. In order to find an adequate barrier configuration to protect the railway at Taxenbach, Salzburg (Austria) and to test its behaviour in respect to a debris flow impact, sets of experimental tests were carried out in a small scaled model respecting the Froude similarity.

Five different basal openings were tested and the results were analyzed in terms of:

volume retained and passed through the barriers;

velocity of the debris flow front along the model;

forces acting on the barrier cables which support the net.

These parameters were taken into account as a starting point to draw some qualitative and quantitative conclusions. The dam behaviour was also considered depending on the purpose to be achieved: partial or total retention of the debris flow with the connected advantages and disadvantages.

Furthermore, the thesis intents to highlight the problems that occur when small scale experiments are led, with a critical analysis on the possibility of extending the obtained test results to the prototype full scale.

2 MATERIALS AND METHODS

Several devices were used in order to investigate the debris flow behaviour in connection with the dam response. Herein the procedure adopted to obtain the experimental data are presented.

2.1 PHYSICAL MODEL

The scaled model of the channel in question was built in the laboratory of IAN-BOKU. The model represents the area object of study (i.e. the prototype) in 1/30 scale (the modeled length of the channel is 3.75 m); this is located at Taxenbach, Salzburg (Austria) about 90 km from Salzburg (Figure 19).

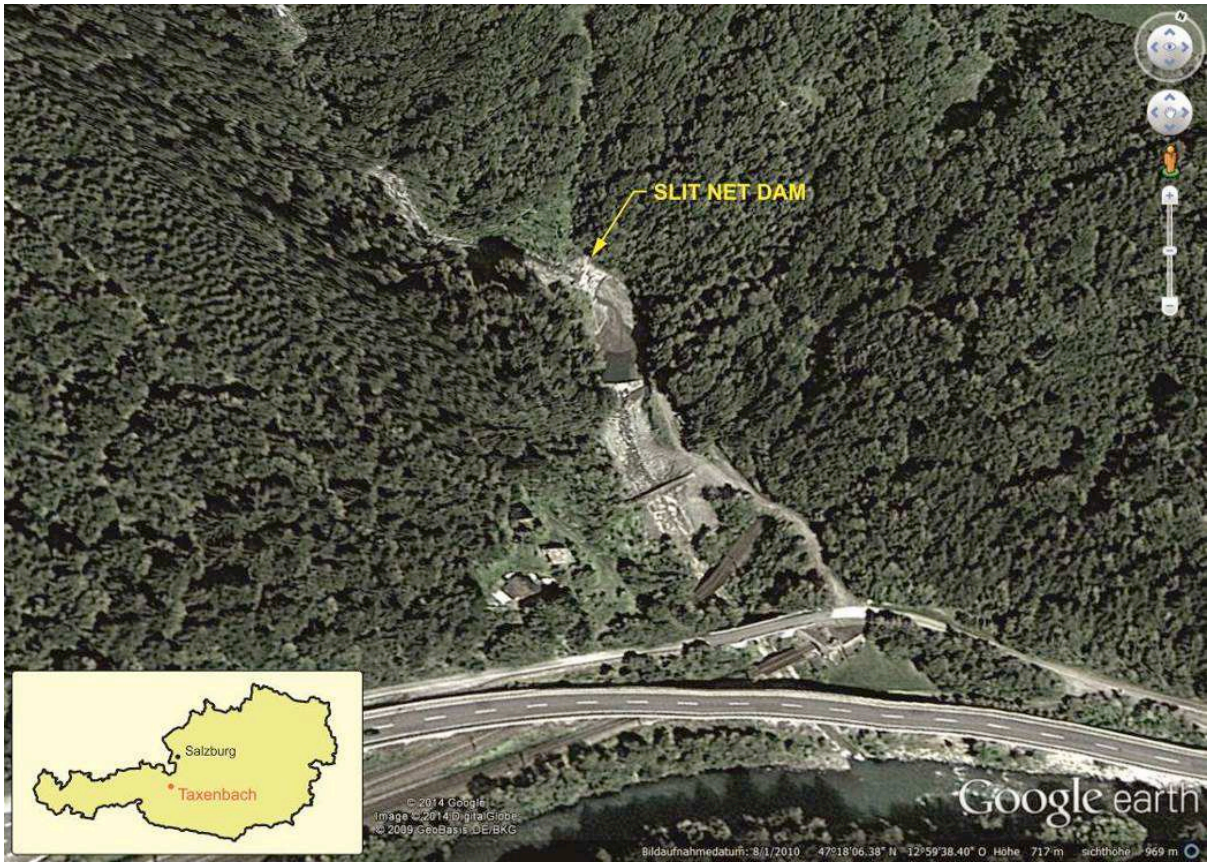

Figure 19. Aerial view of the geographic location: Taxenbach, Salzburg, Austria (from Google Earth).

The area is particularly critical because the stream is close to the rail and road network. The existing situation is characterized by two solid body dams which control the sediment

processes immediately before the railroad. The future slit net dam would be placed before these two dams in order to, depending on the desired purpose, stop completely or partially the incoming debris flow, reducing in this way its energy.

The scaled model was built starting from the field topography in order to represent it on a 1/30 scale. To fulfill a good representation of the reality, 16 sections of the interest area were chosen and reproduced with extruded polystyrene panels (20 cm width) which, when combined each other, formed the final experimental flume. The surface thus formed, was then conveniently covered by simple mortar; in particular the stream bottom was further roughened using a material mixture which represents the scaled granulometry of the prototype stream bottom. Figure 20 shows the three grain size distributions relevant for this study: the green curve represents the prototype material (i.e. the granulometric distribution of the material sampled in the field, in the real scale), the blue curve is the prototype material scaled 1/30 (this represent the "ideal" grain size distribution to be reproduced for the stream bottom model) and the red curve represents the grain size distribution of the material actually used in the model, which was composed by: 30% sand, 30% gravel of 2-4 mm and 40% gravel of 0-32 mm.

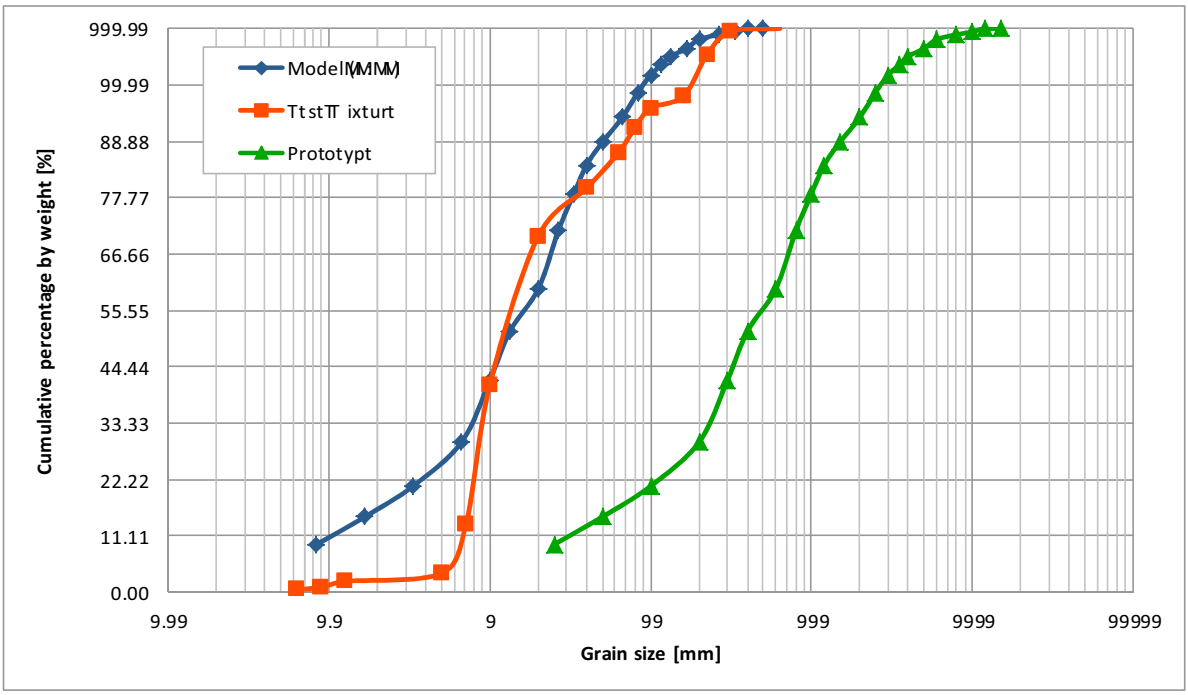

Figure 20. Grain size distribution of the stream bottom material.

In addition to the model surface, on the first part of the model, a channel made of wood panels was built in order to permit the debris flow release. Furthermore, at the end of the

model a closing section with an opening to install the net structure was created. The final model presents a right-hand side length of 3.75 m, a left-hand side length of 3.20 m, a width of 2.40 m and a height of 0.75 m, the mean slope is 5° but it changes along the model according to the prototype morphology; the wood channel is 1.50 m long, 0.40 m width and 0.50 m high, with a slope of 12°. At the end of the model, after the net section, two concrete buckets were placed in order to collect all the debris flow material which passed during the tests and for the successive cleaning of the model. An overview of the construction phases and of the final model is shown in Figure 21, whereas Figure 22 shows the sketch of the model and the measurement devices placement.

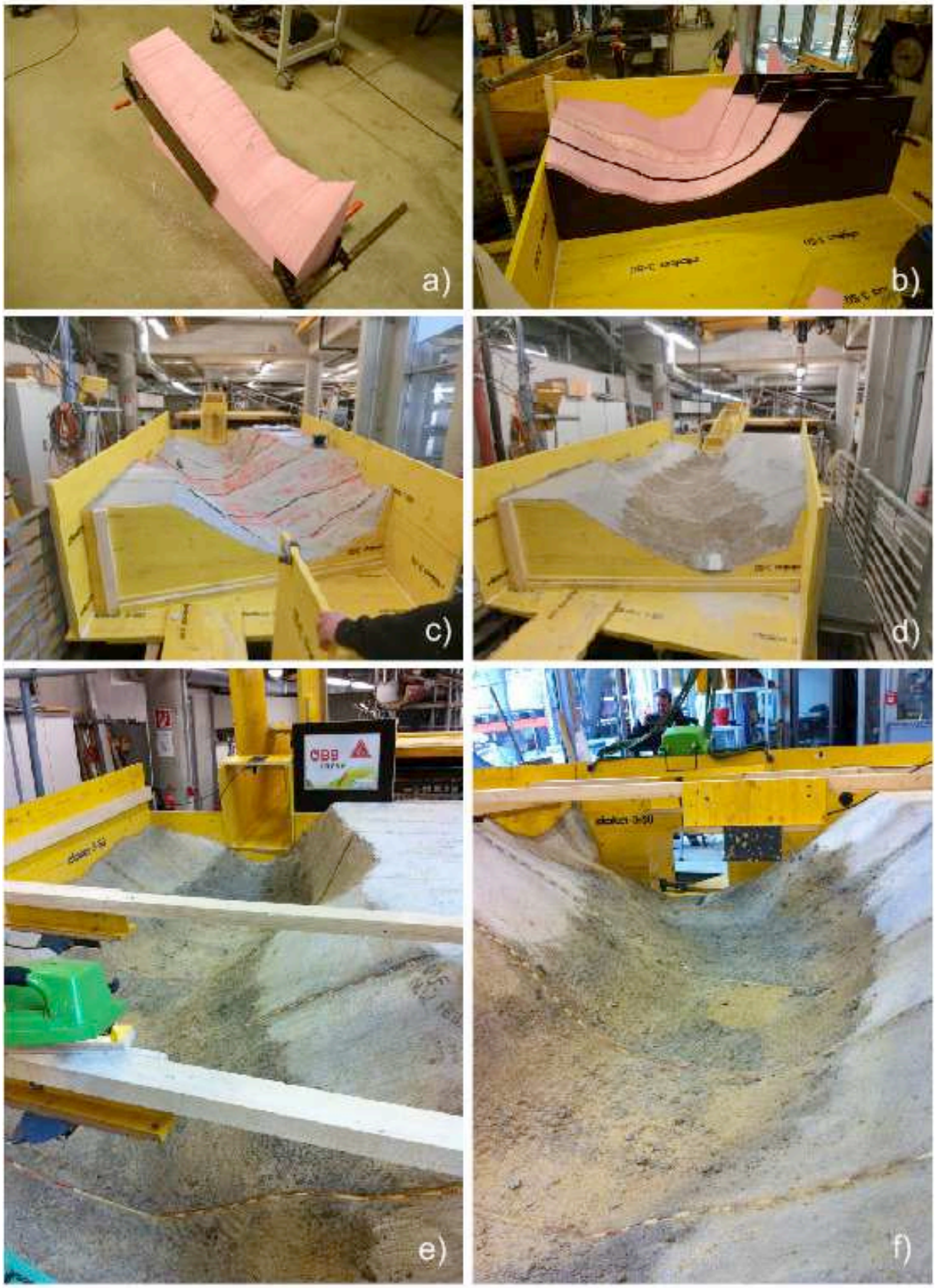

Figure 21. Experimental model built at the Mountain Risk Engineering Laboratory. a) 20 cm width section; b) sections' connection; c) section connected and covered by the first layer of mortar; d) model with the stream bed roughened; e) vision of the upper part (starting channel); f) vision of the lower part (the square hole serves for the net structure placement).

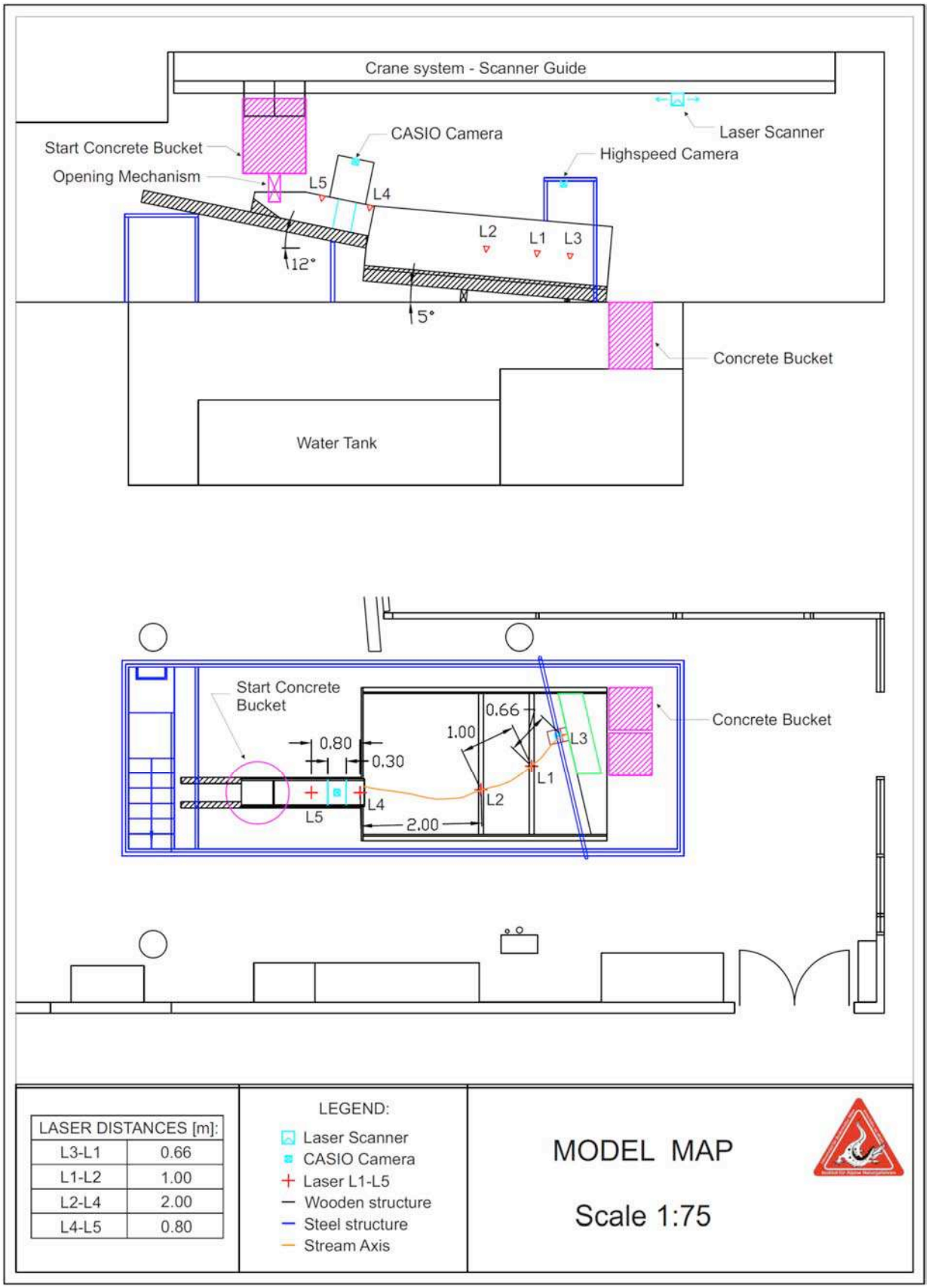

Figure 22. Sketch of the physical model (drawn by Nikolaus Wieser – IAN).

2.2 "SLIT NET DAMS"

The barriers tested in this thesis follow a new technical concept which can be considered as an Open Barrier (see Chapter 1.2.2). If the opening is partially covered, steel beams are usually adopted (Slit beam dam, according to Wehrman et al., 2006; see also Table 4 in the present thesis) (Figure 16) or also grills (Slit grill dam, again according to Wehrman et al., 2006). In the present model the slit opening of the barrier is partially covered by a net element, and therefore we propose here the new term Slit Net Dam. Although it can be considered as an evolution of the previously mentioned dam categories, this solution employing a net is quite new and could lead to good advantages, firstly in terms of easy access for the excavating machines and therefore easy cleaning after debris flow events, with relative low costs when the net has to be replaced due to damages.

The scaled slit net dam was built using plastic elements, set up together in order to reproduce the real slit net dam geometry (Figure 85-87 in APPENDIX A show the slit net dam prototype to be realized on the field). The slit width is fixed and it is equal to 13.3 cm (which corresponds to 4 m in the prototype) whereas the basal opening can be changed adding some extruded polystyrene panels on the slit bottom. The net is made of cotton and presents a square mesh with openings of 1 cm. It is supported by six metal cables (1 mm diameter) every 4 cm, therefore the total net height is equal to 20 cm. Furthermore, two supplementary nets (9 and 12.2 cm height, respectively) were built in order to study the behaviour of the barrier in respect of the overflow problems which were observed during some experiments and to fulfill one test with the opening completely closed. On the slit side six bending beam load cells were placed in order to measure the forces exerted by the flow (Figure 23): they are installed alternately in each side. The load cells measure the forces applied by the flow on the steel cables which are fixed on one side and connected with a pulley (with a diameter of 26 mm) to the load cells on the other side. Every cable was pretensioned before every test start with a force value of 10 N in order to obtain a sufficient stiffness of the net-cables system. The two additional nets are not equipped with cables and load cells, thus along their entire height it was not possible to obtain force values. The details of the slit net dam tested are summarized in Table 7 and Figure 24, where the differences existing between every test are shown. Although the different basal openings are five, the slit net dams tested are eight, depending on the presence or not of additional nets (or of a plexiglass plate in the particular case of Tests 4.2 and Test 4.3).

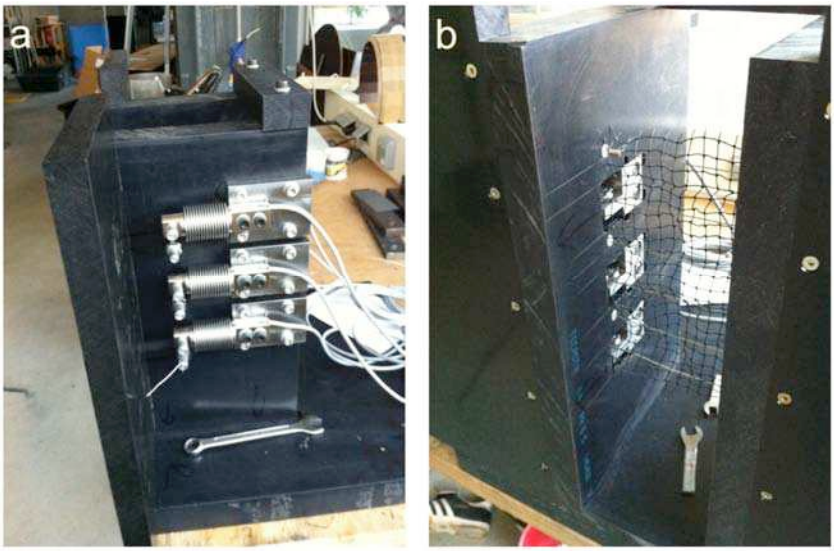

Figure 23. Particulars of the net dam structure: a) load cells on the right side of the dam; b) connection system on the left side (pulleys and fixed cables).

Table 7. Summary of the slit net dams tested.

Run	Date	Slit Net Dam type	Basal Opening [cm]	Net element height [cm]	Note
1.1	9 April 2014	A	8.7	20.0	
1.2	15 April 2014				
1.3	16 April 2014				
1.4	17 April 2014				
2.1	22 April 2014	B	6.0	20.0	
2.2	23 April 2014				
2.3	23 April 2014				
2.4	5 May 2014	C		29.0	Additional net on the upper part
3.1	17 June 2014	D	4.5	20.0	
3.2	17 June 2014				
3.3	18 June 2014				
3.4	12 June 2014	E		29.0	Additional net on the upper part
4.1	6 May 2014	F	3.3	29.0	Additional net on the upper part
4.2	7 May 2014	G			Additional net on the upper part and plexiglass plate on the top
4.3	10 June 2014				
5	6 May 2014	H	0.0	41.2	Additional net on the lower and the upper part

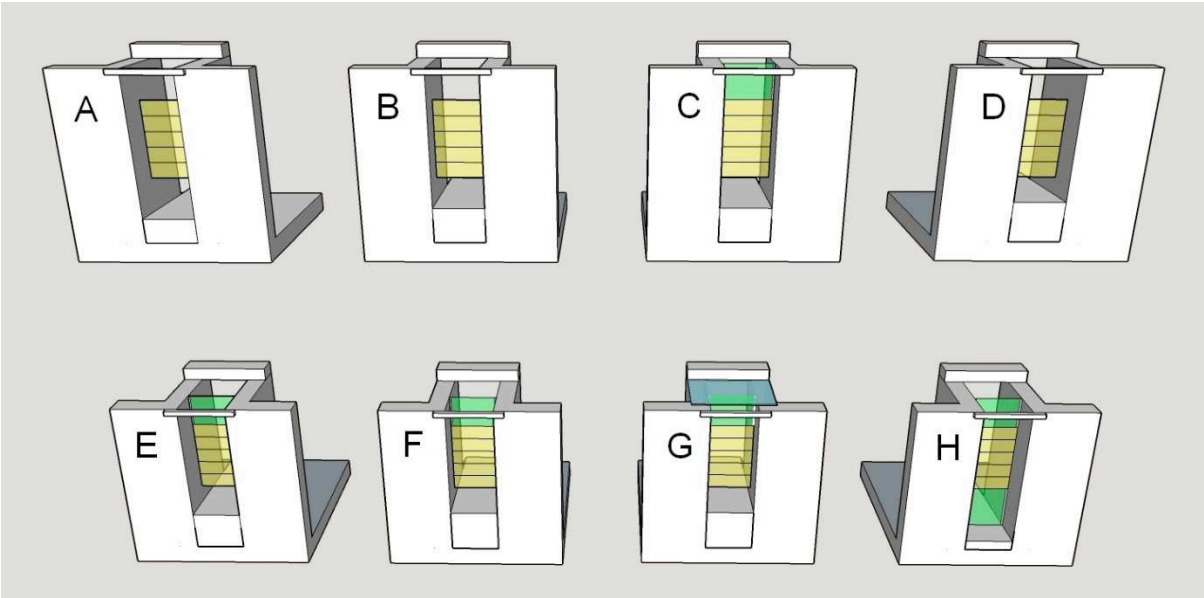

Figure 24. Different typologies of net configurations tested: A) basal opening 8.7 cm; B) basal opening 6.0 cm; C) basal opening 6.0 cm with additional net (shown in green) on the upper part (not equipped with cables and load cells); D) basal opening 4.5 cm; E) basal opening 4.5 cm with additional net; F) basal opening 3.3 cm with additional net; G) basal opening 3.3 cm with additional net and plexiglass plate on the top; H) basal opening 0.0 cm with additional net on the lower and the upper part.

2.3 MATERIAL MIXTURE

The choice of the material mixture to be used on the scaled experiments was guided by samples taken in the field from deposits of a past debris flow event occurred in June 2013. Once the prototype grain size distribution (GSD) was scaled to the model, a GSD for the mixture to be used on the model was chosen. The final debris flow mixture adopted for the tests was composed by loam and coarse sediments with the following percentages: 40% of 0-50 mm gravel, 20% of 2-4 mm gravel, 10% of sand and 30% of loam. The loam in particular, was composed by particles consisting of 26% clay, 60% silt and 14% fine sand. Figure 25 shows the grain size distribution studied to lead the tests: the green curve represents the granulometry distribution of the debris material present in the field (i.e. the prototype grain size distribution), the blue line represents the latter scaled 1/30 and the red curve is the material mixture distribution used on the tests.

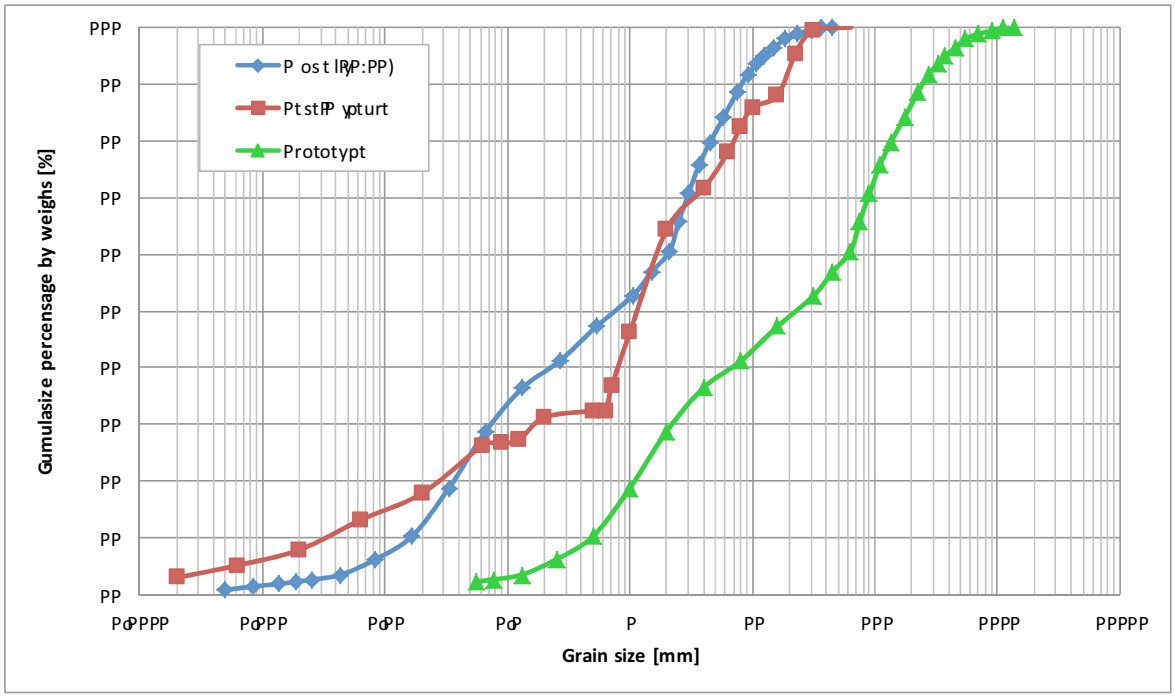

Figure 25. Grain size distribution of the debris flow material.

In addition, Figure 26 shows the grain size distribution of the four different materials which were chosen to reproduce the prototype debris flow and Figure 27 shows the granulometric characteristics of these materials before they were mixed all together.

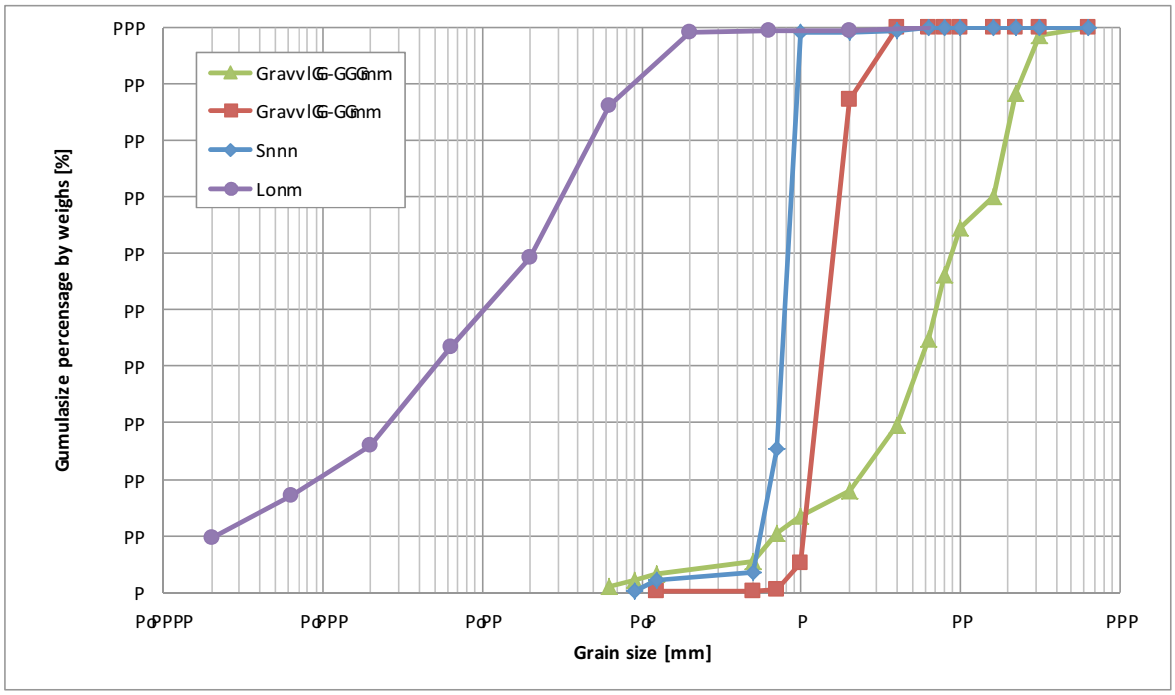

Figure 26. Grain size distribution of the materials used to make the debris flow mixture.

Figure 27. Materials used to prepare the debris flow mixture: a) loam, b) sand, c) gravel of 2-4 mm, d) gravel of 0-50 mm, e) loam mixed with water, f) final mixture on the two concrete buckets.

The material volume released during each test was around 0.40 to 0.47 m^3: the volume consists of the debris flow material described above, plus a certain amount of water. In practice the mixture was prepared starting with a 20% by weight of water and 80% of solid particles (of which 30% composed by fine material and 70% of granular material). From the first to the last test, these percentages changed depending mainly on how much material was lost during the experimental procedures. Effort was made in order to maintain constant the original percentages, although it was really demanding, due the big amount of material used. In fact it was very difficult to have for each test the same material, with the same water content and thus the same conditions. That fact introduces necessarily approximations in the test results, which were taken into account during the analysis of the results.

Figure 28 shows a tri-plot representation for the different percentages by weight of the mixture, in terms of fine and coarse sediments and water content. The percentages of the fine and coarse materials were calculated, known the mixture total weight and the water content of each test (calculated as described in the next paragraph 2.3.1), by assuming constant the percentages of 30 and 70 % of the solid particles.

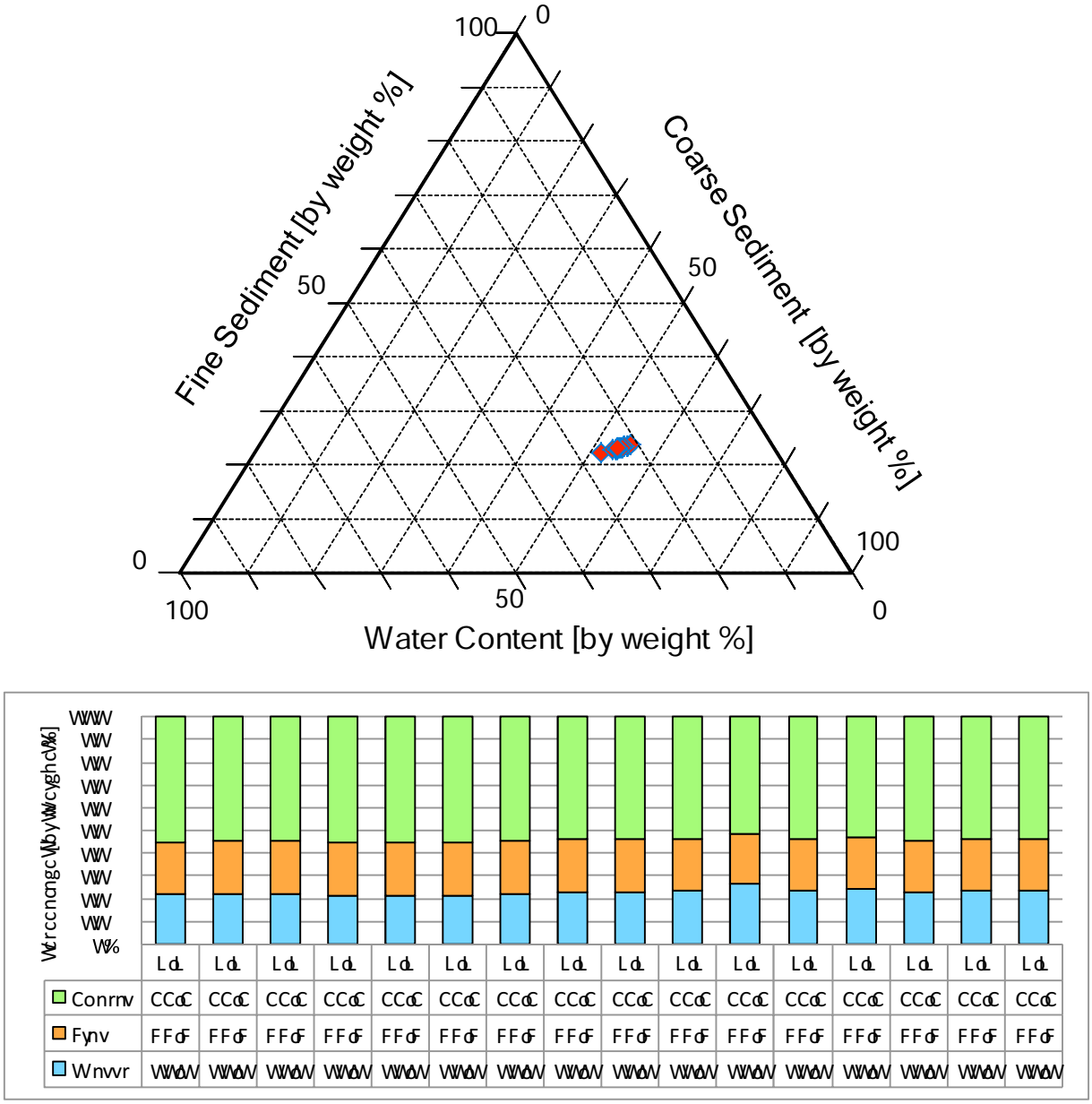

Figure 28. Triangle plot for the mixture components by weight and stacked column chart of the data of each experimental test.

2.3.1 WATER CONTENTS

Since the tests were carried out using a relatively large amount of material with a maximum grain size of 50 mm, it was very difficult to maintain exactly the same conditions for each material mixture. In particular, the water content was the parameter responsible for the greatest variability among tests.

The water content was determined for each test by taking a sample of about 4 kg of material from the release bucket immediately before the beginning of each test. After

weighing the sample of the material and after it dried in the oven at 105°C for at least 24 hours, the water content by weight w was estimated with the following equation:

$$w \quad \frac{m_{wet} \quad m_{dry}}{m_{wet}} \quad 100\% \quad \frac{m_{water}}{m_{wet}} \quad 100\% \tag{13}$$

where m_{wet} and m_{dry} are the sample masses before and after the drying process in the oven and their difference, m_{water}, is the mass of the water.

The variability of this parameter is summarized in Table 8 and Figure 29.

Table 8. Water contents by weight for the experimental tests.

Run	Date	Water content by weight [%]
1.1	9 April 2014	21.66
1.2	15 April 2014	22.08
1.3	16 April 2014	21.73
1.4	17 April 2014	21.52
2.1	22 April 2014	20.99
2.2	23 April 2014	20.94
2.3	23 April 2014	22.09
2.4	5 May 2014	22.92
3.1	17 June 2014	23.00
3.2	17 June 2014	23.62
3.3	18 June 2014	26.36
3.4	12 June 2014	23.75
4.1	6 May 2014	24.13
4.2	7 May 2014	22.52
4.3	10 June 2014	23.49
5	6 May 2014	23.25
	mean ± SD	22.75 ± 1.38

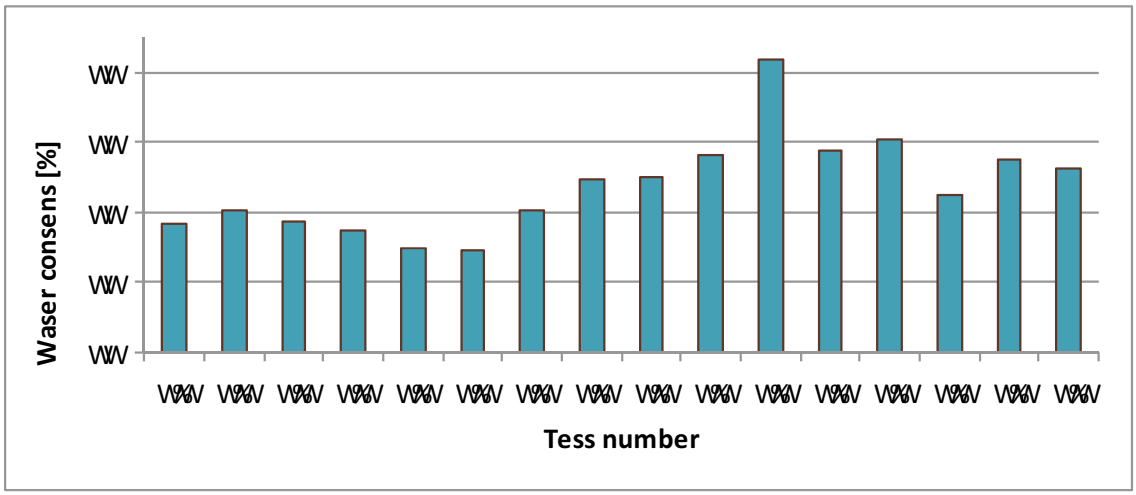

Figure 29. Water content variability for the experimental tests.

It is important to note that these calculations are affected by an approximation because of the little amount of material sampled (about 4 kg) in comparison with the total amount of material used in the tests (about 1000 kg). Furthermore, the measures depended on the site where the samples were taken, since the total masses were not homogeneous although they were properly mixed before the start of each test. This fact can be highlighted observing the diagram in Figure 30 which shows the distribution of the water content among the tests. The theoretical Gaussian curve which is superimposed to the frequency histograms, shows in fact a not perfect symmetrical distribution.

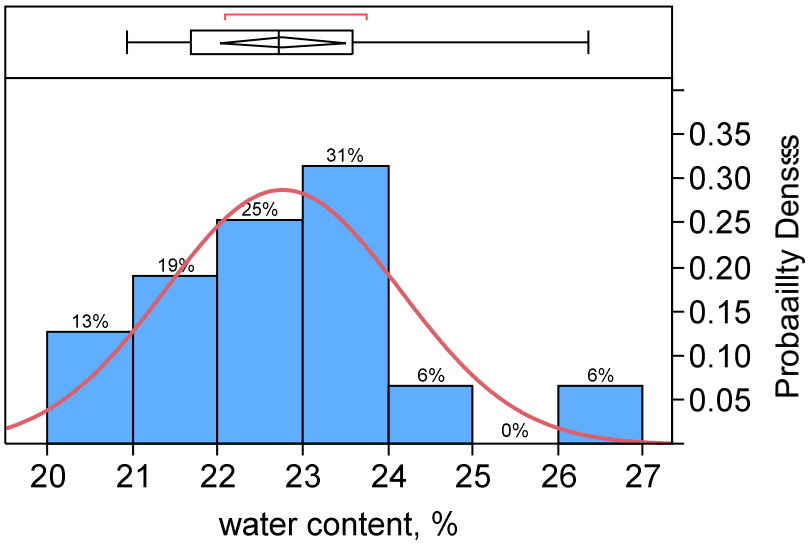

Figure 30. Diagram showing the distribution of the percent water content among the various experimental tests (n=16). Median value is 22.72%.

2.3.2 RELATION BETWEEN d90 AND BARRIER GEOMETRY

Some interesting considerations can be done looking at the relationships between the GSD of the material mixture and the geometry parameters of the slit net dam. As authors have previously observed (Wendeler et al., 2008; Itoh et al., 2013), the dimensions of the net mesh size and also the basal opening, could be related with the d_{90} (90% size of sediment distribution) or the d_{95} (95% size of sediment distribution) of the debris flow material. Figure 31 shows the d_{90} and the d_{95} values of the test mixture which were equal to 17.48 mm and 21.98 mm respectively.

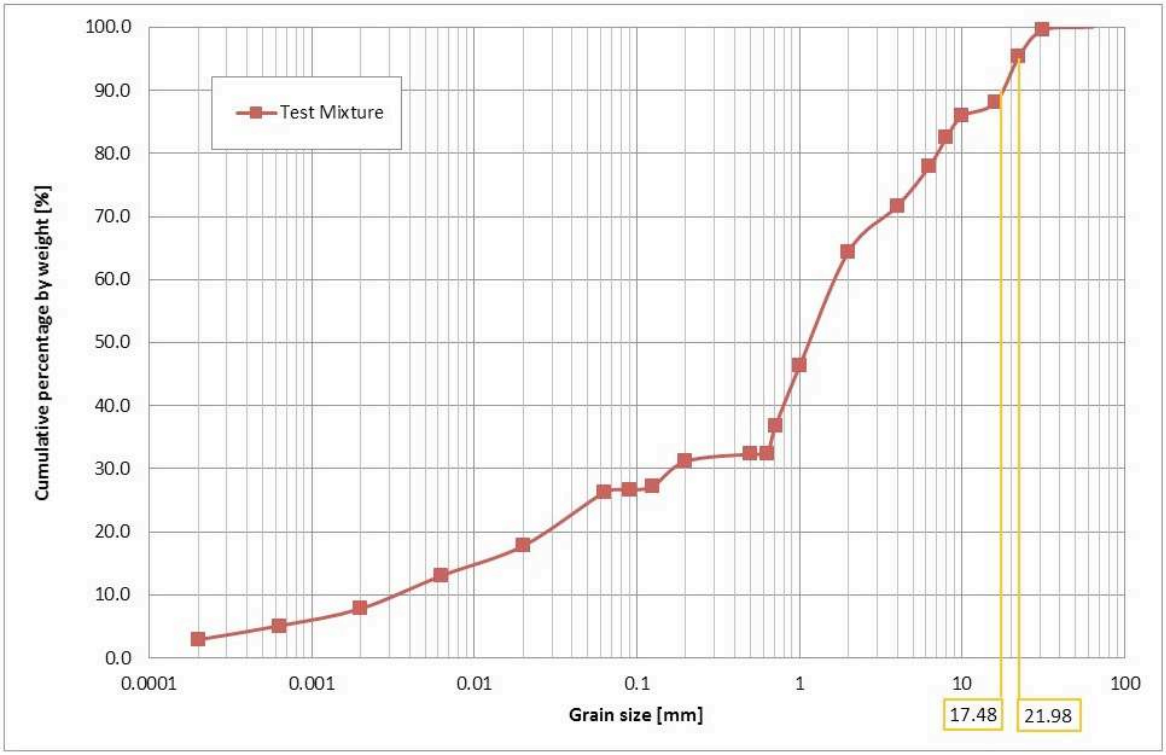

Figure 31. Evaluation of d_{90} (90% size of sediment distribution of the debris flow mixture) and d_{95} (95% size of sediment distribution of the debris flow mixture) as interpolation from the logarithmic representation of the grain size distribution.

Final conclusions regarding the slit net dam prototype configuration (i.e. which are the best basal opening and mesh size for the prototype) were done depending on the test mixture and hence on the slit net dam with the results obtained from the scaled model.

In Table 9 some relations among the d_{90} and the d_{95} and the different basal opening tested are shown. In addition, other relations can be done looking at the mesh size which was the same during each test (Table 10).

Table 9. Geometric relations between d_x and slit net dam basal opening.

d_x Test Mixture value [cm]		Basal Opening [cm]	Slit Net Dam type	Ratio [basal opening/d_x]
d_{90}	1.748	8.7	A	$4.98 \cdot d_{90}$
		6.0	B, C	$3.43 \cdot d_{90}$
		4.5	D, E	$2.57 \cdot d_{90}$
		3.3	F, G	$1.89 \cdot d_{90}$
d_{95}	2.198	8.7	A	$3.96 \cdot d_{95}$
		6.0	B, C	$2.73 \cdot d_{95}$
		4.5	D, E	$2.05 \cdot d_{95}$
		3.3	F, G	$1.50 \cdot d_{95}$

Table 10. Geometric relations between d_x and net mesh size.

d_x Test Mixture value [cm]		Net Mesh Size [cm]	Slit Net Dam type	Ratio [net mesh size/d_x]
d_{90}	1.748	1.00	A, B, C, D, E, F, G, H	$0.57 \cdot d_{90}$
d_{95}	2.198	1.00	A, B, C, D, E, F, G, H	$0.45 \cdot d_{95}$

2.4 MEASUREMENT DEVICES

The measurement devices used during the tests consisted of:

Five Baumer laser distance sensors (model OADM 20I6480/S14F; Figure 32a), placed in different positions (Figure 22) to gain measures of the debris flow depths during the tests. These measures were used to obtain the flow velocities between the laser sensors and were taken with a frequency of 1200 Hz.

One Sick laser scanner LMS400 (Figure 32b) which provided a scan of the model after each test with a scanning frequency of 360 Hz, in order to obtain data for the deposition volume analysis.

One Optronis high speed camera (model CR3000x2; Figure 32c) capable of capturing 1200 frames per second with a resolution of 1280x800 pixels; it was used to obtain the front velocities of the flow, immediately before the slit net dam.

Three cams: two Actionpro X7 and one GoPro Hero, arranged in different positions, in order to acquire videos of the tests and thus to achieve a qualitative vision of each test.

One CASIO camera (model Exilim EX-ZR1000) positioned on the wood inlet channel between the laser sensors L4-L5, with the aim to obtain a qualitative vision of the flow close to the start concrete bucket, immediately before the debris mixture starts to flow in the model.

Six HBM bending beam load cells (model Z6FC3; Figure 32d) installed on the net sides, with a nominal load of 200 N in order to measure the forces applied by the flow on the net cables. The acquisition frequency was of 1200Hz.

For data recording an amplifier (company HBM, model MCGplus) was used to transfer the signals measured by the laser distance sensors and the load cells to a laptop. The acquisition software Catman (Version 6.0) was adopted for acquiring, visualizing and analyzing the data measured. The laser scanner and the high speed camera were directly connected to the laptop which recorded the relative measures (Figure 33).

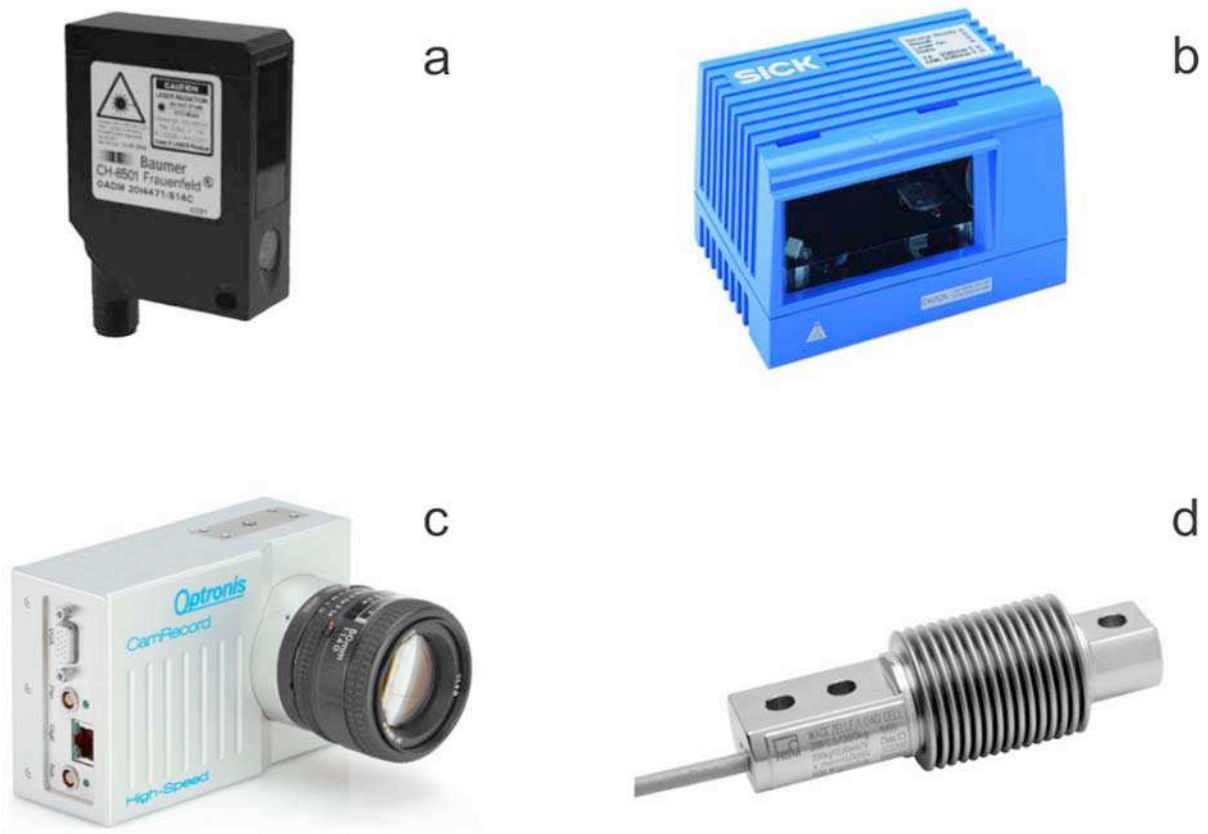

Figure 32. Measurement devices: a) laser distance sensors; b) laser scanner; c) high speed camera; d) bending beam load cell.

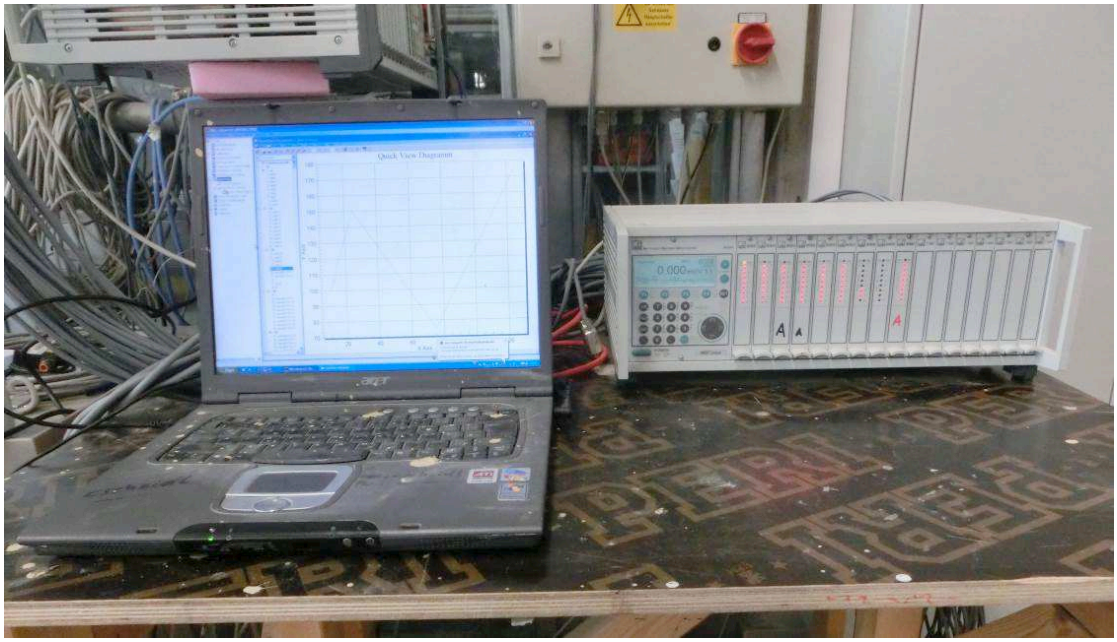

Figure 33. Laptop and amplifier used to record the measured data.

2.5 TEST PROCEDURE

In order to discover the behaviour of this particular type of slit dam, different basal opening configurations were tested. As previously shown in Table 7 and Figure 24, they are different in terms of basal openings and total net heights.

In total sixteen experiments were carried out; this restricted number was due to the large amount of material (with a total mass around 1 ton) that has to be prepared for each test.

Prior to every test run, the mixture collected in the two concrete buckets (which contain the material of the previous test, Figure 27f) was mixed in order to homogenize the material and to avoid particle sedimentation on the buckets' bottom. The ready material was then poured into a unique big concrete bucket with a full capacity of 0.53 m^3. Once the bucket was filled up, a sample of the mixture was collected to analyze the water content of the test; subsequently the distance from the mixture surface and the upper edge of the bucket was measured, in order to estimate the total volume (and mass) of the mixture released in each test. The concrete bucket was then positioned above the start of the inlet wood channel, and after every measuring devices were turned on, the bucket basal opening was opened lifting the basal lever. In this way the material starts to run and hits the net at the end of the model. After the flow was stopped and velocities, forces and debris flow depths were measured, the relative instrumentations were removed from the measure sections in order to permit the scanning of the model area by the laser scanner. At the end of this last measure, cleaning procedure starts, with the aim to restore the same initial conditions for the successive test.

2.6 MEASUREMENTS AND DATA

Since the aim of this work was to investigate and characterize the behaviour of a slit net dam model, different configurations were tested and compared according to different parameters. In this context the major parameters of interest are volumes, velocities and forces: they are described below, in order to explain the methods used to obtain them.

2.6.1 VOLUMES

Volume values were investigated in terms of retained material by the dam and passed (and also lost) material through the dam. Starting from the knowledge of the volume, obtained with the measure of the distance from the material level surface to the concrete release bucket

upper edge, it was possible to obtain the value of the material volume released in each test. After each test was run, the laser scanner provided a scan of the model area with the deposited material. The scan results were given in terms of xyz data and were then elaborated with the software Surfer (Golden Software, Inc., Golden, CO, USA), a grid-based mapping program which provided different types of output maps to best represent the data (Figure 34). Furthermore, the software allows to calculate the volume between two different surfaces thanks to the Grid Volume command, which only required a lower and an upper surface grid files: the first one is given by the scan of the empty model (Figure 35a) while the second one is given by the scan with the debris flow deposited (Figure 35b). In order to obtain more accurate results, the maps were cut to remove the volumes not interesting for the purpose of calculating, with the Blank function provided by the software. The volume calculated in this way refers to the retained volume, i.e. the volume of the material which was deposited or retained on the model.

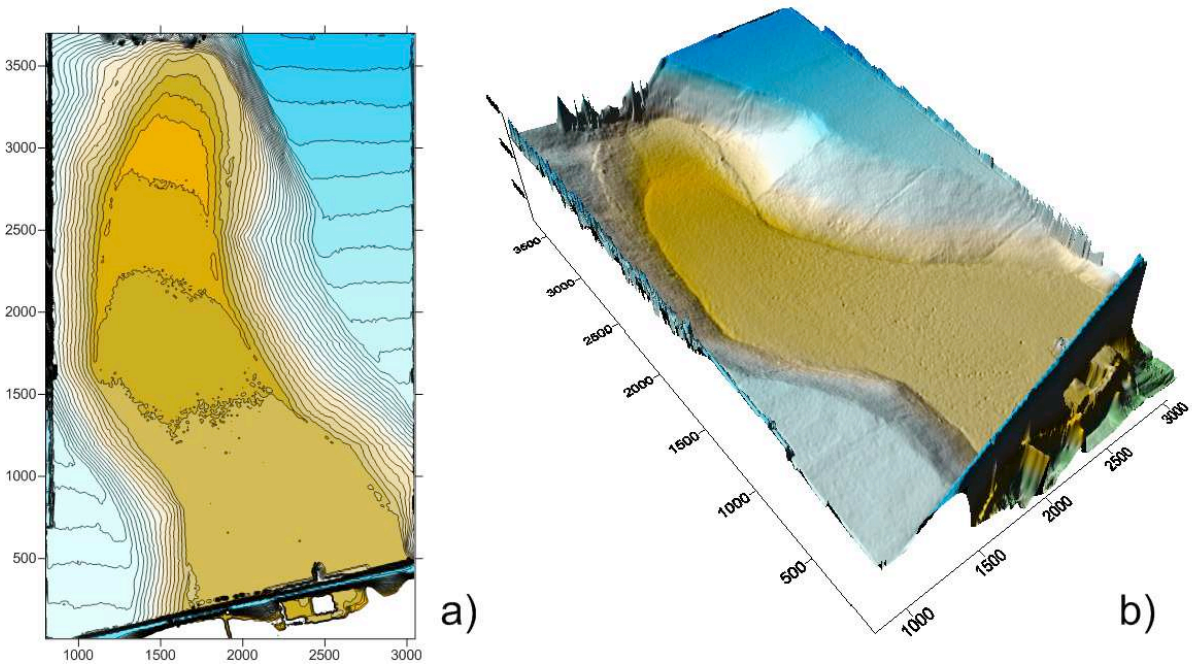

Figure 34. Example of the output maps provided by Surfer: a) contour map and b) 3D surface for Test 4.1.

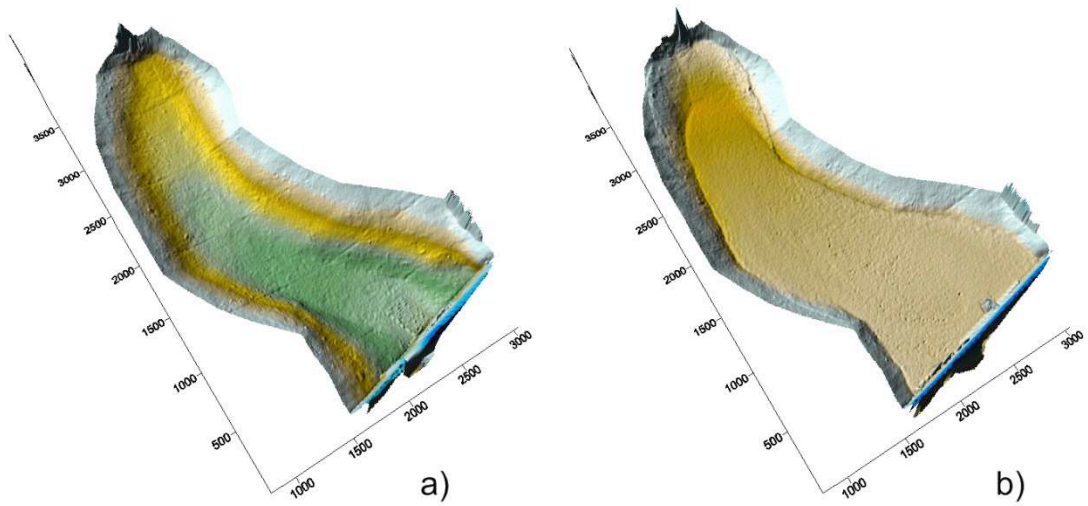

Figure 35. 3D surface for Test 4.1: a) empty model and b) model with the debris deposited used to calculate the retained volume.

Once the computation with Surfer was made, it was possible to calculate an estimate of the passed volume material as a difference between the total volume released and the retained volume. These volume calculations were affected by some approximations: the retained volume obtained with the laser scan did not take into account the percentage of material lost during each test. This lost material percentage was composed by four components: the material deposited on the wood inlet channel (which was inaccessible to the laser scanner), the material deposited on the bucket internal surface, the material which passed through the barrier and the material sprayed out of the model in the released part immediately under the basal lever bucket. As a consequence, this fact introduced an error on the final volume data. Assuming that the material loss was constant on each test, comparisons among the tests were made. As an example of the size of these losses, in Figure 36 the losses occurred during the Test 4.1 are shown.

Figure 36. Losses of the Test 4.1: a) material deposited in the inlet channel, b) material passed through the net, c) material deposited on the bucket internal surface.

Another consideration should be done regarding the volume scans of the tests since some problems were observed concerning the lower part of the model. In this part, a noise due to the presence of the instrumentations (such as connection cables or other materials located out of the model), were registered. These instruments are quite close to the wood panel which closed the section and may introduce a difference between two scans if they present different positions. These differences could lead then to an error on the final volume calculated, because they are computed as an additional volume. The problem can be well understood thinking to the elevation of a certain material inside a box: the upper surface is defined by the level of the material inside the box while the lower surface is defined by the bottom level of the box. If the scans of two boxes present differences in the boxes' shapes, the computation results to find the volume inside the box full of material, are probably wrong. For this reason, these little differences observed in the scans, could introduce an additional error to the measures.

2.6.2 VELOCITIES

Front average velocity values were obtained with the data provided by the laser distance sensors and by the high speed camera. As described above, the laser distance sensors were placed along the model in different positions (Figure 22) from the inlet channel, to the net closed section. Front average velocities were obtained watching the time taken from the debris flow front to travel the known distance between two sensors (which is known for all of them). Figure 37 shows an example of a debris flow depth-time diagram of the Test 1.4 for the laser sensors L2-L1 (which are located in the middle of the model). As Figure 38 shows, the travel time was then obtained from a zoom of the diagram part of interest. The travel times and then the velocities were calculated with the same procedure for all the couples of sensors.

Unlike the laser distance sensors, the high speed camera was placed above the net with the lens which looked at a grid panel specifically installed on the net bottom. This grid panel allowed the identification of the debris flow front position at a certain time. In order to calculate the average velocity close to the net, the software TimeBench (Optronis GmbH, Kehl, Germany) provided by Optronis was used. The software allows to analyze the video recordings of the high speed camera thanks to a function which permits to roll the different frames of the video. A generic front velocity was hence calculated as the ratio between the space traveled by the debris flow front on a grid space of 5 cm (immediately before the net) and the time taken to cover it. As an example, Figure 39 shows two different frames used to calculate the average velocity for the Test 1.4 with TimeBench software.

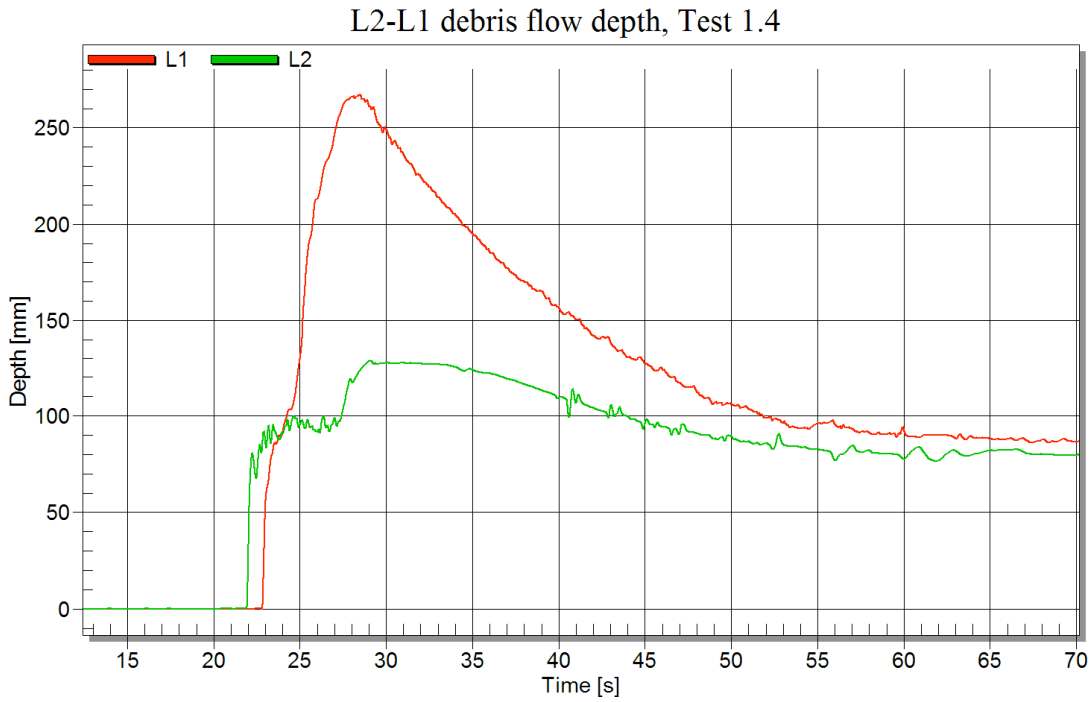

Figure 37. Depth-time diagram for the laser distance sensors L2-L1 provided by Catman software for Test 1.4.

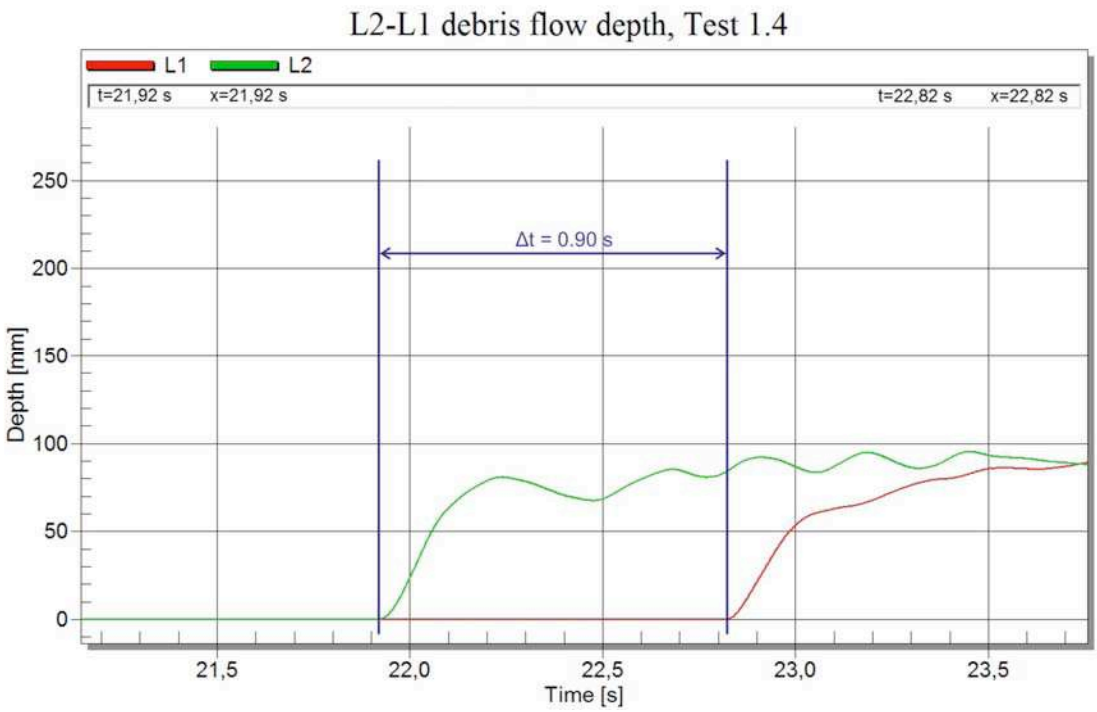

Figure 38. Debris flow travel time calculation for Test 1.4.

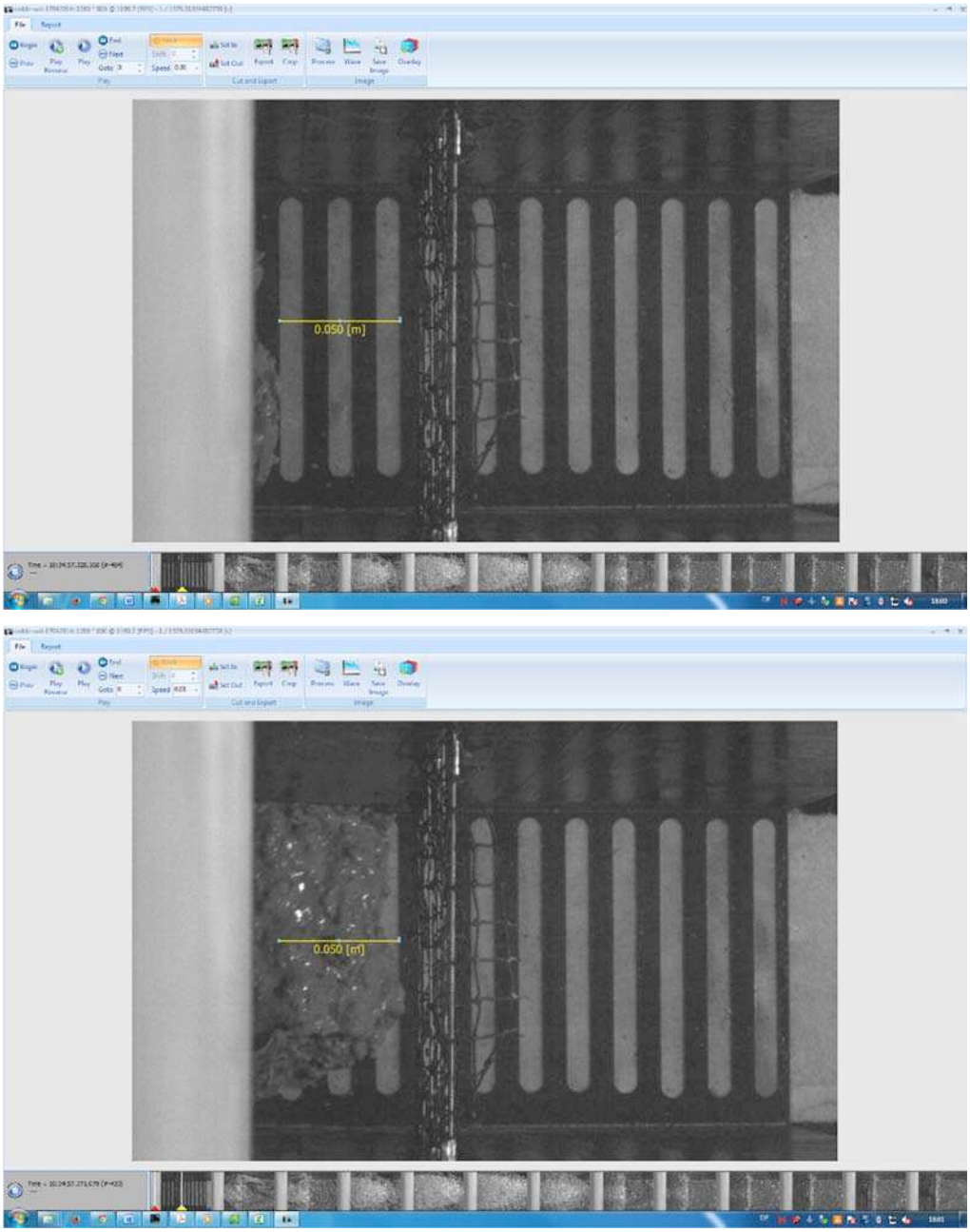

Figure 39. Top views of two different frames from the high speed camera, immediately above the slit net dam section (Test 1.4).

2.6.3 FORCES

Force measures were obtained using the Catman software which allows to acquire and analyze the signals transmitted by the load cells to the amplifier. The forces were sampled with a sample rate of 1200 Hz and then automatically filtered with a Bessel low-pass filter with cutoff frequency of 5 Hz. Each load cell measure was then given in terms of a force-time diagram (Figure 40) which shows the force exerted by the flow on each cable.

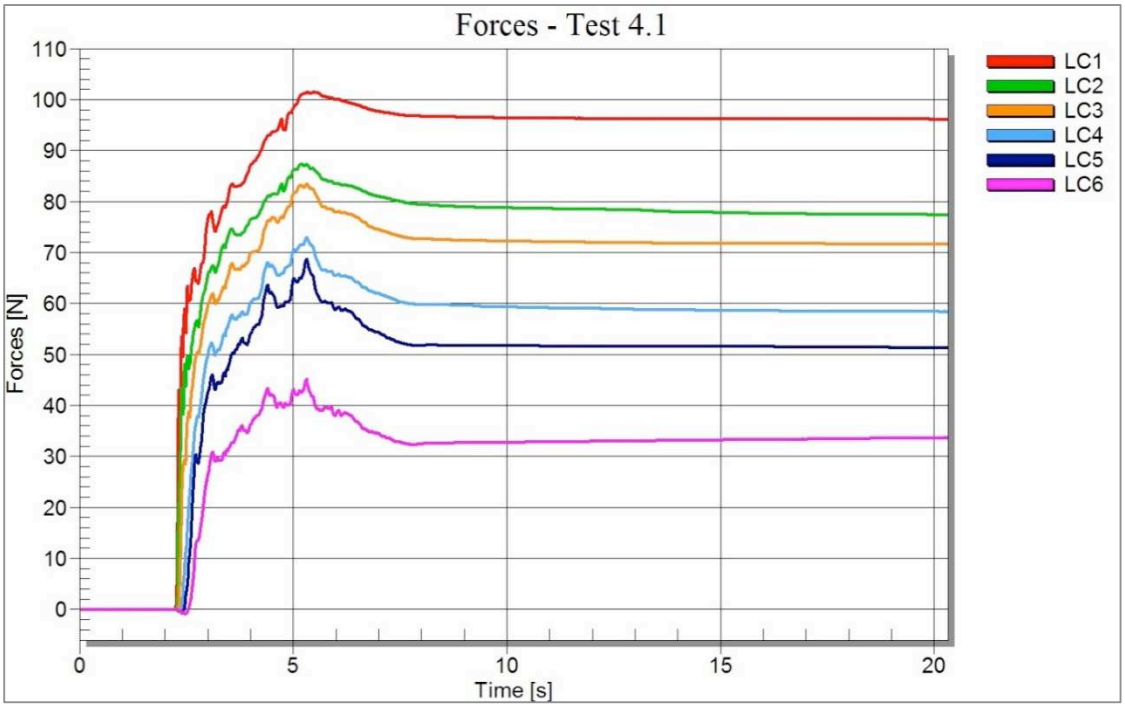

Figure 40. Example of Force-Time diagram provided by the Catman software, for Test 4.1.

The forces measured by the load cells are tensile axial forces, therefore these force values are not the impact (frontal) forces due to the debris flow but the forces which relate with the axis of the cables.

In order to understand the behaviour of the load cells, different known weights were applied at half-way length of the cables and the related loads measured by the load cells were recorded. In total three different tests were done changing, in addition, the pretension of the cables which were equal to 2.5, 5.0 and 10.0 N. The results of the tests are explained by the diagram of Figure 41 where it is possible to note that the points, for the case of the test with 10 N of pretension, show a high coefficient of determination equal to 0.986.

The final pretension which was chosen for the tests was equal to 10.0 N; this value gave a sufficient stiffness for the net system. The pretension was hence applied to the cables prior to each test run.

During the tests some problems were observed in relation to the lamps used to illuminate the slit net dam section. It was in fact observed that, if these lamps illuminate the net (and hence the cable and load system) for too much time, they can influence the load cells measures showing fluctuations on the diagram results. This was due probably to the heat produced by the lamps and this inconvenience was avoided switching on them an instant before the test was run and then switching them off after the flow finished its motion.

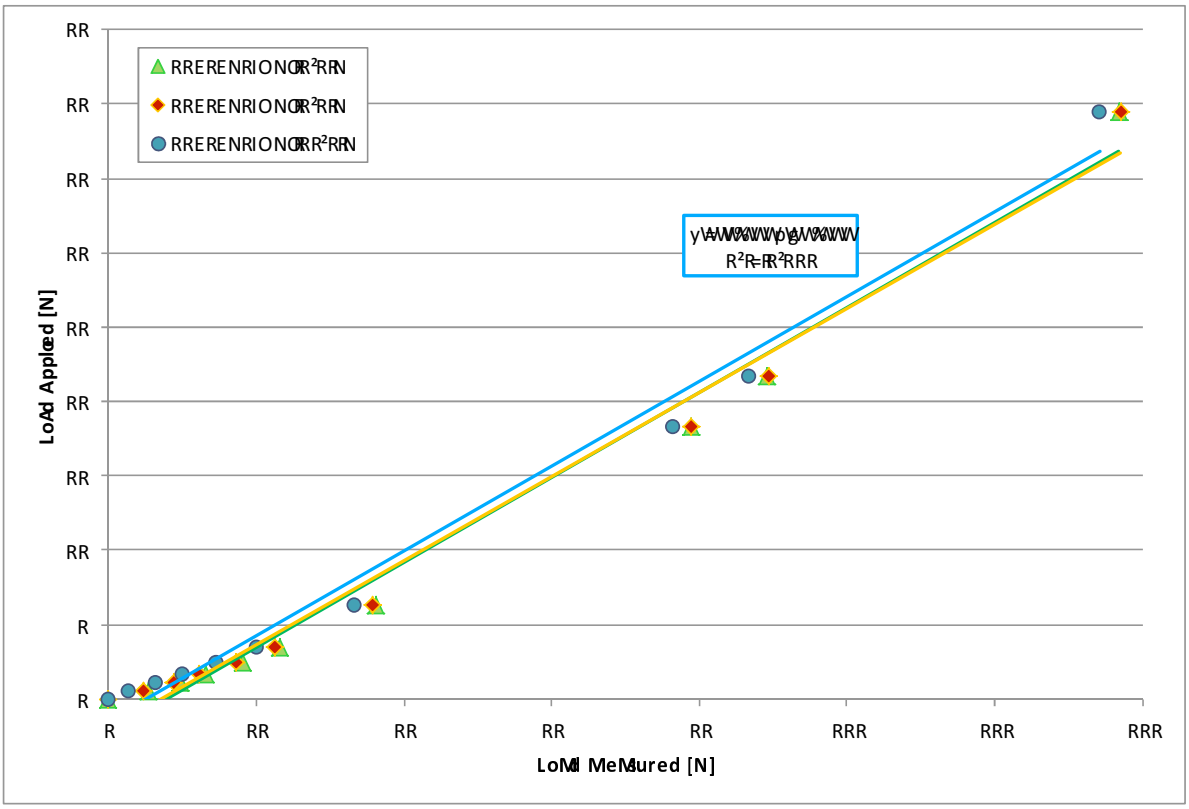

Figure 41. Loads applied and measured with different pretensions.

Cable mechanics

From a mechanical point of view, it was assumed that the debris flow which acts on one cable, loads it with a constant distributed load q_{imp}. This load, which was assumed to act only on the horizontal plane, transmits as a consequence a tensile axial force T along the cable which has an horizontal component H (constant along the x direction, i.e. it is equal for both the cable edges $H_A = H_B$) and a vertical component V (Figure 42). As Brighenti et al. (2013) suggested, if the deformations of the cable are limited (around 10-15% of the cable length), the tensile axial force T can be assumed approximately equal to the horizontal component H along the entire cable. Therefore, the forces measured by the bending beam load cells refer directly to the tensile axial forces, since the deformations observed were limited.

Because no devices to measure impact pressure were arranged, the impact load of the debris flow is not known. An estimation of the impact force F_{imp} was derived from the relation obtained during the pretensioning tests described earlier:

$$F_{imp} \quad 0.286\ T \quad 0.1470 \qquad (14)$$

This force value refers to an ideal concentrated load acting on the middle of the cable. By dividing this force along the entire cable length l, the distributed load q_{imp} applied by the debris flow was calculated:

$$q_{imp} \quad \frac{F_{imp}}{l} \tag{15}$$

Furthermore, it is possible to calculate the value of the tensile axial force in the y direction which is the same for both the edges of the cable:

$$V_A \quad V_B \quad \frac{F_{imp}}{2} \quad \frac{q_{imp}\, l}{2} \tag{16}$$

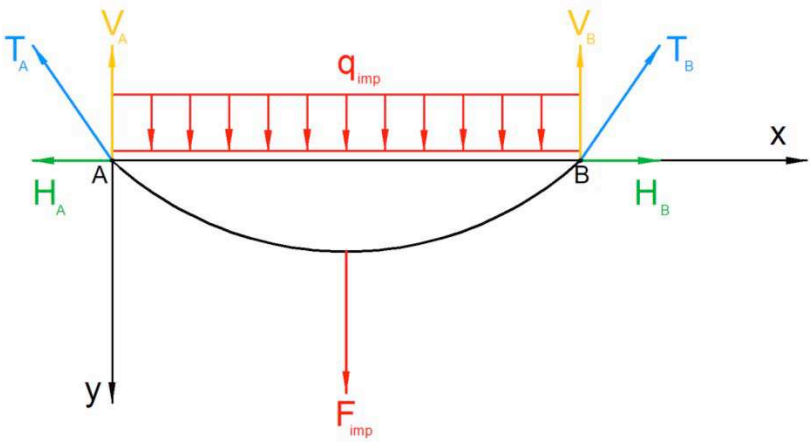

Figure 42. Scheme of the forces acting on a cable of the slit net dam.

It should be noted that these considerations do not take into account the real-scale deformations of the cables. In the real cases, the cables are subjected by complex deformations, since the forces act on different planes (not only along the horizontal plane as assumed herein). Furthermore, in the real net barriers dissipation elements (ring brake system) are usually provided, in order to reduce the tensions in the cables. Therefore, the force values obtained from the experimental tests of this thesis, are probably valid only for qualitative conclusions. Even though with these approximations, the forces from the model to the prototype were however scaled, according to the theory illustrated in Chapter 1.3.3.

3 EXPERIMENTAL RESULTS

In this chapter a summary of the results obtained from the experimental tests, with the methods described in Chapter 3 are presented. The results shown herein are grouped according to the five different basal openings tested.

3.1 TYPE 1 TESTS (basal opening of 8.7 cm)

The first series of experiments was carried out with a basal opening of 8.7 cm, which corresponds to 261 cm in the prototype. As expected, the debris flow passed through the basal opening in each of the four runs and the net actually influenced the debris flow motion. Analyzing the video footage it is possible to recognize five main sequences: first the debris flow which comes from the inlet channel reaches the barrier section and starts to pass through the basal opening (Figure 43a), then the level increases and the net starts to stop the debris flow (Figure 43b), afterward the flow reaches the net top and starts to overflow (Figure 43c and 43d). Finally, when the material released from the bucket finishes, the level behind the net starts to decrease with a successive stop of the overflow and the material passing through the net (Figure 43e and 43f).

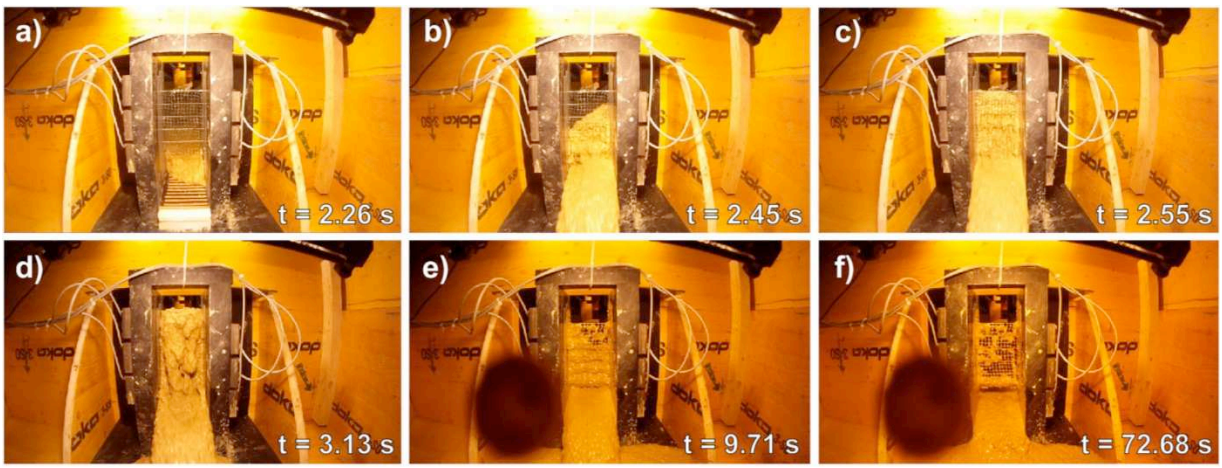

Figure 43. Debris flow sequences observations for Test 1.3: a) debris flow reaches the net section, b) level increases behind the net, c) level reaches the top of the net, d) overflow phase, e) level decreases, f) end of the test with stationary flow.

Table 11 summarizes the volume data and the water contents of the mixture, obtained according to the methods described in Chapter 2.6.1. As the results show, with a basal

opening of 8.7 cm most of the material passed the barrier, even though a not negligible percentage was permanently retained and deposited behind it (mean value of 28.44%).

Table 11. Volume data and water contents of the debris flow mixture for type 1 tests.

Run	Released material	Retained material		Passed or lost material		Water content by weight
	[m^3]	[m^3]	[%]	[m^3]	[%]	[%]
1.1	0.466	0.144	30.94	0.322	69.06	21.66
1.2	0.473	0.133	28.20	0.340	71.80	22.08
1.3	0.466	0.125	26.84	0.341	73.16	21.73
1.4	0.458	0.127	27.80	0.331	72.20	21.52
mean	0.466	0.132	28.44	0.333	71.56	21.75
± SD	0.006	0.009	1.76	0.009	1.76	0.24

Four debris flow average front velocities were calculated from the laser distance sensors and the high speed camera according to the methods described in Chapter 2.6.2. Table 12 shows these velocity values which are termed according to the positions of the measurement devices: inlet velocity v_{inl} from lasers L5-L4, middle model velocity v_{mid} from lasers L2-L1, end model velocity v_{end} from lasers L1-L3 and high speed camera velocity v_{HSC}.

Table 12. Debris flow average front velocities for type 1 tests.

Run	v_{inl}	v_{mid}	v_{end}	v_{HSC}
	[m/s]	[m/s]	[m/s]	[m/s]
1.1	2.35	0.82	1.71	0.92
1.2	2.96	1.11	2.29	1.25
1.3	2.86	1.09	1.66	1.15
1.4	2.76	1.11	2.02	1.18
mean	2.73	1.03	1.92	1.13
± SD	0.27	0.14	0.30	0.14

As the results show, there is a clear trend that the average velocities change their magnitude along the model, in particular it is possible to note that the highest values occurred in the inlet channel (i.e. just after the release) while the lower values occurred in the middle of the model. Moreover, after that point the debris flow increases again its velocity and then decreases one more time when it reaches the barrier section. This change of velocities can be

attributed to the variation of slope and geometry along the model. A graphic representation is shown in Figure 44, where the average front velocities trends along the model axis can be easily observed.

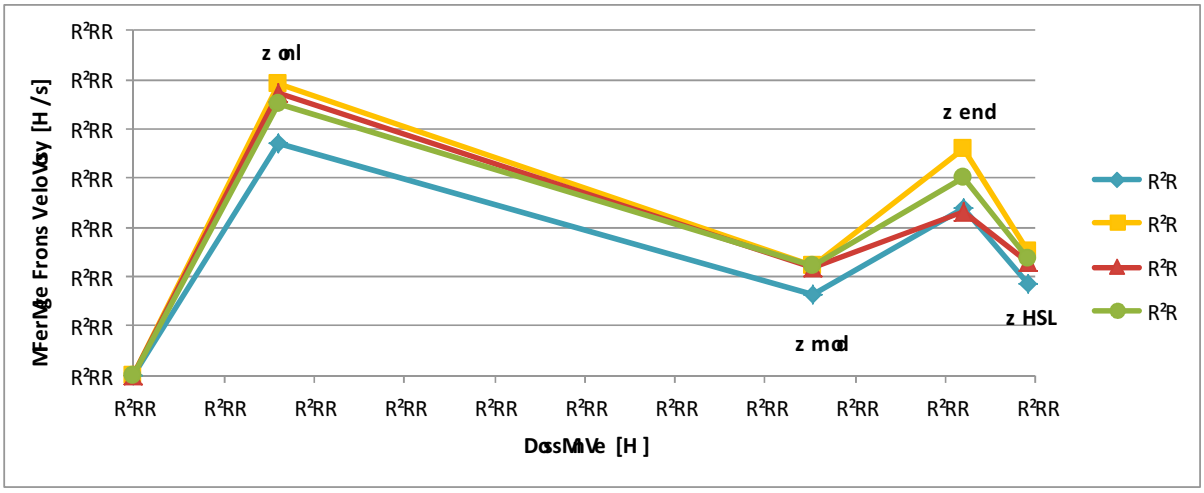

Figure 44. Average front velocities along the model for type 1 tests.

The last parameter of interest which was analyzed is represented by the maximum tensile axial forces exerted by the debris flow on the cables, measured by the load cells and later recorded by the Catman software (as described in Chapter 2.6.3). In this study only the peak force values were considered, since they represent the most important condition for designing the net system. Table 13 summarizes all the measurements obtained from the load cells, according to their layout shown in Figure 45.

Table 13. Maximum tensile axial forces from the load cells measurements for type 1 tests.

Run	LC1 [N]	LC2 [N]	LC3 [N]	LC4 [N]	LC5 [N]	LC6 [N]
1.1	35.86	53.23	44.12	34.36	23.65	12.34
1.2	41.94	69.81	55.61	43.45	33.73	19.45
1.3	56.21	73.14	61.82	49.27	38.53	20.71
1.4	56.31	79.62	64.19	58.00	39.96	29.21
mean	47.58	68.95	56.44	46.27	33.97	20.43
± SD	10.33	11.24	8.97	9.94	7.38	6.92

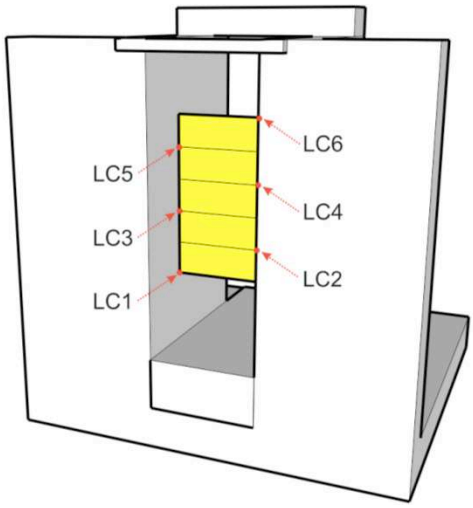

Figure 45. Layout of the load cells, indicated with their respective cell number.

A representation of the data is shown in Figure 46, where the maximum forces are related to the net height. For this series of experiments, we find that the highest force values occur on the second cell starting from the bottom (i.e. LC2). The other forces measured are smaller and decrease in descending order from cell 2 to cell 6.

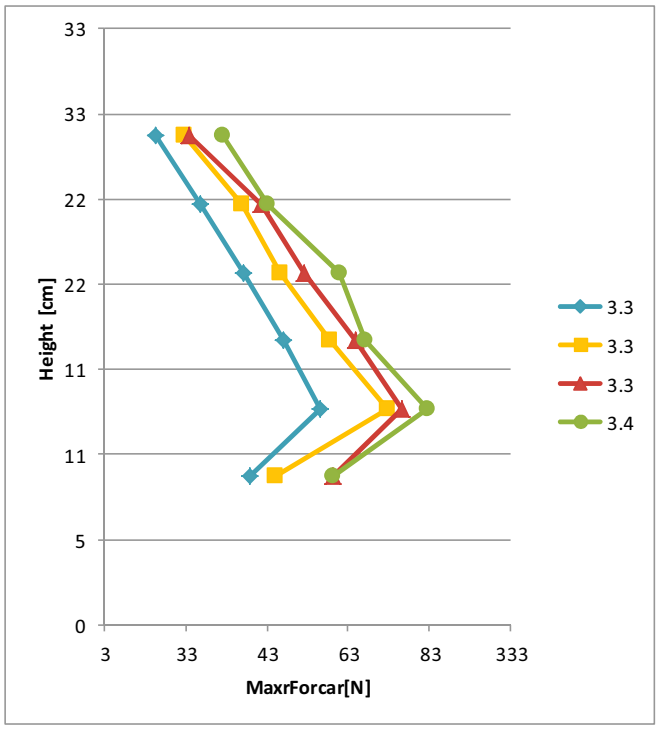

Figure 46. Tensile axial forces along the barrier height for type 1 tests.

A detailed time series of forces measured by the load cells are also shown in Figure 47 for the four experiments of type 1 tests. As it is possible to note from the charts, the force

trends show a fast rise and then a decrease until a final constant value. The results of this latter are sometimes not zero, even though the debris flow had already flowed and stopped. This fact can be explained by the observation that some material was deposited in the net (and also on the cables) thus causing a non-null value on the load cell measures (Figure 48).

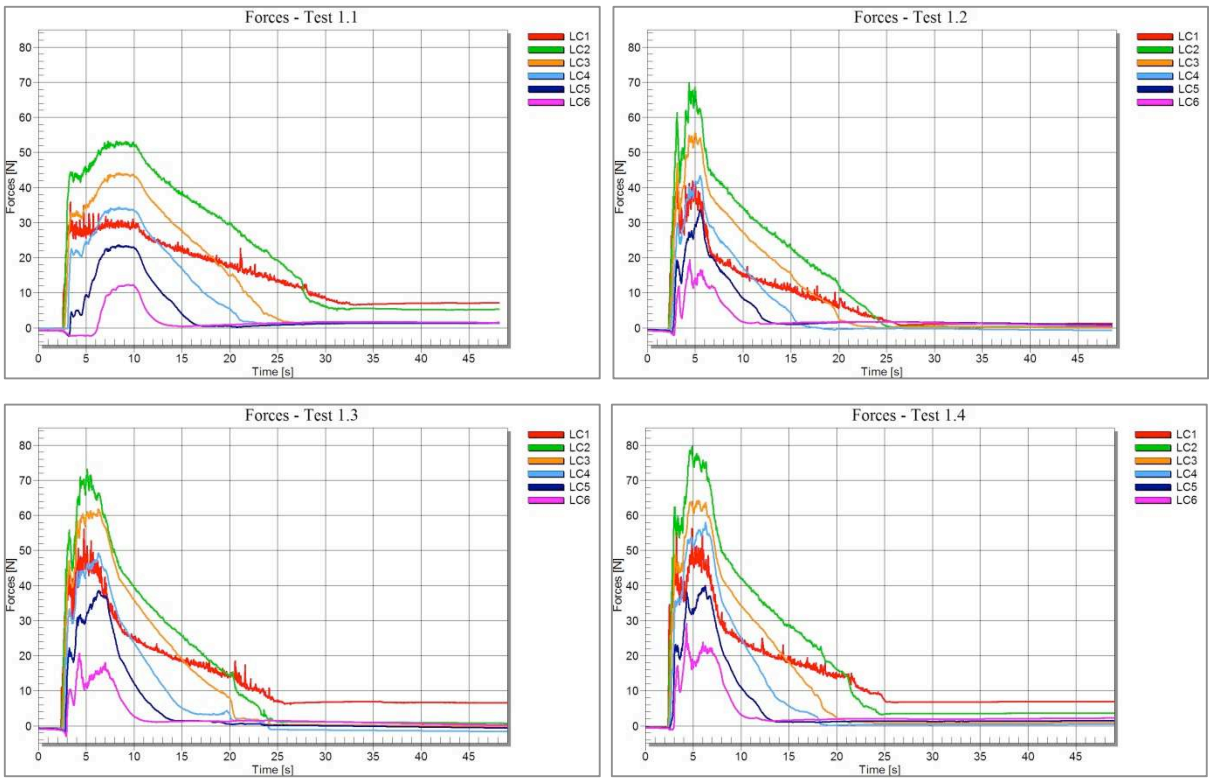

Figure 47. Force vs time charts for type 1 tests.

Figure 48. Example of material deposited on the net and on the cables at the end of the Test 1.1.

3.2 TYPE 2 TESTS (basal opening of 6.0 cm)

For the second series of experiments the basal opening was reduced to 6.0 cm (180 cm in the prototype scale). In order to understand the role of the net height, the last test (2.4) was carried out with an additional net on the top (which was 9 cm high). This expedient was originally thought in order to avoid the overflow phenomena which were observed during the previous experiments. As a result of the installation, Test 2.4 shows a positive results since no material overflowed the top of the additional net.

In terms of material retention also during these series, the debris flow passed through the basal opening, showing a behaviour similar to the type 1 tests. The volume data measured are summarized in Table 14.

Table 14. Volume data and water contents of the debris flow mixture for type 2 tests.

Run	Released material	Retained material		Passed or lost material		Water content by weight
	[m^3]	[m^3]	[%]	[m^3]	[%]	[%]
2.1	0.450	0.123	27.43	0.327	72.58	20.97
2.2	0.450	0.117	26.01	0.333	73.99	20.94
2.3	0.450	0.115	25.63	0.335	74.37	22.09
2.4	0.427	0.123	28.81	0.304	71.19	22.92
mean	0.444	0.120	26.97	0.325	73.03	21.73
± SD	0.012	0.004	1.45	0.014	1.45	0.96

Table 15. Debris flow average front velocities for type 2 tests.

Run	v_{inl}	v_{mid}	v_{end}	v_{HSC}
	[m/s]	[m/s]	[m/s]	[m/s]
2.1	2.79	1.04	2.02	1.33
2.2	2.67	1.10	1.90	1.20
2.3	2.67	1.00	1.75	1.15
2.4	2.58	0.96	2.08	0.97
mean	2.68	1.02	1.94	1.16
± SD	0.09	0.06	0.14	0.15

Also for this series it is possible to note that the average front velocities present the same trend described for the type 1 tests: lower values on the middle of the model and just before

the net section and higher values on the inlet channel and on the end of the model (Table 15 and Figure 49).

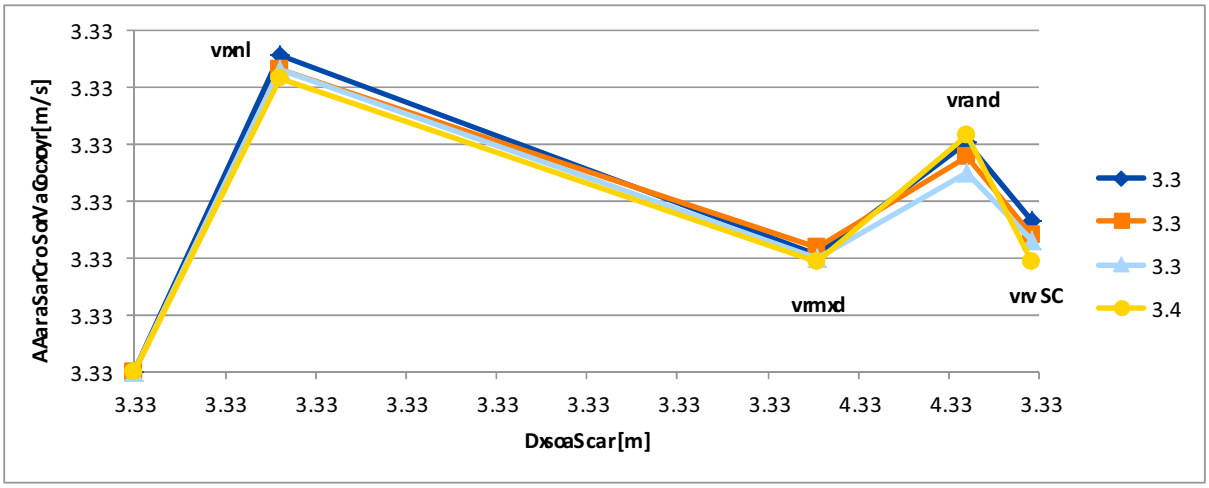

Figure 49. Average front velocities along the model for type 2 tests.

In terms of tensile axial forces the four tests present similar values and trends (Figure 50 and Table 16), with the exception of Test 2.3 which shows lower force values for all the cells and a maximum value for the higher cell (LC6). This could be due to larger particle size of the debris flow mixture, which caused an increase of the measured force as a result of their impact.

Table 16. Maximum tensile axial forces from the load cells measurements for type 2 tests.

Run	LC1 [N]	LC2 [N]	LC3 [N]	LC4 [N]	LC5 [N]	LC6 [N]
2.1	59.74	85.20	75.91	63.78	51.82	26.61
2.2	67.69	83.25	82.87	58.30	50.04	24.31
2.3	51.09	61.98	57.61	47.07	38.78	34.84
2.4	61.29	84.68	79.17	65.06	53.50	32.39
mean	59.95	78.78	73.89	58.55	48.54	29.54
± SD	6.84	11.23	11.22	8.20	6.66	4.90

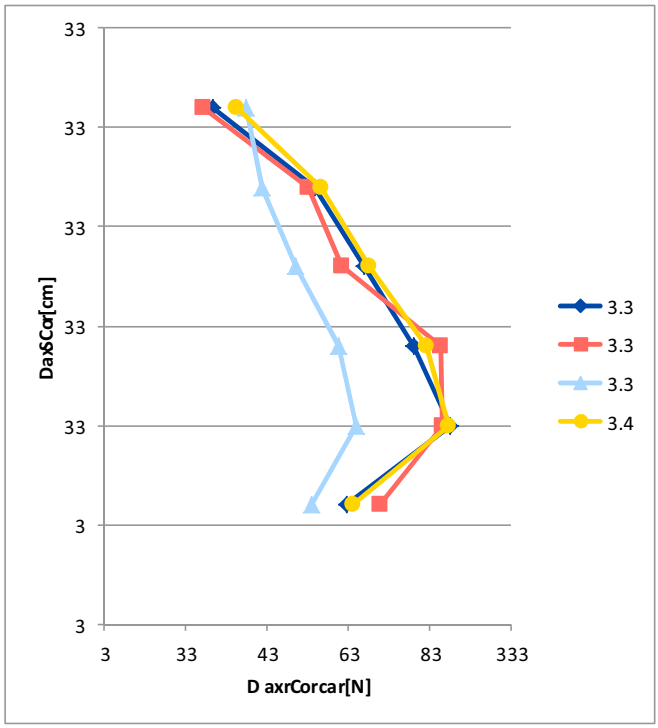

Figure 50. Tensile axial forces along the barrier height for type 2 tests.

Finally, in Figure 51 force vs time charts are shown, where a similar trend already observed for type 1 tests can be noted.

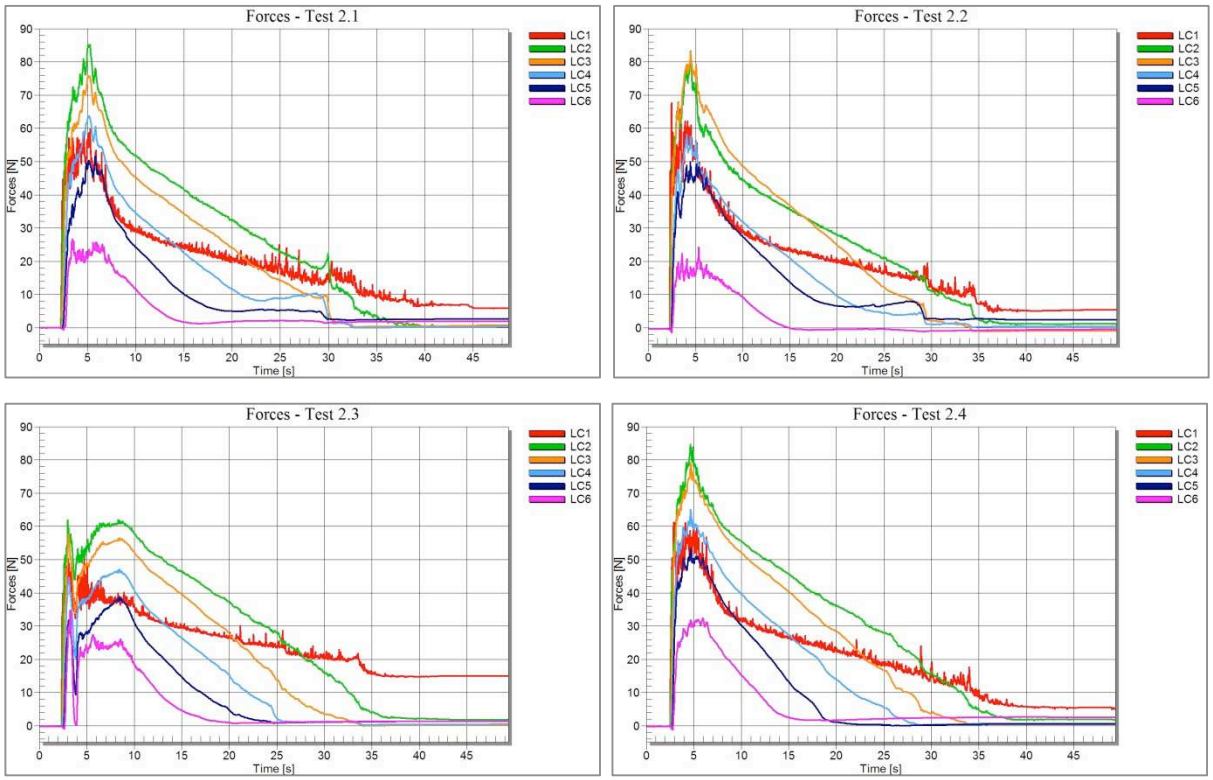

Figure 51. Force vs time charts for type 2 tests.

3.3 TYPE 3 TESTS (basal opening of 4.5 cm)

Type 3 tests were carried out with a basal opening of 4.5 cm, corresponding to 135 cm in the prototype. The first three tests presented had a net element height of 20 cm (net type D), while the fourth test had an additional net on the upper part with a total height of 29 cm (net type E). Unlike the previous tests, for this series the debris flow began to be retained. Tests 3.1, 3.2 and 3.4 showed high percentages of retention, while Test 3.3 allowed the passage of the flow under the basal opening, with a percentage of retention substantially minor. This may be explained by the water content measured from the test samples (Figure 52): for Test 3.3, the water content shows a value of 26.36%, higher than the other three tests. This fact highlights the importance of the water content for the barrier retention capacity, suggesting that the greater the water content (mixture therefore more fluid) the greater the quantity of material that passes through the barrier.

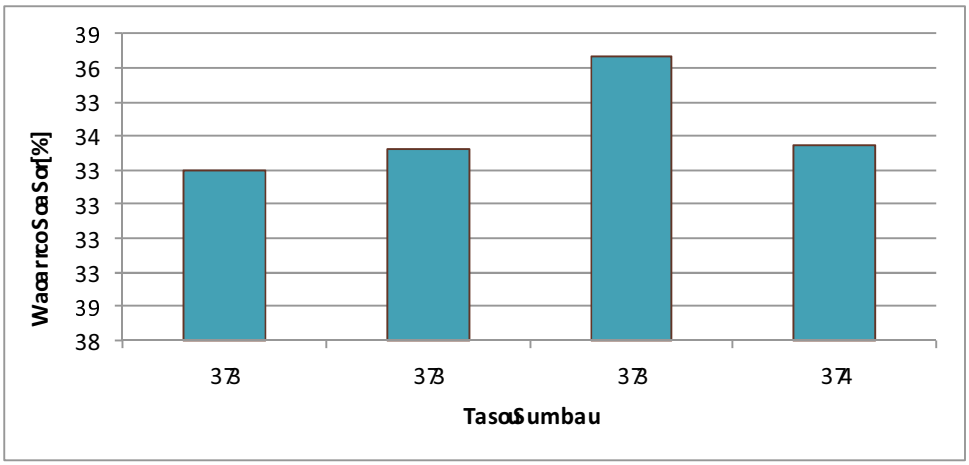

Figure 52. Water content values for type 3 tests.

Test 3.1 and 3.2 show similar retained volumes (Table 17), with a high value of retention (around 80% of the entire volume released). Test 3.3 allowed the passage of the debris flow and, for this reason, presents a limited percentage of material retained (31.19%). Finally, due to the additional net, Test 3.4 presents the higher percentage of retained material (92.71%). Tests 3.1 and 3.2 showed a similar overflow phase, whereas Test 3.3 showed a minor overflow (due to the passage of the flow under the net) and Test 3.4, having an additional net, showed the smallest overflow (see also Chapter 4.1 where overflow phenomena are described in terms of duration). A qualitative overview of the barriers after the test runs is shown in Figure 53 where their different retention capacities are clearly visible.

Table 17. Volume data and water contents of the debris flow mixture for type 3 tests.

Run	Released material	Retained material		Passed or lost material		Water content by weight
	[m^3]	[m^3]	[%]	[m^3]	[%]	[%]
3.1	0.404	0.322	79.61	0.082	20.39	23.01
3.2	0.404	0.323	79.92	0.081	20.08	23.62
3.3	0.404	0.126	31.19	0.278	68.81	26.36
3.4	0.400	0.371	92.71	0.029	7.30	23.75
mean	0.403	0.285	70.86	0.118	29.14	24.18
± SD	0.002	0.109	27.14	0.110	27.14	1.49

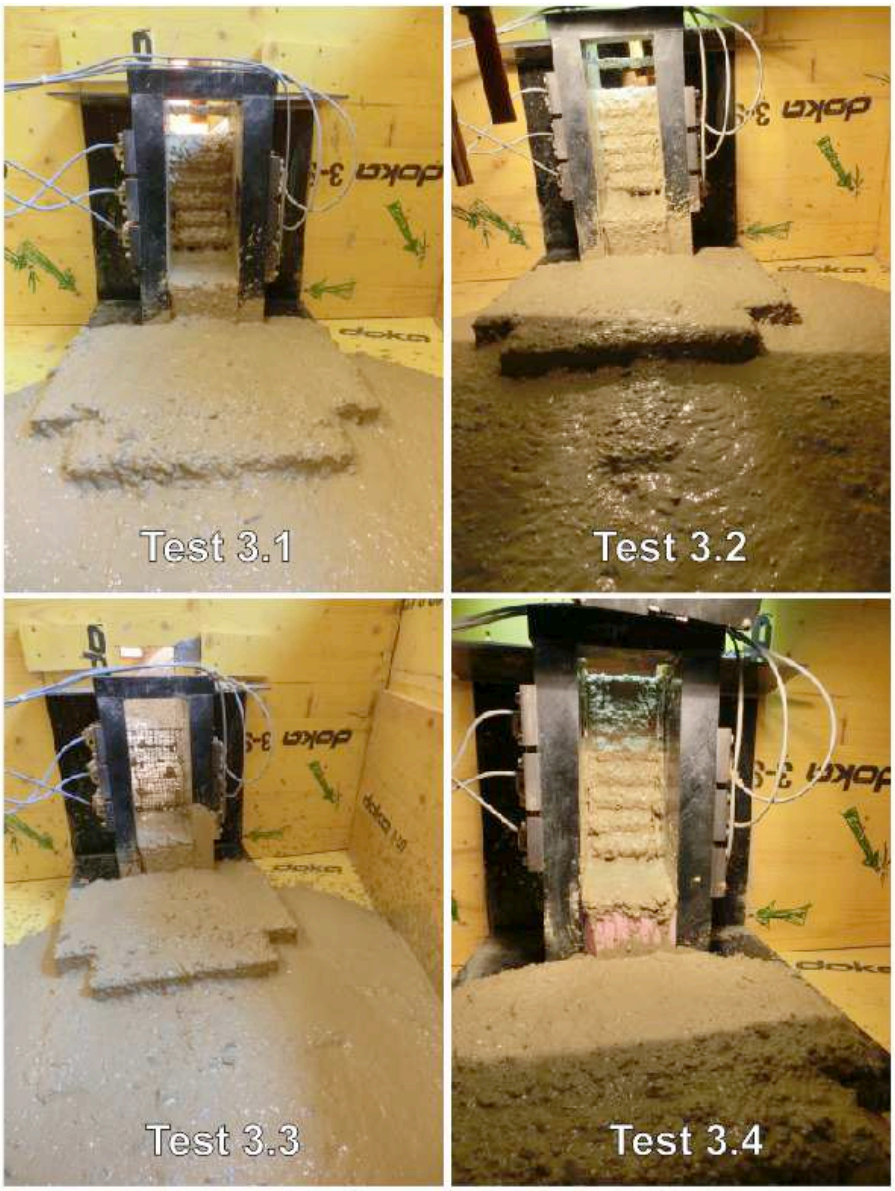

Figure 53. Barriers overviews at the end of type 3 tests.

For these test series a great variability appears in the inlet velocities (Figure 54 and Table 18). This may be an artefact due to problems while releasing the mixture from the tank: when the bucket basal lever was lifted, the first material which left the tank presented a compacted shape as though a sort of stopper was formed on the bucket's bottom. This little mass of material came out very slowly in a first moment and was then followed by the rest of the mixture which came out with the same traits usually observed in the past tests.

Table 18. Debris flow average front velocities for type 3 tests.

Run	V_{inl} [m/s]	V_{mid} [m/s]	V_{end} [m/s]	V_{HSC} [m/s]
3.1	1.57	0.88	1.11	0.69
3.2	2.00	0.77	1.45	1.30
3.3	1.31	0.79	1.66	1.18
3.4	2.22	0.92	1.11	0.98
mean	1.78	0.84	1.33	1.04
± SD	0.41	0.07	0.27	0.27

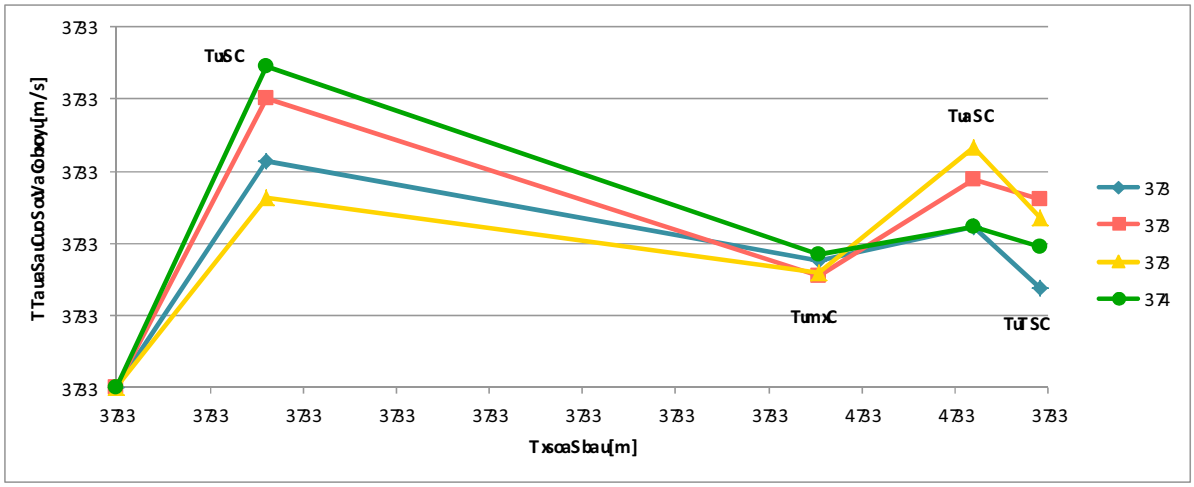

Figure 54. Average front velocities along the model for type 3 tests.

Unlike the previous type 1 and type 2 tests, this test series presents the highest force values at the first load cell (LC1) - and not instead at the second cell LC2 - for three of the four tests run (Figure 55 and Table 19). This fact leads to speculate that the presence of big particles on the debris flow front could influence the measures because of their impacts.

The material deposited behind the barrier permanently exerts a final constant force value which is minor compared to the peak force, but great enough to be considered as significant (Table 20, Figure 55 and Figure 56).

Table 19. Maximum tensile axial forces from the load cells measurements for type 3 tests.

Run	LC1 [N]	LC2 [N]	LC3 [N]	LC4 [N]	LC5 [N]	LC6 [N]
3.1	118.17	85.97	71.24	65.57	56.70	38.08
3.2	92.79	90.27	73.61	59.87	52.97	32.58
3.3	84.20	90.81	69.90	55.79	47.20	31.77
3.4	109.88	84.25	80.20	69.74	64.72	43.68
mean	101.26	87.83	73.74	62.74	55.40	36.53
± SD	15.52	3.22	4.57	6.15	7.34	5.53

Table 20. Final constant tensile axial forces from the load cells measurements for type 3 tests.

Run	LC1 [N]	LC2 [N]	LC3 [N]	LC4 [N]	LC5 [N]	LC6 [N]
3.1	86.51	63.66	53.17	42.78	30.89	17.28
3.2	70.16	63.96	58.63	39.68	32.5	13.33
3.3	1.48	0.48	0.26	0.04	0.41	0.00
3.4	101.32	75.74	67.96	53.26	45.28	27.7
mean	64.87	50.96	45.01	33.94	27.27	14.58
± SD	44.13	34.12	30.45	23.33	19.03	11.45

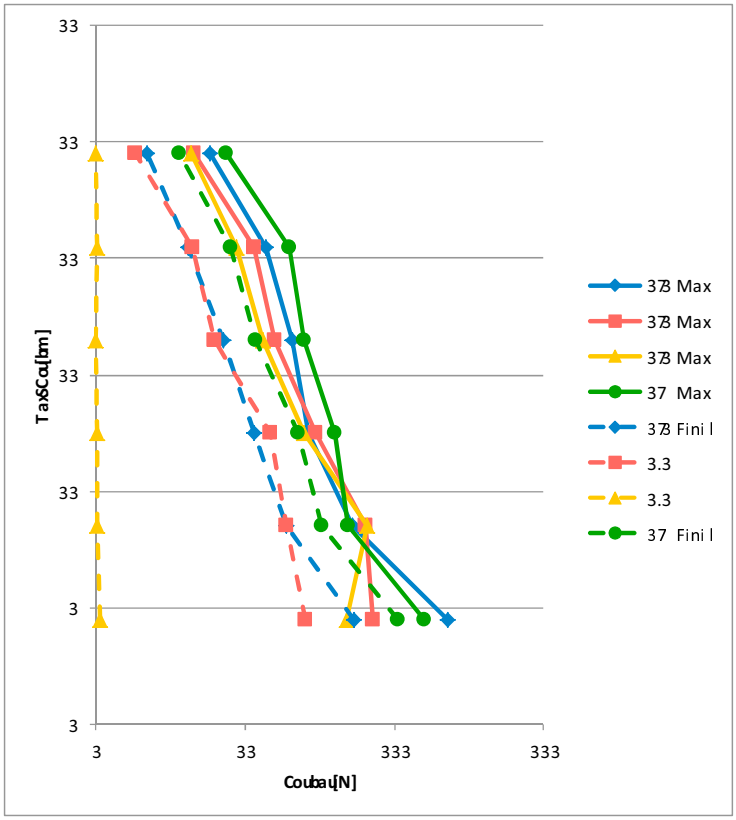

Figure 55. Tensile axial forces along the barrier height for type 3 tests: maximum and final values (shown respectively with continuous and dashed lines).

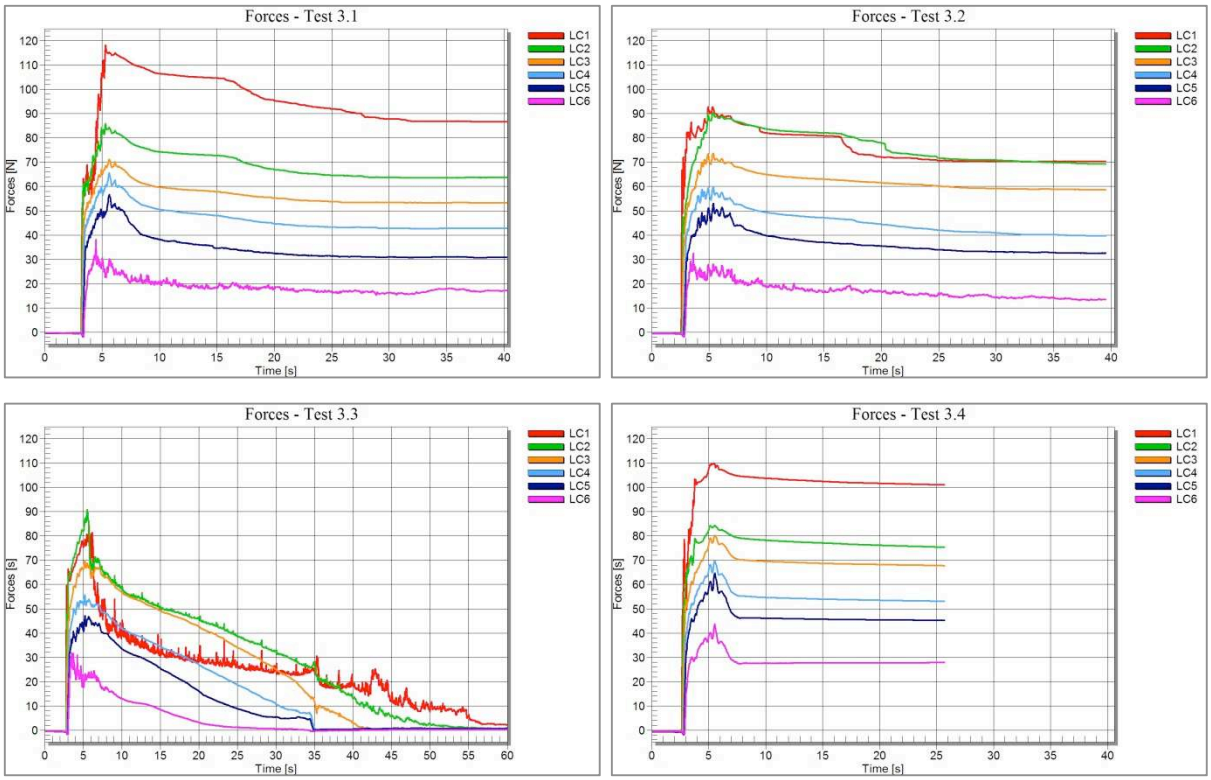

Figure 56. Force vs time charts for type 3 tests.

3.4 TYPE 4 TESTS (basal opening of 3.3 cm)

The three type 4 tests were run with a basal opening of 3.3 cm, corresponding to 100 cm in the prototype. All the barriers used had a net element height of 29 cm (i.e. with the presence of the additional net on the top) but with the difference that Test 4.2 and 4.3 were run with the presence of a plexiglass plate on their top (Figure 57). This expedient was adopted to investigate the influence of an ideal infinite net height. As a consequence, the material which passed through the barrier was due only to the basal opening (before it was occluded) and not to the overflow phenomena. This artifice obviously is not representative of the reality, but gives useful information to study the retained volumes entity. It is important to note that since the plexiglass plate acts like an additional barrier, it influences the flow in a different way in comparison with the previous tests. In terms of results, problems could occur only with the force measures, since velocities were measured before the debris flows reached the plexiglass plate and since volumes were not related with this problem.

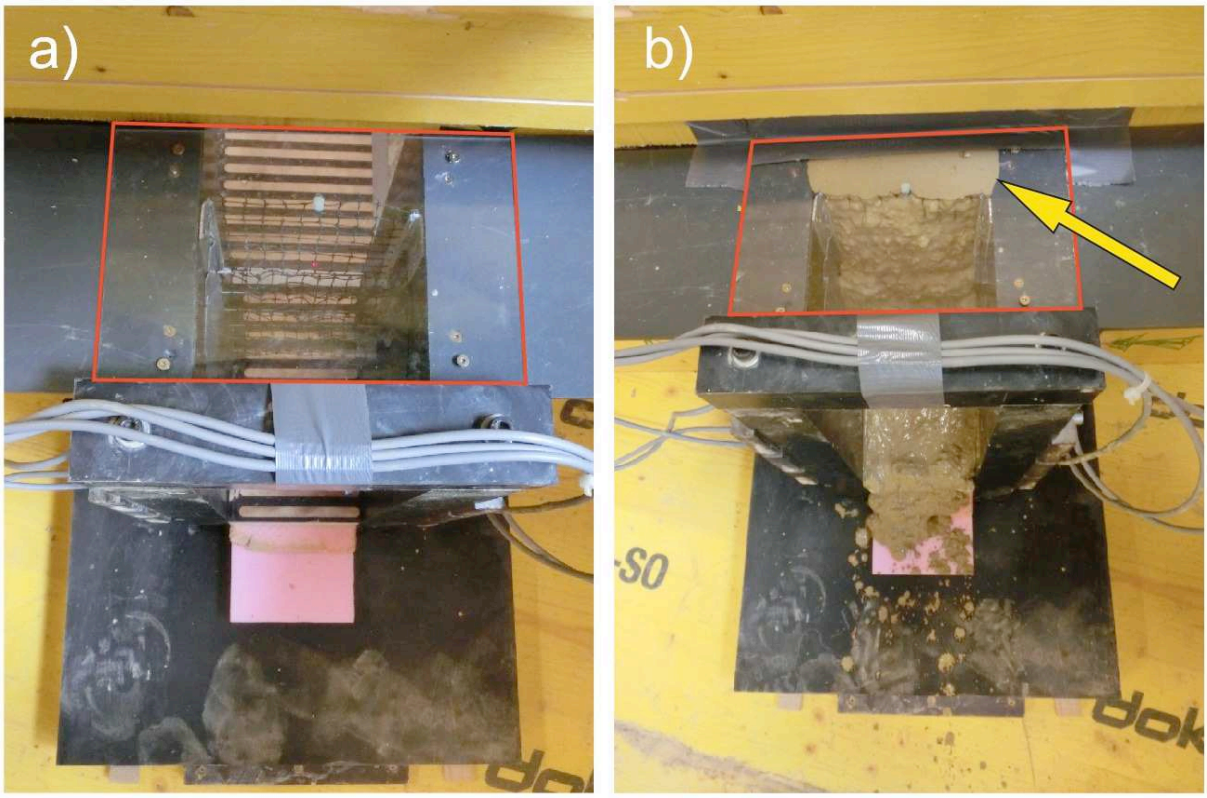

Figure 57. Particular of the barrier used in Test 4.2: a) barrier before the debris flow release (the plexiglass plate is highlighted with a red square), b) barrier at the end of the test, with the debris flow which filled the total net height (yellow arrow).

Generally all the tests with this slit net dam type had a high retention capacity (Table 21). Test 4.1 shows a highest percentage of material passed with respect to the other ones because of the lack of the plexiglass plate which did not avoid the overflow. Therefore, for this first test, the material which passed the barrier is due to the small percentages of the volumes which passed through the basal opening and more material that overflowed the top of the additional net. Tests 4.2 and 4.3 showed similar retained values; the existing differences on the results can be due to the possible losses which were observed during the tests (Chapter 2.6.1). A qualitative overview of the material passed over the barrier is shown in Figure 58.

Table 21. Volume data and water contents of the debris flow mixture for type 4 tests.

Run	Released material	Retained material		Passed or lost material		Water content by weight
	[m^3]	[m^3]	[%]	[m^3]	[%]	[%]
4.1	0.442	0.401	90.58	0.042	9.42	24.13
4.2	0.404	0.386	95.54	0.018	4.47	22.52
4.3	0.404	0.383	94.90	0.021	5.10	23.49
mean	0.417	0.390	93.67	0.118	6.33	23.38
± SD	0.022	0.009	2.70	0.110	2.70	2.49

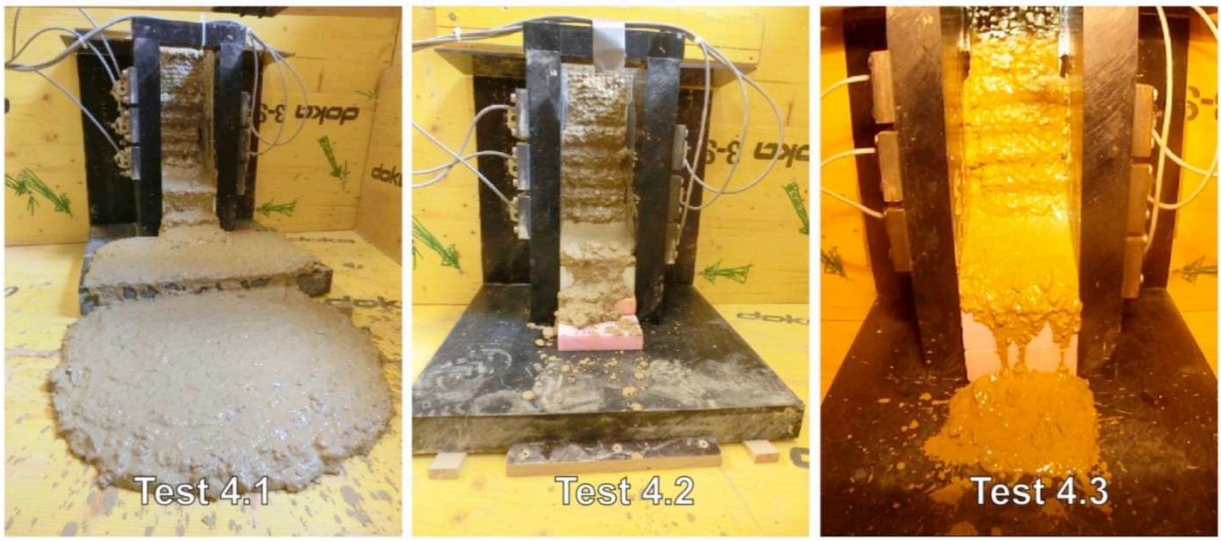

Figure 58. Overview of the passed material for type 4 tests.

Also for this series of tests, it is possible to note a major variability for the inlet channel velocities (Table 22 and Figure 59).

Table 22. Debris flow average front velocities for type 4 tests.

Run	V_{inl} [m/s]	V_{mid} [m/s]	V_{end} [m/s]	V_{HSC} [m/s]
4.1	2.50	1.09	1.55	1.28
4.2	2.76	1.04	1.41	1.18
4.3	1.90	1.04	1.25	1.01
mean	2.39	1.06	1.405	1.15
± SD	0.44	0.03	0.15	0.14

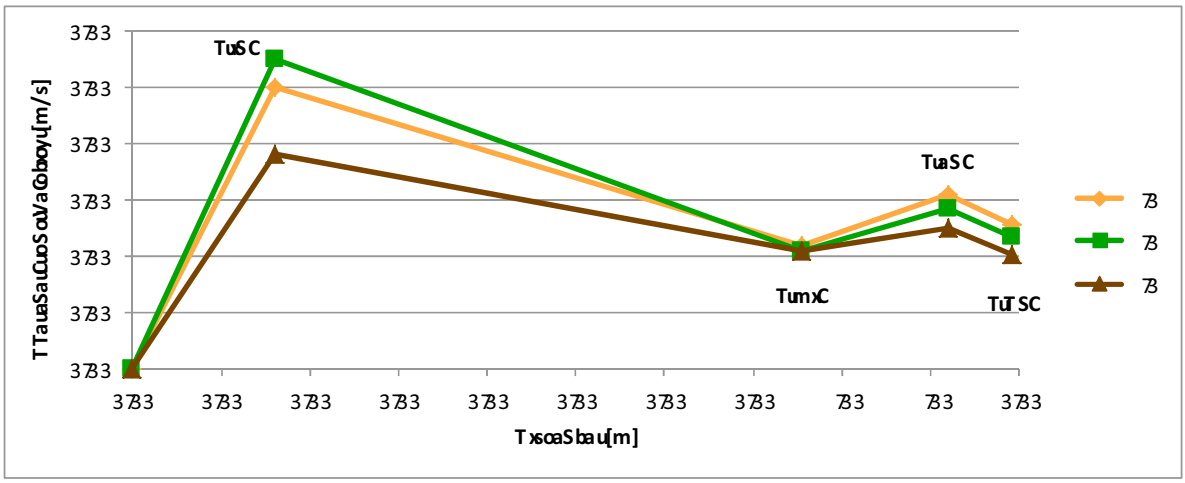

Figure 59. Average front velocities along the model for type 4 tests.

Even though the presence of the plexiglass plate during Tests 4.2 and 4.3 may have influenced the debris flow in a different way, tensile axial forces were however measured and collected (Table 23 and Table 24). Observing the results for the Test 4.1, run with a barrier which had not the plexiglass plate, it is possible to note that the force trends (Figure 60 and Figure 61) are similar to the ones observed for the Tests 4.2 and 4.3 (which had the plexiglass plate). This suggests that the results obtained may give however valid values.

Table 23. Maximum tensile axial forces from the load cells measurements for type 4 tests.

Run	LC1 [N]	LC2 [N]	LC3 [N]	LC4 [N]	LC5 [N]	LC6 [N]
4.1	101.43	87.24	83.41	72.93	68.72	45.17
4.2	83.78	95.19	79.89	73.58	69.14	49.79
4.3	84.77	85.15	70.79	69.31	64.95	43.23
mean	89.99	89.19	78.03	71.94	67.60	46.06
± SD	9.92	5.30	6.51	2.30	2.31	3.37

Table 24. Final constant tensile axial forces from the load cells measurements for type 4 tests.

Run	LC1 [N]	LC2 [N]	LC3 [N]	LC4 [N]	LC5 [N]	LC6 [N]
4.1	96.09	77.24	71.54	58.07	51.13	33.83
4.2	72.88	85.82	66.92	58.10	49.65	32.87
4.3	74.19	77.46	60.06	56.74	49.81	29.65
mean	81.05	80.17	66.17	57.64	50.20	32.12
± SD	13.04	4.89	5.78	0.78	0.81	2.19

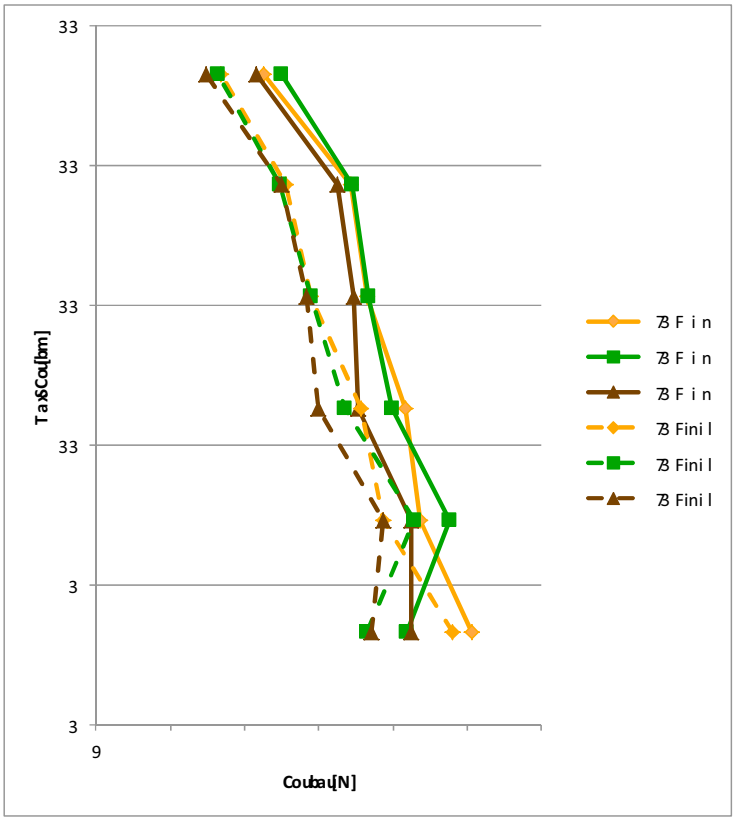

Figure 60. Tensile axial forces along the barrier height for type 4 tests: maximum and final values (shown respectively with continuous and dashed lines).

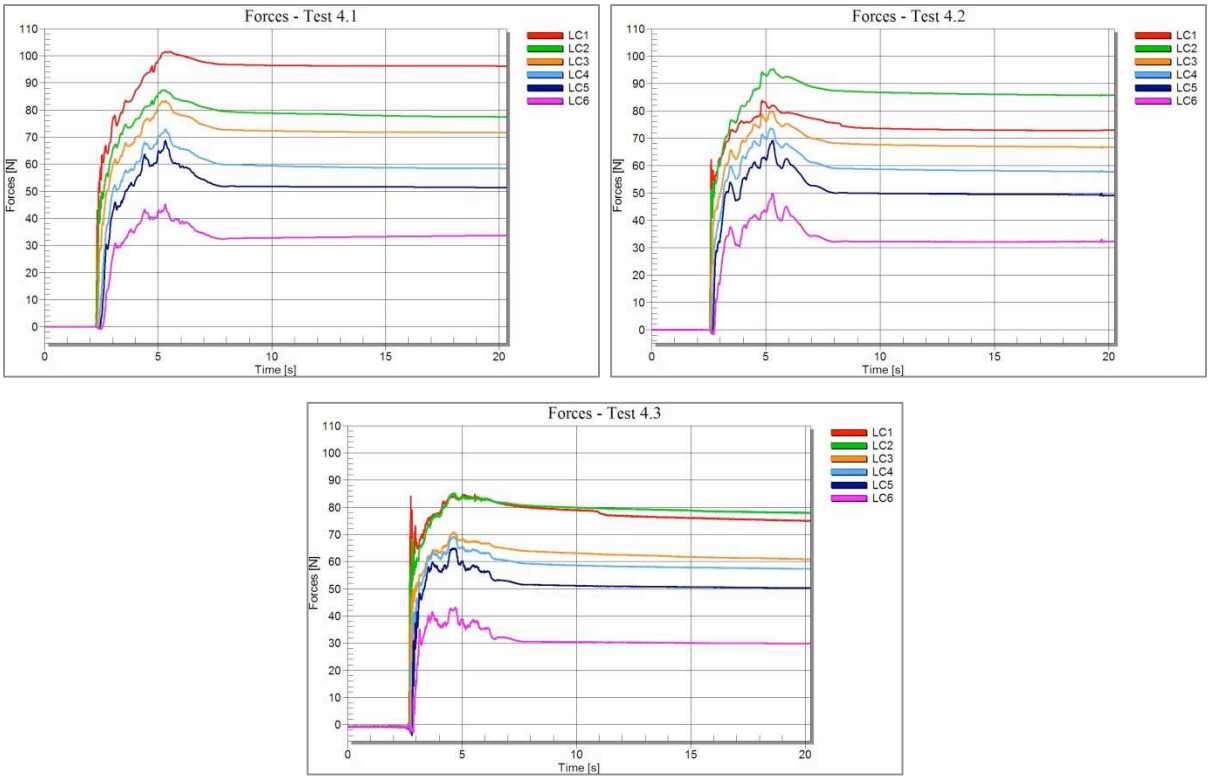

Figure 61. Force vs time charts for type 4 tests.

3.5 TYPE 5 TEST (no basal opening)

To test the retention efficiency of a slit net dam completely closed on its entire opening by a net element, one test was carried out. This test represents the limiting condition. To lead this particular net configuration a further additional net of 12.2 cm was adopted, in order to cover the lower part of the opening and thus to increase the total net height. Therefore the total net height was equal to 41.2 cm, quite sufficient to avoid possible overflow phenomena.

For this test an incoherence was noted between the passed material percentage (Table 25) and the passed material amount optically observed (Figure 62) since they showed no comparable results. Despite no measures of the losses were taken during the tests and therefore no precise information of these are available, it is possible to conclude that no negligible losses occurred in the first part of the model. As described in Chapter 2.6.1, these losses can be quantified as material deposited on the inlet channel, in the released bucket or material sprayed off the model nearby the released section. Since the aim of this test was only to demonstrate that a slit dam with its entire height covered by a net, would retain most of the debris flow material, the test can be considered as positive.

Table 25. Volume data and water contents of the debris flow mixture for type 5 test.

Run	Released material	Retained material		Passed or lost material		Water content by weight
	[m^3]	[m^3]	[%]	[m^3]	[%]	[%]
5	0.419	0.389	92.68	0.031	7.32	23.25

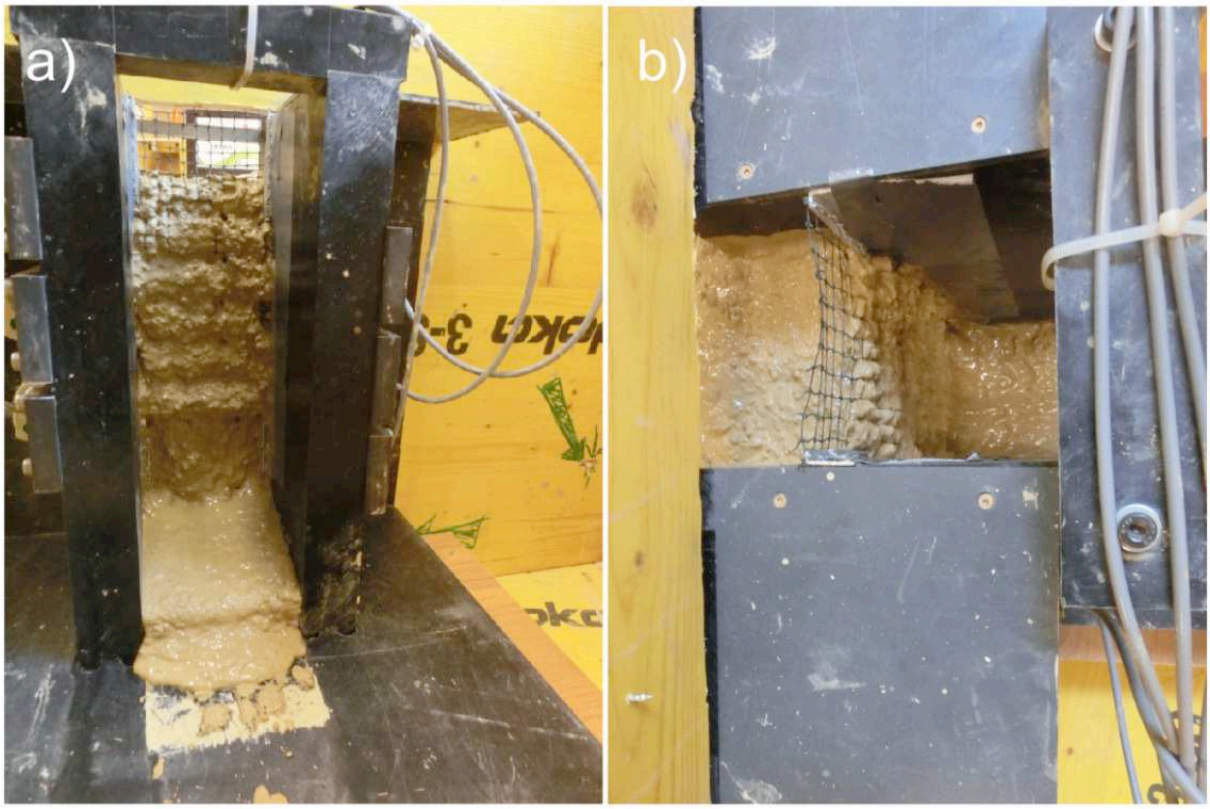

Figure 62. Passed material amount for type 5 test: a) front view, b) upper view.

Debris flow average front velocities are summarized in Table 26 and their trend is shown in Figure 63 where it is possible to note that even for this series, it appears to be similar to the ones observed in the previous experiments.

Table 26. Debris flow average front velocities for type 5 test.

Run	v_{inl}	v_{mid}	v_{end}	v_{HSC}
	[m/s]	[m/s]	[m/s]	[m/s]
5	2.67	1.12	1.48	1.00

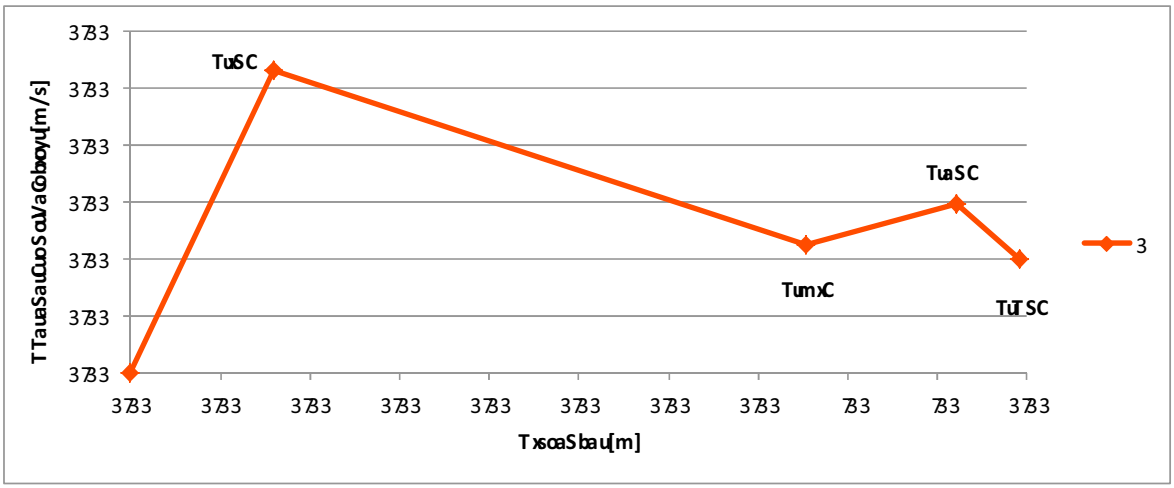

Figure 63. Average front velocities along the model for type 5 test.

Since the lower additional net was not equipped with load cells, no force information were obtained for this first net part. Therefore, the force values were recorded starting from the end of the lower additional net, i.e. starting from 12.2 cm from the model bottom. The results of the measures are show in Table 27 for the maximum forces and in Table 28 for the final constant forces. Figure 64 shows the force trends along the barrier height where it is possible to note the typical trend detected in the previous tests, i.e. higher values on the lower part and lower values in the upper part, with a maximum force value measured by load cell LC2. Finally, Figure 65 shows the force vs time chart.

Table 27. Maximum tensile axial forces from the load cells measurements for type 5 test.

Run	LC1 [N]	LC2 [N]	LC3 [N]	LC4 [N]	LC5 [N]	LC6 [N]
5	69.82	71.07	59.35	46.75	37.72	21.79

Table 28. Final constant tensile axial forces from the load cells measurements for type 5 test.

Run	LC1 [N]	LC2 [N]	LC3 [N]	LC4 [N]	LC5 [N]	LC6 [N]
5	61.94	34.85	14.13	60.53	51.40	24.79

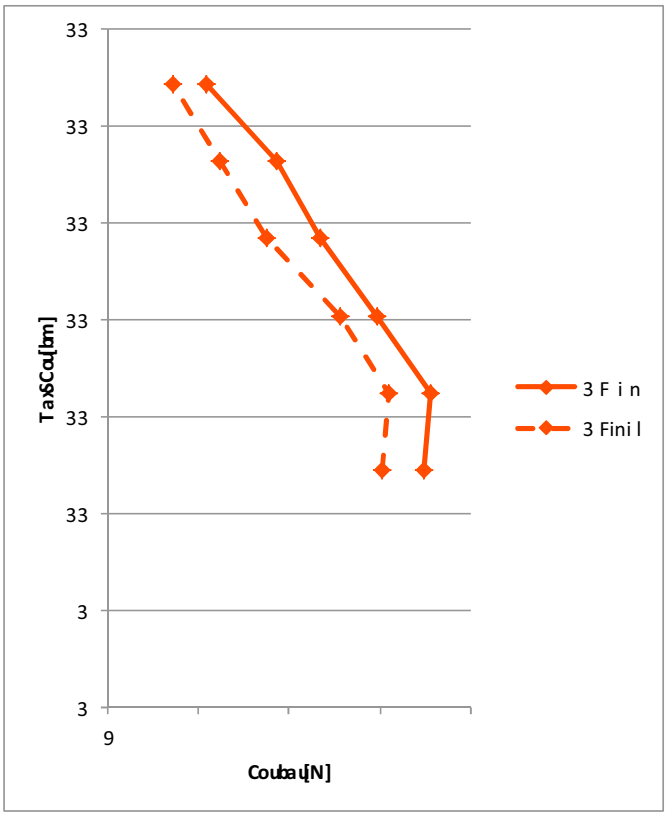

Figure 64. Tensile axial forces along the barrier height for type 5 test: maximum and final value (shown respectively with a continuous and a dashed line).

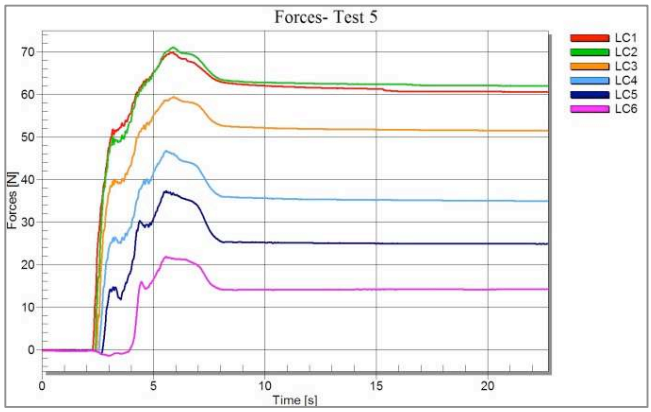

Figure 65. Force vs time chart for type 5 test.

4 DISCUSSION

This chapter provides the discussion of the results presented in the Chapter 3. A particular focus is given to the comparison of the results of the five different basal openings, as well as a critical discussion of the problems observed on the execution of the tests and the elaboration of the data. Furthermore, when it was possible, the results found were compared with those presented in the Literature by other authors.

4.1 RETENTION EFFICIENCY

As observed in the previous Chapter 3, the five different barrier configurations tested have shown different retention capacities (Figure 66; see also APPENDIX C where the 3D surfaces provided by the software Surfer are reported). In particular type 1 and type 2 tests have shown similar retention capacities, with percentages of retention ranging from 25.63 to 30.94 % of the entire volumes released. For type 3 tests there is a significant onset of high retention efficiency due to a lower basal opening (4.5 cm). Test 3.3 showed a retention capacity comparable to those observed for type 1 and type 2 tests because the debris flow was not retained by the barrier. For type 4 and type 5 tests a greater retention was observed, with percentages ranging from 90.58 to 95.53 %. As a result, this suggests that a certain basal opening would distinguish the case of partial or total retention of the material released.

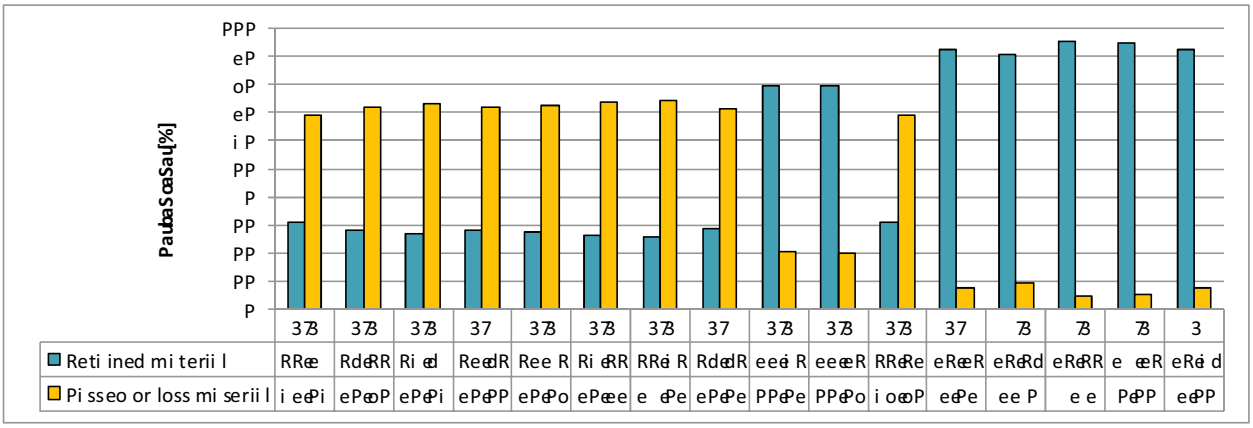

Figure 66. Summary of the percentages of retained and passed or lost material for the entire set of experiments.

Figure 67 shows a 3D plot of the passed or lost material and the retained material (both variables are each other directly related and here expressed as percentage) as a function of the

basal opening of the barriers tested. The ellipse joins the experimental points of the different test types and gives a general pattern of the phenomenon: larger basal openings allow the passage of a greater amount of material (and hence a lower percentage of retained material) whereas smaller basal openings show greater percentage of retained material. It must be noted that between the partial or complete retention showed by the experimental points, an evident gap exists. This fact clarifies the existence of a certain basal opening which would distinguish the flow behaviour (as highlighted just above). As Figure 68 shows, if through the experimental data points a theoretical curve fitting is performed using a sigmoid model with variable slope, an estimated range for a critical basal opening lies in between the values of 4.1 and 5.1 cm (which correspond to the points where the sigmoidal curve starts and ends, respectively). The value of basal opening that has a 50% probability to allow the passage of the material may be calculated as 4.6 cm (see legend of Figure 68 for details). Further investigations, with more basal openings in the range between 4.5 and 6.0 cm, might allow the discovery of a more accurate discriminant value.

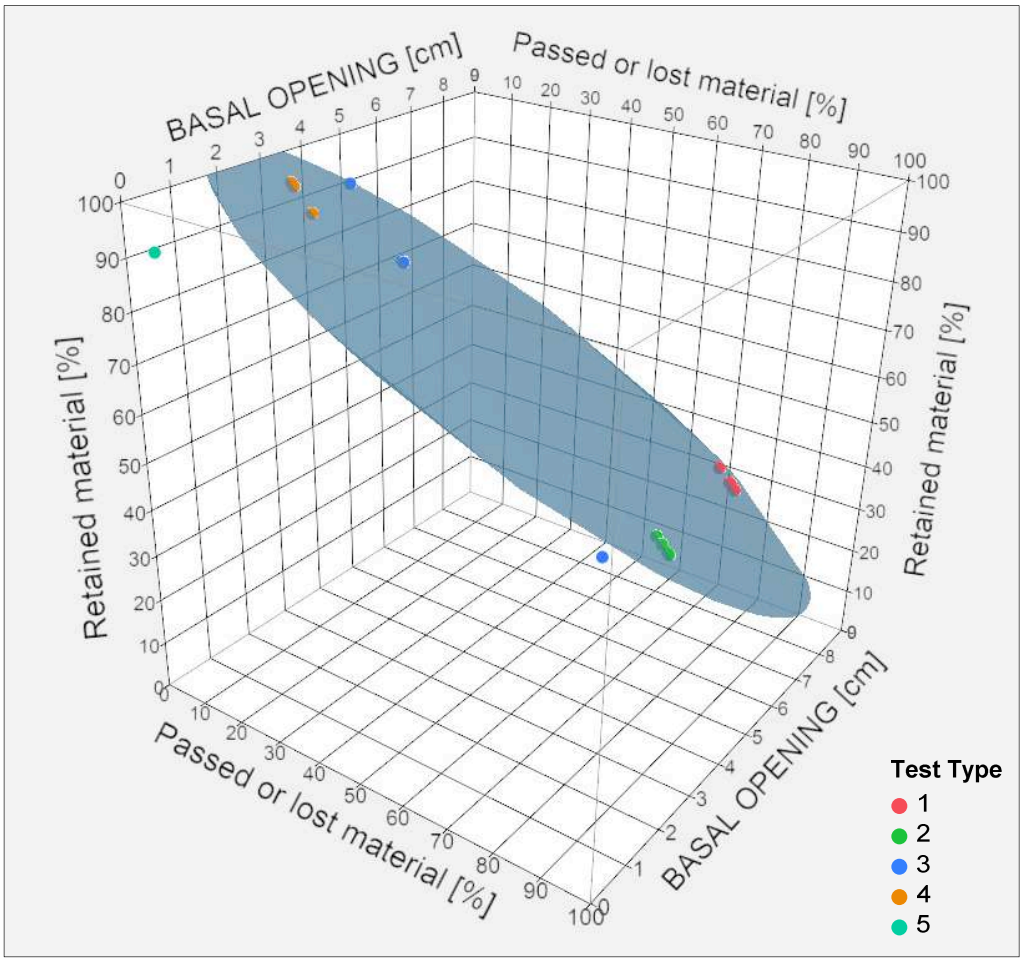

Figure 67. 3D plot of passed or lost material and retained material as a function of the basal opening of the barrier.

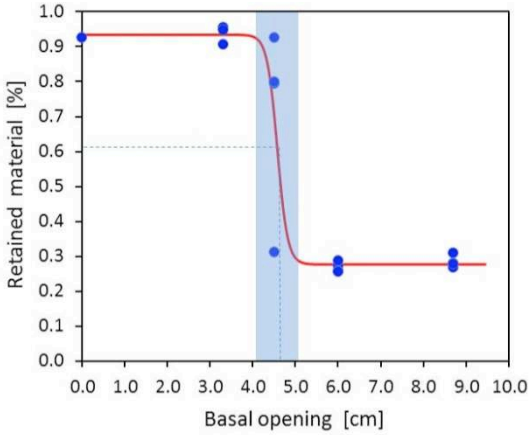

Figure 68. Sigmoidal curve fitting of retained material vs basal opening data. The curve follows the general equation:

$$Y \quad min \quad \frac{max \quad min}{1 \quad e^{(K \quad X)h}}$$

where Y is the retained material, X is the basal opening, min and max are respectively the lower and the highest values of Y, h is the slope and K is the flex point, corresponding to the value of basal opening that has a 50% probability to allow the passage of the material.

Besides basal opening parameter, also the net element height (see Table 7 for the net type data) should be taken into account as a contributor to the amount of passed or retained material. In order to investigate the role of both parameters, a multiple regression analysis was performed. The results are reported in Table 29 where it is possible to note that the net element height parameter does not contribute signicantly to the regression, as well as the interaction between net element height parameter with basal opening parameter. The basal opening remains as the only significant parameter contributing to the retaining process; in addition, Table 30 shows the simple linear regression of the parameters, demonstrating that this simple model, at least as first approximation, can be adopted.

Table 29. Multiple regression analysis of the basal opening and net element height parameters vs retained material.

R^2	0.6565			
R	0.8102		p=0.004* (ANOVA)	
Terms	Estimate	Std Error	t Ratio	Prob>|t|
Intercept	58.199	55.529	1.05	0.3153
BASAL OPENING	-8.073	3.466	-2.33	0.0381*
Net Element Height	1.833	1.759	1.04	0.3180
(BASAL OPENING) (Net Element Height)	0.344	0.348	0.99	0.3423

* statistically significant parameter

Table 30. Simple linear regression between basal opening vs retained material.

R^2	0.6206			
R	0.7877		p=0.0003* (ANOVA)	
Terms	Estimate	Std Error	t Ratio	Prob>|t|
Intercept	110.052	12.583	8.75	<.0001*
BASAL OPENING	-10.174	2.126	-4.78	0.0003*

* statistically significant parameter

Retention efficiency has also proved to be dependent on the net element height as well as the basal opening. Indeed, the flow can pass under or over the net element and as a result, the total duration of the debris flow phenomenon shows different magnitudes. Therefore, in order to quantify these problems, overflow times and total debris flow durations were estimated from the high speed camera video (using the software TimeBench) and from the laser distance sensor measures (assuming as t=0 the moment when the flow overflowed the last net cable for the overflow estimation, and the time when the flow passed the L4 section for the total duration estimation). According to the data collected depending on the different basal openings and the net element heights (Table 31), some considerations can be done. The results show that slit net dam type A, due to a major basal opening, takes less time to allow the passage of the debris flow than slit net dam B. Furthermore this latter, due to a minor basal opening, allows the passage of a lower quantity of material and, as a result, more material overflows the net with a consequent increase of the overflow duration. For the Tests 3.1 and 3.2 (slit net dam type D) instead, the overflow time is much higher. Moreover, observing the video recording, it was possible to note the different intensity assumed by the overflow: in particular, after the basal opening was occluded, the remaining material overflowed first really fast and then more slowly (when the flood wave decreased) until the retained material behind the barrier became stationary. Test 3.3, which is of the same type (D) of these latter, shows a smaller overflow and total debris flow durations since the basal opening did not stop the material. In this case the barrier behaviour is similar to those observed during type 1 and type 2 tests, with the difference that more material overflowed the net top (thus the overflow duration was greater than the ones observed for type 1 and type 2 tests) and the emptying process was longer, due to the smaller basal opening. Finally, Test 3.4 (with a major total height) shows as a consequence a smaller overflow duration and thus a fast retention. Type 4 tests, with the exception of Test 4.1, showed no overflows due to the presence of the plexiglass plate on the top which was specifically developed to avoid the

overflow phenomena. Even if they had the artifice represented by the plexiglass plate, these tests showed small debris flow duration, and hence a fast retention phase. Observing the results of the Test 4.1 it is possible to note a similarity in comparison to the ones obtained from Test 3.4, which presents 1.2 cm of difference on the basal opening (and hence on the total height). In particular it is possible to note that Test 4.1, with a smaller total height, shows higher overflow and debris flow total durations than the Test 3.4. Finally, the results of type 5 test (no basal opening) show similar results to the Tests 4.2 and 4.3 since they both stopped the flow in the lower and upper part of the barrier.

Table 31. Overflow and debris flow durations.

Run	Slit Net Dam type	Basal Opening [cm]	Net element height [cm]	Total height [cm]	$\Delta t_{OVERFLOW}$ [s]	$\Delta t_{Debris\ Flow}$ [s]
1.1	A	8.7	20.0	28.7	n.d.[1]	63.35
1.2					4.36	73.48
1.3					4.81	72.68
1.4					4.99	67.20
2.1	B	6.0	20.0	26.0	7.07	80.28
2.2					8.47	77.71
2.3					9.10	79.46
2.4	C		29.0	35.0	No overflow	89.49
3.1	D	4.5	20.0	24.5	115.02	118.55
3.2					110.78	114.12
3.3					12.32	89.40
3.4	E		29.0	33.5	2.91	8.21
4.1	F	3.3	29.0	32.3	3.39	9.22
4.2	G				No overflow	8.29
4.3						8.30
5	H	0.0	41.2	41.2	No overflow	8.84

[1] No data available due to an accidental cut of the end of the video which did not allow to observe the entire overflow phenomenon.

Additional graphic representation is given in Figure 69, where a histogram resumes the duration data evaluated in this time analysis. Furthermore, Figure 70 shows a chart where the barrier total heights (i.e. the sum of basal opening and net element height) are reported versus the debris flow total durations. The trend of the regression line suggests that when the total

height decreases, the debris flow total duration increases. This hypothesis seems to be confirmed by the statistically significant correlation coefficient (R=0.745, p=0.0009) which suggests that a significant linear relation between the data exists.

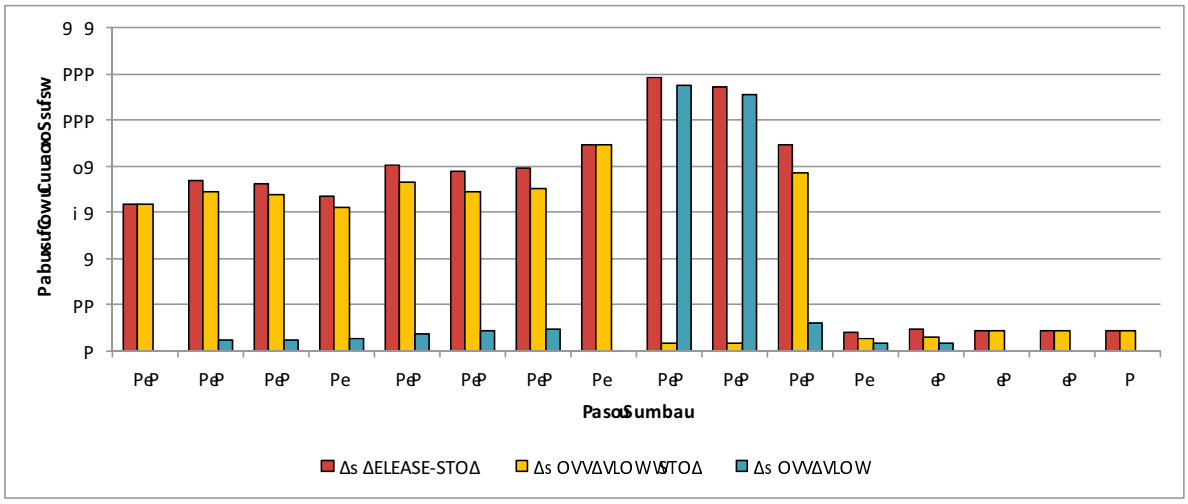

Figure 69. Debris flow durations for the experimental tests.

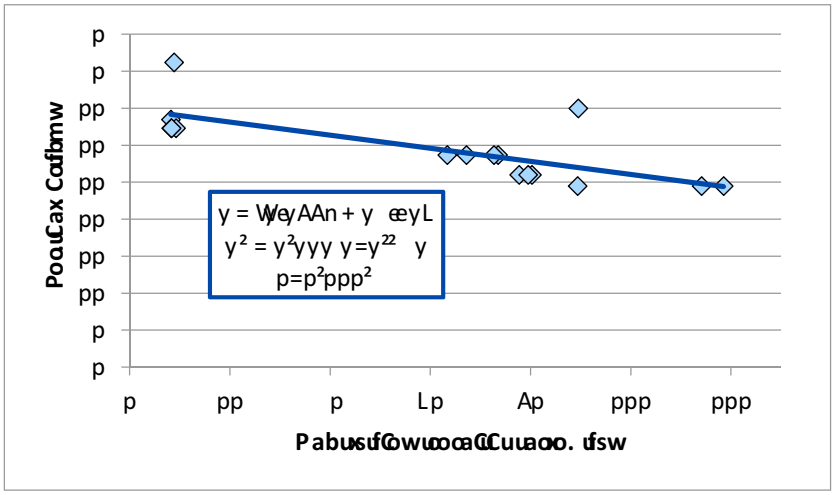

Figure 70. Total barrier Height vs Debris flow total duration. Inset: parameters and statistical evaluation of the linear regression among data points.

A final consideration must be done regarding the material volume released during the experimental tests. The duration of a certain phenomenon generally depends on the volumes involved and more material released means more time for a barrier to dissipate the phenomenon. In this work the volumes released during the experiment ranged from 0.40 to 0.47 m^3 (mean value 0.43 ± 0.03 m^3), with a maximum variation of 15%. Despite the presence of this deviation, in this context the duration considerations were however done in order to give a general overview of the phenomena.

4.2 VELOCITY TRENDS AND WATER CONTENT ROLE

As shown in Figure 44, 49, 54, 59, 63, average front velocities change their magnitude along the model. The greatest velocities occurred in the inlet channel, i.e. immediately after the debris flow released. This can be explained because, in this part of the model, the flow was not influenced by the roughness of the bottom, since it flowed on the inlet channel which was made of smooth wood. The next middle velocities v_{mid}, were instead influenced by the roughness of the stream bottom and as a consequence they showed a smaller magnitude. Further on, the debris flow reached the end part of the model (just before the barrier) and showed velocity values higher than the middle velocities but smaller than the inlet velocities. The increase of these values could be due to the variation of slope and geometry along the channel. Finally, when the debris flow arrived on the barrier it decreased its velocity, showing velocities quite similar to the ones obtained from the middle of the channel. This decrease appears to be due to the different roughness of the stream bottom: in this part of the model in fact, the flow came in contact with the different roughness offered by the grid panel (used in order to easily obtain the velocity measures, as described in Chapter 2.6.2). Furthermore the flow front could be influenced by the barrier wall which started to contrast the debris flow wave.

An overview of all the data measured is shown in Figure 71 while Figure 72 shows the data variability. Focusing on the latter, it is interesting to note that the middle velocities show the smaller variability with a standard deviation equal to 0.121 m/s (mean value 0.992 m/s), whereas inlet velocities show the major variability (SD = 0.483 m/s, mean value 2.410 m/s).

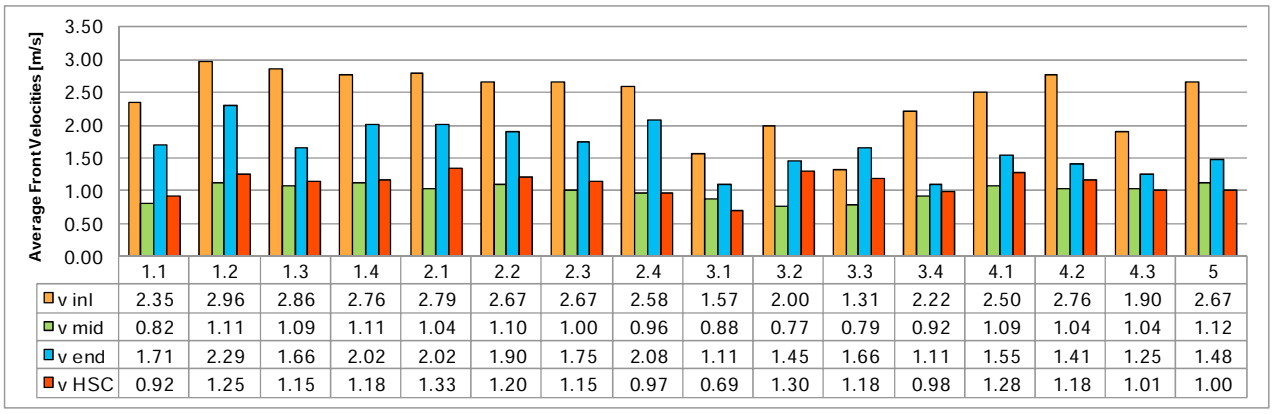

	1.1	1.2	1.3	1.4	2.1	2.2	2.3	2.4	3.1	3.2	3.3	3.4	4.1	4.2	4.3	5
v inl	2.35	2.96	2.86	2.76	2.79	2.67	2.67	2.58	1.57	2.00	1.31	2.22	2.50	2.76	1.90	2.67
v mid	0.82	1.11	1.09	1.11	1.04	1.10	1.00	0.96	0.88	0.77	0.79	0.92	1.09	1.04	1.04	1.12
v end	1.71	2.29	1.66	2.02	2.02	1.90	1.75	2.08	1.11	1.45	1.66	1.11	1.55	1.41	1.25	1.48
v HSC	0.92	1.25	1.15	1.18	1.33	1.20	1.15	0.97	0.69	1.30	1.18	0.98	1.28	1.18	1.01	1.00

Figure 71. Average front velocities for all the sixteen tests carried out.

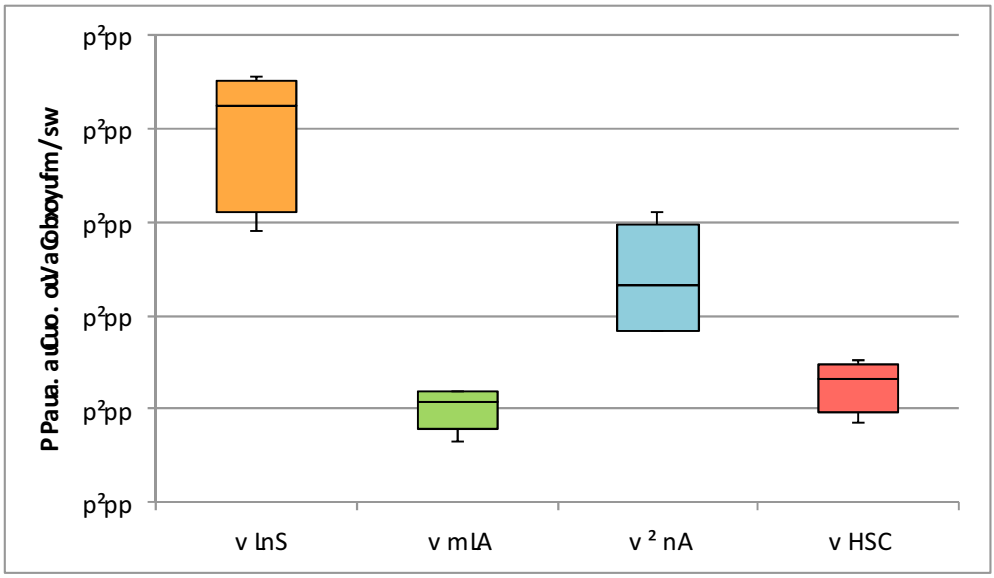

Figure 72. Box plot representation of the velocities along the model for all the tests (n=16).

In order to understand the origin of the velocity variability, an attempt was made observing the water content data. During the tests executions more turbulent characteristics were observed for the mixture with greater water contents, suggesting that with the increasing of the water content, also the velocity values increase in turn. Instead, looking at the diagrams of Figure 73 this fact seems to be not true. Although the correlation coefficient of the interpolation lines is not high (but statistically significant for the presence of a regression in cases a,b,c), it is possible to observe that a negative value for the slope always occurs. Thus, this analysis shows that when the water content increases, the velocity decreases. Therefore, the results are unexpectedly in contrast with the original observations and with the evidences found in literature. For example, Iverson et al. (2010) during large-scale experiments have observed that the velocity generally increases with the increase of water content. In this context, however, it is important to remember the source of variability introduced by the place where the samples (used to obtain the water contents) were taken. Indeed, as already discussed in Chapter 2.3.1 the measures could be strongly influenced by this fact and the measured water contents could be probably not representative for the entire bulk masses.

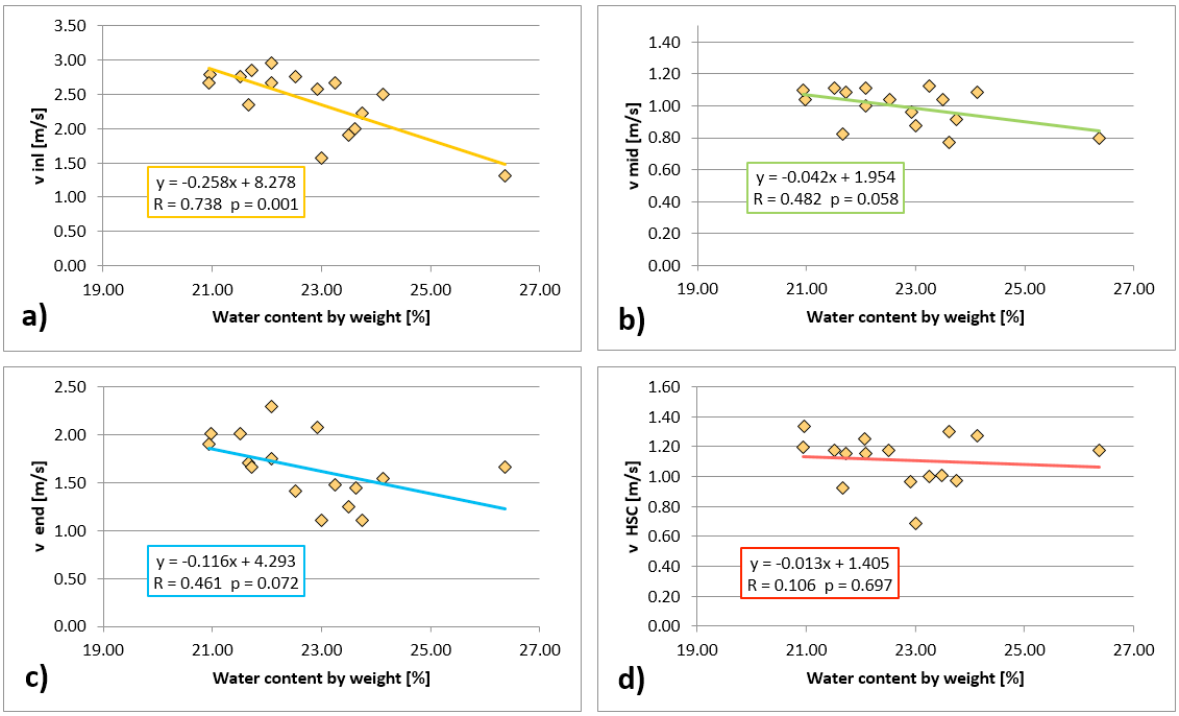

Figure 73. Velocities along the model as a function of the water content by weight [%] of the debris flow mixtures: a) inlet channel, b) middle channel, c) end channel, d) high speed camera.

4.3 FORCE TRENDS AND FLOW BEHAVIOUR

The force values presented in Chapter 3 have shown different results and trends. As appears from Figure 74 and Figure 75 the first difference that can be noted is related to the final forces measured. Indeed, tests which have retained most of the material released (Tests 3.1, 3.2, 3.4, 4.1, 4.2, 4.3 and 5), have shown constant and permanent force values on the load cells. Instead, tests which permitted the flow of most of the material, showed almost zero values except for negligible forces caused by the material which sometimes remained deposited on the net element.

Observations of the peak values of each tests reveal that the highest values measured were not always on the same load cell but sometimes change. In particular the highest values were observed for the load cell LC2 with the exception of Tests 3.1, 3.2, 3.4 and 4.1 which have shown the greater value on load cell LC1. This fact suggests the importance of the debris flow mixture which impacts against the net: as authors have previously observed (Zhang, 1993; Hu et al., 2011; Scheidl et al., 2013) the presence of big particles (boulders) on the debris flow front can cause higher values on the measures due to the strong collisions exerted.

Furthermore, the role of the basal opening should be highlighted. In fact this distance from the first cable of the net and the stream bottom influences the flow in different ways since larger basal opening allows the passage of the flow, while smaller basal opening stops it.

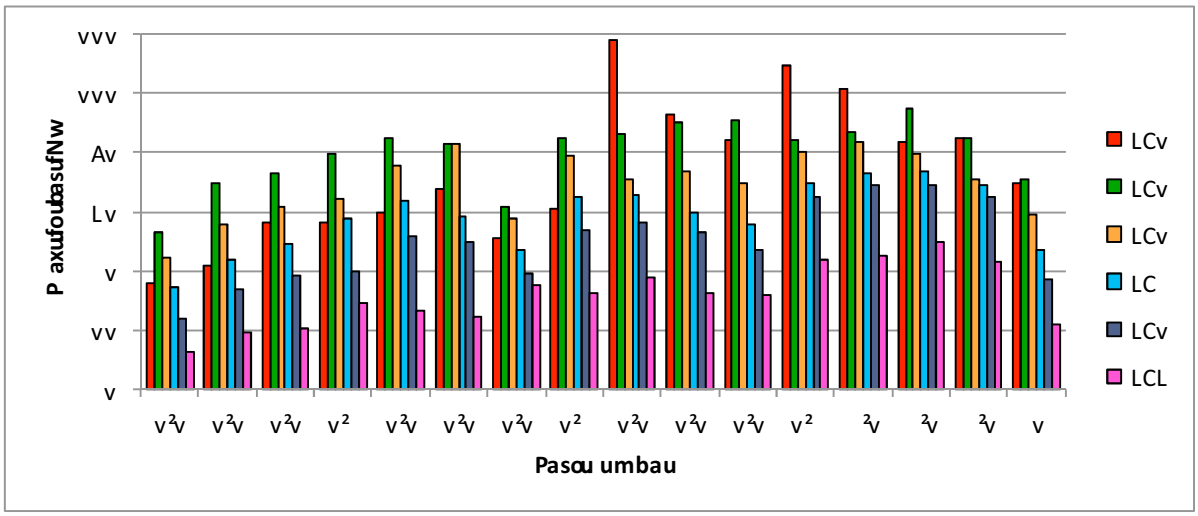

Figure 74. Maximum tensile axial forces measured by the load cells for the sixteen experimental tests.

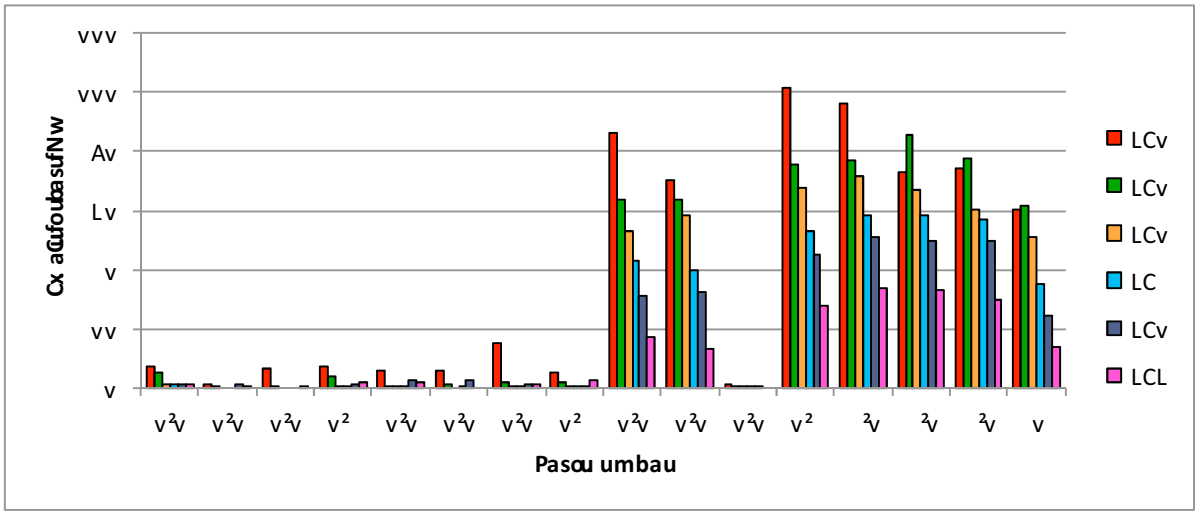

Figure 75. Final tensile axial forces measured by the load cells for the sixteen experimental tests.

Another interesting observation can be done looking again at the force trends. In fact it is possible to identify up to three distinct peaks on the force value time-series (Figure 76 shows an example of the force measured over time for the Test 2.3 where two peaks are easily recognizable for all the load cells recordings). In order to investigate the origin of these peaks,

video recordings were analyzed and compared with their respective force charts in terms of time.

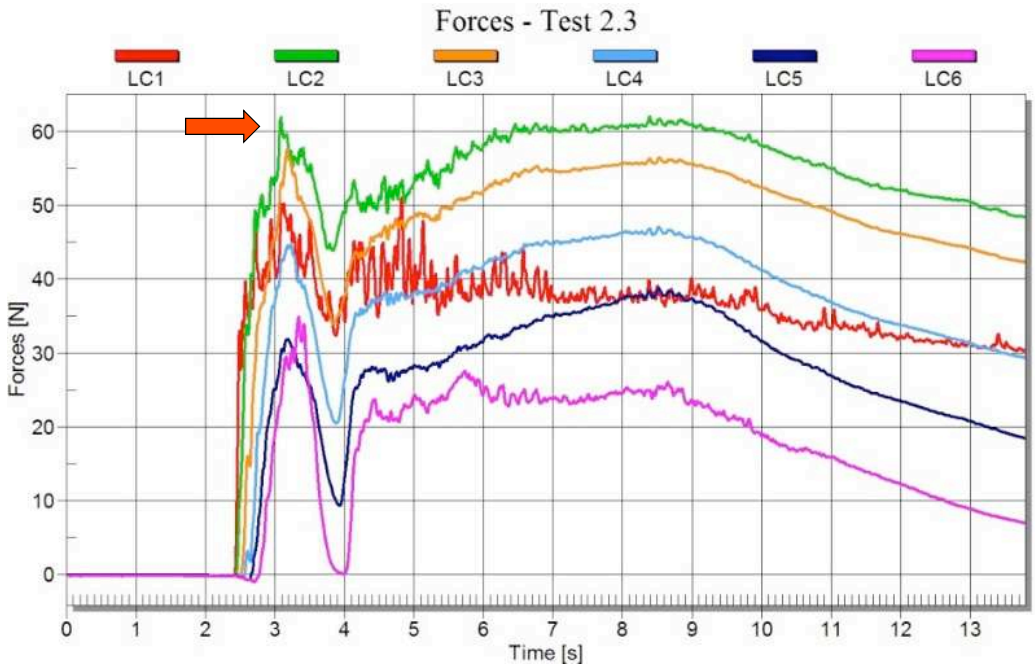

Figure 76. Force vs time for Test 2.3. Particular of the peaks in the curves, the biggest one is indicated by a red arrow.

As an example, Figure 77 shows the most important points of the force trend of Test 2.3 for the last cell LC6, which have been related to the video sequences provided by the high speed camera (Figure 78, vision above the net) and the GoPro (Figure 79, lateral vision of the model). Looking at the recordings, it was possible to note that when the debris flow reached the barrier section, it was affected by the lateral walls of the barrier and, as a consequence, a reflected wave was generated. The point (b) in Figure 77 corresponds to the first peak which occurred 3.34 s after the flow have passed the L4 section (i.e. at the end of the inlet channel) and represents the peak of the first impact onto the cable. After that, the wave felt inside the model and went counter-current, colliding against the incoming debris flow which continued to flow. The reflected wave then collapsed into itself and the level behind the net decreased with a consequent hollow in the curve (point c). The remaining debris flow continued to act through the barrier and a second peak (with a lower value in comparison with the first one) was then reached (point d). Finally, when the debris flow material released from the inlet channel begins to finish, the level behind the net decreases and consequently the forces in turn begin to decrease (point e and f).

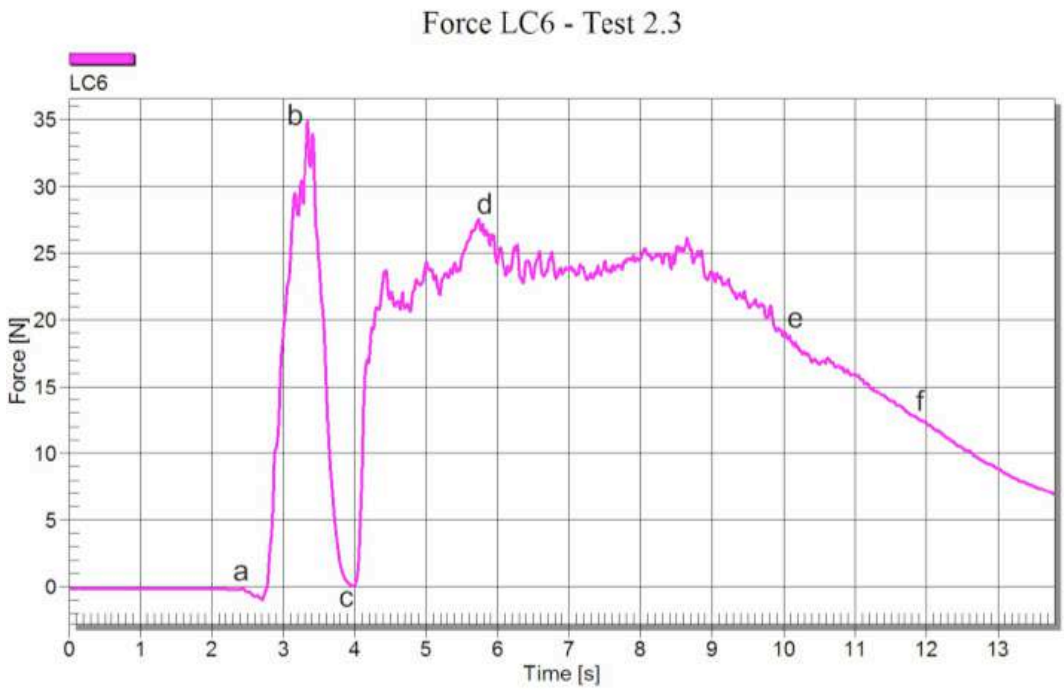

Figure 77. Particular of the force vs time chart for the load cell LC6 during the Test 2.3 (the letters refer to the particular time sequences shown in **Figure 78** and in **Figure 79**).

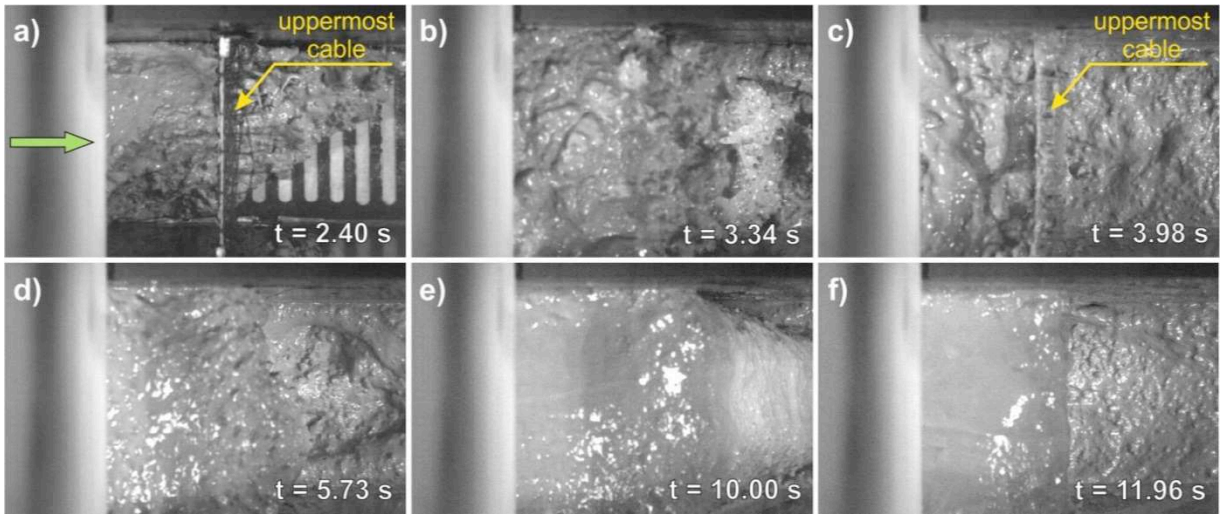

Figure 78. Evolution of the flow in the net section from the high speed camera view for Test 2.3: a) flow arrives to the net (the flow direction is indicated by an arrow), b) flow level above the last net cable and consequent overflow, c) decrease of the flow level and temporary stop of the overflow (the uppermost cable is not affected by the debris flow and it is notable), d) increase of the flow level and second overflow, e) the overflow continues and the flow shows differences on the mixture, f) overflow starts to end.

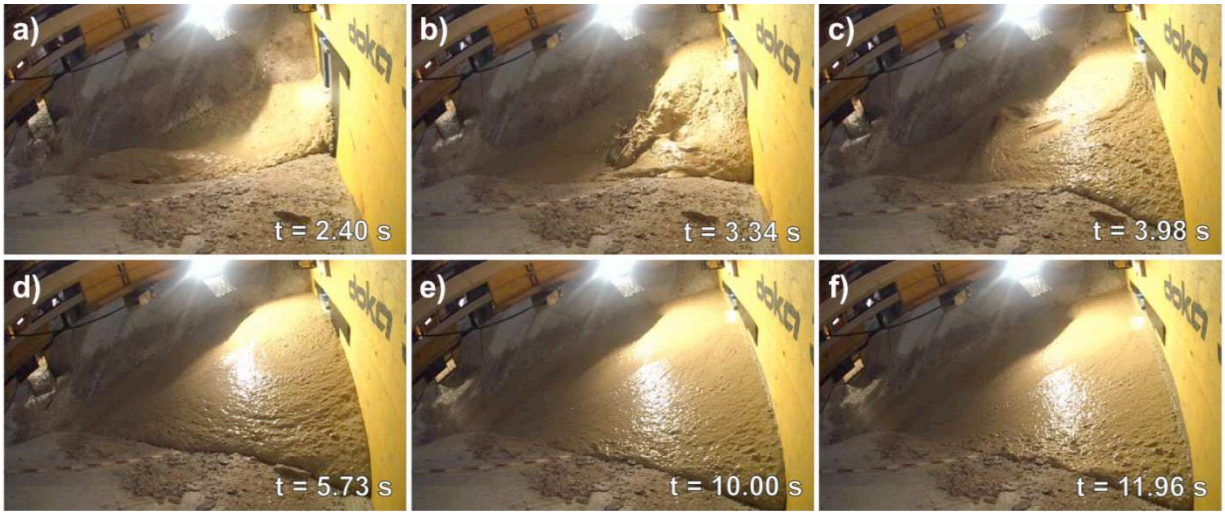

Figure 79. Evolution of the flow in the model from the GoPro camera lateral view for Test 2.3 (the time steps are the same of **Figure 78**).

A further consideration can be done observing the qualitative aspect of the debris flow mixture (especially from the high speed camera vision, Figure 78): during the first sequences the debris flow appears in fact composed by a greater percentage of coarse particles while on the last sequences (end of the last overflow) it appears more fluid. This fact suggests that a grain-size segregation phenomenon occurs during the debris flow experiments and supports the hypothesis that the larger particles are present on the flow front (this would explain the large values measured on the first peaks, during the first wave).

A second example is given additionally for Test 1.4, during which two main peaks with also three rising phases were observed. Figure 80 shows the force trend for the last cell LC6 and Figure 81, together with Figure 82, show the debris flow sequences related with the most important force points. Unlike the previous case, here it is possible to note that the greater peak was not the first one (corresponding to the reflected wave fully developed) but the second one (corresponding to the reflected wave collapsed). This fact could be related to the barrier total height (basal opening plus net element height) which was greater than the previous case of 2.7 cm and hence acted on the flow in a different way.

The flow behaviour herein observed, characterized by the development of a reflected wave when the debris impacted against the barrier, looks similar to the one described by Canelli et al. (2012) during their small-scale tests (see also Chapter 1.3.1). As these authors have observed, although their conclusion refers to a different model, it is possible that the successive peaks which were developed after the first one, were due to an overpressure generated by the reflected wave. This complex phenomenon is not easy to study (especially

with the devices adopted for the present work, which were not designed to investigate this aspect), thus only a qualitative observation of the flow evolution can be herein proposed.

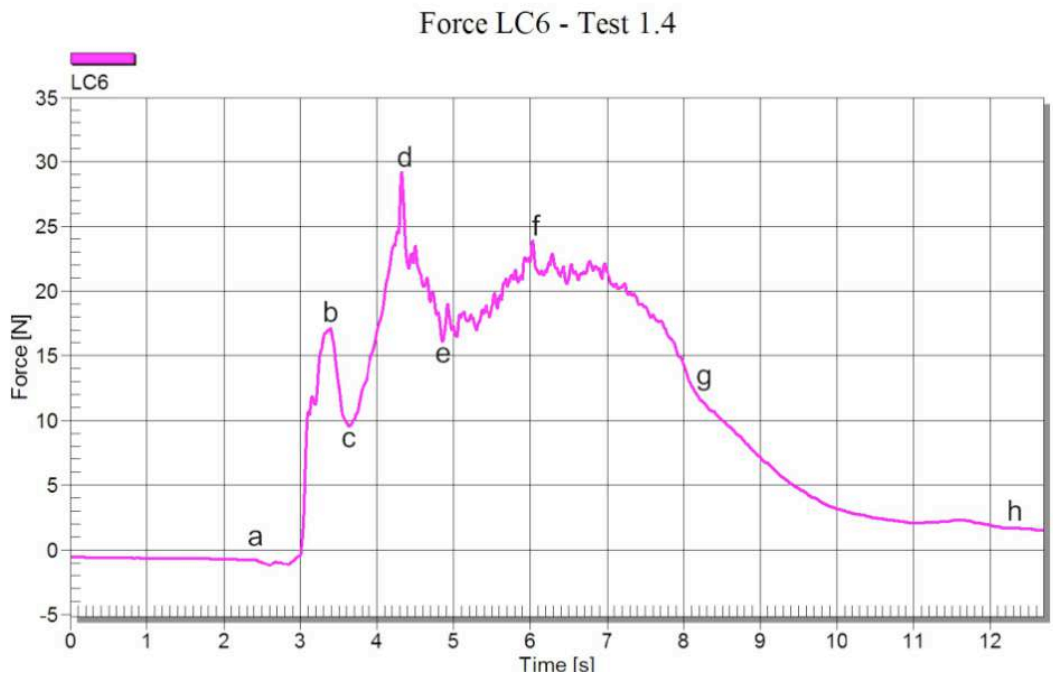

Figure 80. Force vs time chart for the load cell LC6 during the Test 1.3 (the letters refer to the time sequences shown in **Figure 81** and in **Figure 82**).

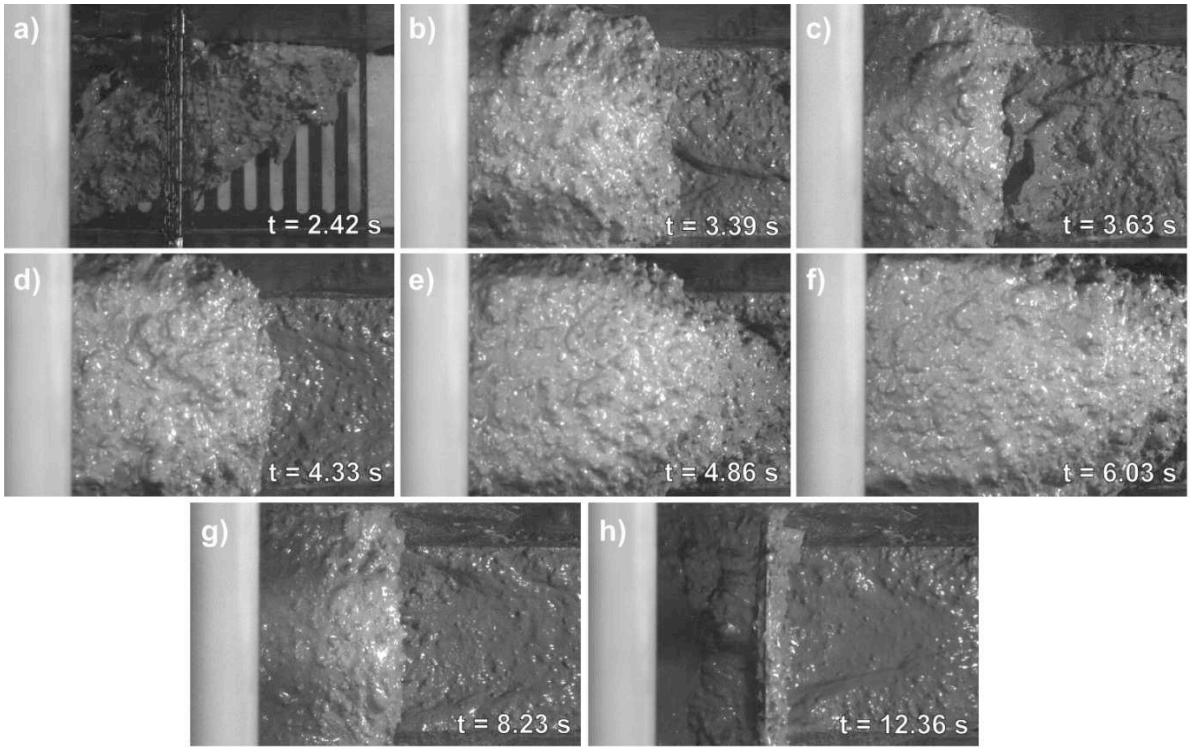

Figure 81. Evolution of the flow in the net section from the high speed camera view for Test 1.4.

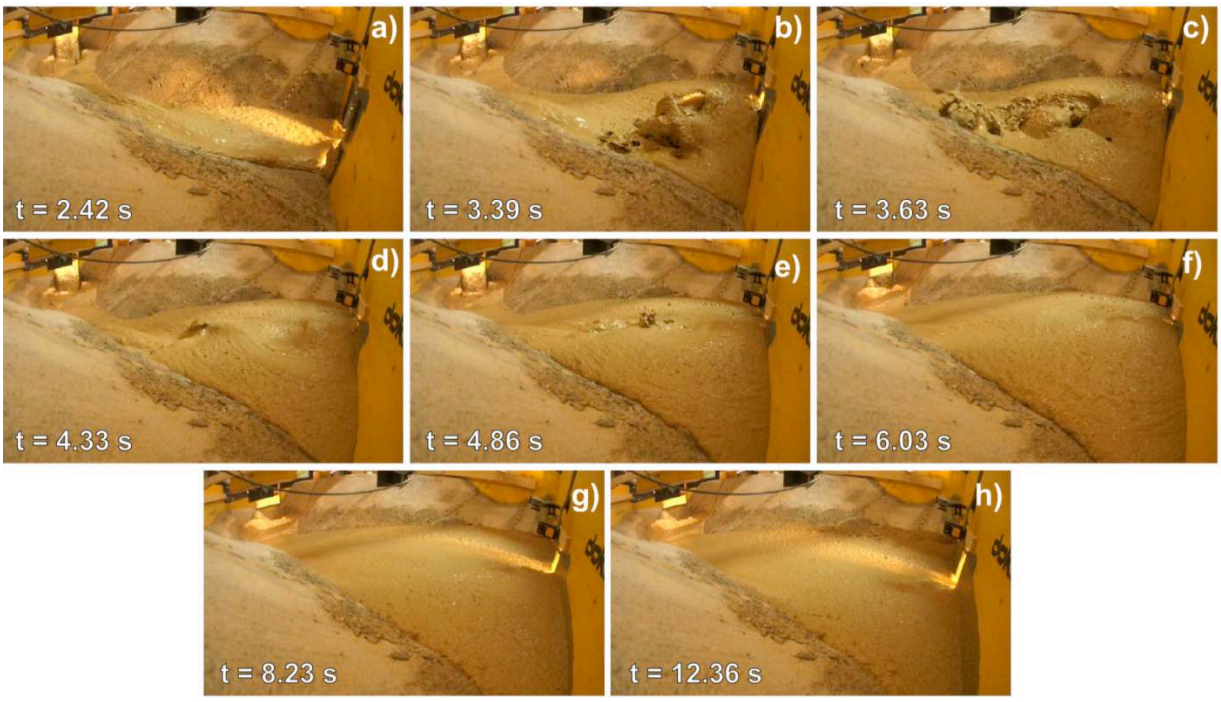

Figure 82. Evolution of the flow in the model from the GoPro camera lateral view for Test 1.4 (the time steps are the same of **Figure 81**).

In order to better understand the impact phenomenon, a further frame sequence with time steps of 0.15 s, is shown in Figure 83 (see also APPENDIX B which shows the sequences for the other experiments). The images were taken from the GoPro camera installed on the right side of the model which has recorded videos of each tests with 240 fps. The flow evolution shows clearly the development of the reflected wave due to the impact of the debris flow against the barrier wall. This flow behaviour leads to the consideration that this type of barrier works, in a first moment, as a solid body dam since the flow behaves like it impacted against a rigid wall. This suggests that the net element does not provide an immediate discharge of the flow, but stops it in a first moment and then allows a slower material release.

Figure 83. Debris flow impact sequences (with Δt=0.15 s) for Test 1.4. Vision from the GoPro camera (240 fps), lateral view.

4.4 SCALED DATA

Since the experimental tests were carried out in a small-scale model in order to understand the behaviour of a prototype slit net dam, a critical analysis on the possibility to extend the values obtained from the model to the prototype scale was proposed.

The tests were achieved according to the Froude scaling concept (Chapter 1.3.3) which requires the equality of the Froude number for both the model and the prototype (equation 10). For this work the Froude number is equal to F_r 1.90 and was calculated with respect to the debris flow front close to the net barrier section. That value falls into the range typically calculated from field observations which is equal to 0.5 - 2 (Hübl et al., 2009) and leads to the conclusion that the model could comply with the real debris flows which occur in nature, if only Froude scaling is concerned.

In this context the main results in terms of volume retained, debris flow front velocities and maximum tensile axial forces are reported (Table 32), according to the model scale adopted, which was equal to 1/30.

Table 32. Model and Prototype quantities for the experimental tests.

Run	MODEL				PROTOTYPE		
	Volume Retained [m³]	[1]Front Velocity [m/s]	Maximum tensile axial force (in LC_) [kN]		Volume Retained [m³]	Front Velocity [m/s]	Maximum tensile axial force [kN]
1.1	0.144	1.71	0.053	(LC2)	3'889	9.34	1'437
1.2	0.133	2.29	0.070	(LC2)	3'604	12.56	1'885
1.3	0.125	1.66	0.073	(LC2)	3'373	9.11	1'975
1.4	0.127	2.02	0.080	(LC2)	3'436	11.04	2'150
2.1	0.123	2.02	0.085	(LC2)	3'333	11.04	2'300
2.2	0.117	1.90	0.083	(LC2)	3'161	10.41	2'248
2.3	0.115	1.75	0.062	(LC2)	3'115	9.59	1'673
2.4	0.123	2.08	0.085	(LC2)	3'322	11.38	2'286
3.1	0.322	1.11	0.118	(LC1)	8'683	6.07	3'191
3.2	0.323	1.45	0.093	(LC1)	8'717	7.92	2'505
3.3	0.126	1.66	0.091	(LC2)	3'402	9.11	2'452
3.4	0.371	1.11	0.110	(LC1)	10'015	6.07	2'967
4.1	0.401	1.55	0.101	(LC1)	10'821	8.47	2'739
4.2	0.386	1.41	0.095	(LC2)	10'420	7.75	2'570
4.3	0.383	1.25	0.085	(LC2)	10'350	6.87	2'299
5	0.389	1.48	0.071	(LC2)	10'494	8.09	1'919

[1] Front velocity values refer to the measures got from the end part of the model (v_{end}).

The results obtained show reasonable values for the volumes and the velocities but questionable values for the cable forces. Prototype scaled forces seem in fact to be much higher than the results measured in real scale problems. DeNatale et al. (1999) for example, during real scale experiments carried out in the USGM flume on different net barriers, have found maximum force values of 40 kN (Figure 84). Wendeler et al. (2007) reported field tension forces measured by load cells installed at the ends of the ropes. The forces relate to a real debris flow event occurred in 2006 which impacted against a net barrier and gave values equal to 150 kN for top support rope and 248 kN for bottom support rope.

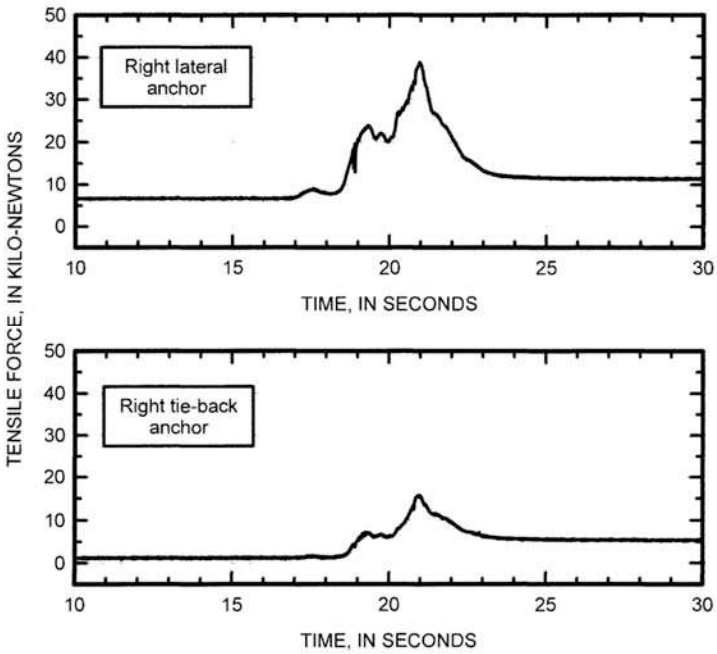

Figure 84. Anchor cable forces measured by DeNatale et al. (1999) during real-scale tests at the USGS flume in Oregon, USA (test #2); figure taken from DeNatale et al. (1999).

Since the forces obtained after the scaling calculation have shown too high values, this could suggest that the results herein obtained are overestimated. One reason for this is attributed to the imperfect scaling of debris flow dynamics. As explained in Chapter 1.3.3 and outlined in detail by Iverson (1997), scaling of all relevant forces acting in a two-phase mixture such as debris flows (inertia of two solids and fluids, grain-grain interactions, fluid resistance, solid fluid interaction, gravity,…), is practically impossible. Froude scaling only considers inertia and gravity of a quasi one-phase material. Therefore a lot of other force combinations are neglected. However, this study only investigates the effect of the basal opening geometry on the flow of a solid-fluid mixture.

Another issue is the experimental setup itself: although no proofs about a possible malfunctions of the load cells were gained, it is possible that the wrong values obtained are due to the net dam model. The barrier structure was in fact made with plastic material and the cable system composed by pulleys and load cells were mounted on it. It is possible that the measures were influenced by the deformation of the plastic which composed the barrier, since great sensitivity was observed during the calibration phase of the barrier.

Therefore, the force values presented herein should be considered of qualitative but not quantitative relevance.

5 CONCLUSIONS

The present thesis work has shown the response of a small-scale slit net dam towards a debris flow simulation. The research aims were achieved and the experimental tests and analysis produced valuable results. This chapter summarizes the final conclusions and suggests further possible investigations that could be planned in order to better understand the behaviour of this particular type of barrier.

5.1 CONCLUDING REMARKS

The design of this kind of barrier, and hence the choice of the suitable basal opening, must be done depending on the purpose to be achieved. If the aim is only to oppose the debris flow events, with a reduction of their impact energy and a gradual release of the material, high basal opening can be adopted. In particular, since no great differences were observed in the barrier behaviour during type 1 and type 2 tests, a basal opening of 2.60 or 1.80 m can indifferently be chosen. The adoption of this kind of basal openings could be useful in those cases when the barriers are located in impassable places because if the debris flow is completely retained, it would be a problem to reach the place with the excavating machines which want to restore the original conditions. On the opposite, if the aim is to completely stop the debris flow events (because of the presence of high hazards to humans and infrastructure safety), a smaller basal opening must be adopted. Moreover, a completely closed slit net dam (i.e. with no basal opening) could be more appropriate, since a basal opening too close to the limit between total and partial retention, could lead to unwanted or unpredictable results. Finally, it is important to underline the advantages of having a net element as covering of the opening: practical aspects such as easy restoration (or replacement) in case of damages of the net components and economical aspects related to the lower costs in comparison to huge concrete barriers. As a result, these considerations suggest that this new type of barrier, together with the modern barriers entirely composed by a net structure, can be considered as a valuable alternative to the classic barriers made entirely of reinforced concrete.

The observations of the flow behaviour have shown the presence of a reflected wave which was developed behind the barrier. This aspect has led to the conclusion that this kind of barrier is capable to temporarily limit the debris flow power and then to work in order to drain the remaining material. However, it appears that this particular behaviour is strongly dependent on the slit dam width, net mesh size, basal opening, mixture composition and

material released volume. This suggests that a change in one of these factors could lead to completely different results and, for this reason, the data herein obtained cannot be considered of general validity, but should be intended only for this specific case.

The scaled results have highlighted the problems which occur when small scale experiments are carried out (scale effects). In particular, this work led to the conclusion that great attention must be taken especially when force observations are required. In this sense, large-scale experiments seem more appropriate to better study these phenomena although they require more efforts than small-scale laboratory tests. However, the study of a barrier behaviour against debris flow problems with this kind of small-scale experiments, leads to obtain first useful conclusions to help in the design of these active measures. This work showed that when designing the net, special focus should be given to the two lowermost cables (which are the most stressed). Probably a deforming break element could be included to decrease the tensile axial force in the cables.

5.2 FURTHER RESEARCH

The present work focused on the study of the behaviour of a slit net dam with different basal openings. Although it contributed to the knowledge of this particular type of barrier, further topics could be investigated as well as a greater number of runs for each basal opening could be performed, in order to prove the reliability of the results. Furthermore, a larger number of experimental replicates could permit a more accurate statistical analysis.

The first improvement that could be done regards the investigation of different net mesh size, since only one type was tested here and more attention was given to the basal openings. In particular, it would be interesting to find the mesh limit which distinguishes the complete or the partial passage of the material through the net. The future investigations could be fulfilled continuing to use the d_{90} of the material mixture as a comparison parameter between different mesh sizes.

The tests were carried out with only one type of mixture which wanted to represent the material composition of the field where a possible barrier would be built. Other tests with different mixtures are strongly recommended since the barrier response could change depending on it. In particular, it could be interesting to observe the barrier response by changing the water contents, the d_{90} of the material, or adding larger particles in the mixture, in order to simulate catastrophic debris flows with huge boulders.

Barrier response was tested with a volume material which ranged from 0.40 to 0.47 m^3 with a fast and unique release. A further investigation could be planned testing different volumes released (also with successive, temporally distinct, releases) and also testing the case of long time events, long enough to observe uniform flow conditions. Moreover, the case of an erodible bed during the debris flow event, would be also interesting to study.

Finally, since this work has shown the limit of this kind of small-scale experiments and in order to obtain correct scaled values (especially for the forces), the role of the scale effects must be further clarified.

ACKNOWLEDGEMENTS

Although this page is located at the end of this thesis work, I consider it as one of the most important. I think that human relations are essential for every person and, for me in particular, they have a big significance. For this reason, here I would like to thank some people without whom this work would not have been possible. In particular, I am thankful to the following persons:

Prof. Roland Kaitna and Prof. Johannes Hübl, for giving me valuable suggestions and always clever ideas to develop my thesis. They definitely made this experience possible from the beginning to the end.

Prof. Simonetta Cola, for introducing me into the world of the debris flows, teaching me her knowledge with passion and dedication.

Martin Falkensteiner, for helping me a lot during the execution of the experimental tests and for giving me amazing climbing (and friendly) days in Vienna.

Friedrich Zott, for his precious and patient assistance with the measurement devices.

Nikolaus Wieser, for welcoming me into the project immediately when I arrived at Boku, giving me the possibility to work together with him.

My climbing friends in Padua, with them I passed some of the best days of my life visiting amazing places. They made me to understand that to be happy we just need to go and stay outdoor (better with a great climbing wall in front). Just some important persons: Matteo, Carlo, Sara, Fede, Sofia, Luigi, Maurizio, Marco, Alessio, Flavio, Matte, Mattia, Jacopo, Luca, Pietro, Aldo, and many others… A big thanks to all of you!

My father and my mother, for helping and supporting me a lot during these years. They taught me how to stay in this world with happiness, how to give the right importance to the things. They always gave me the support to make what I liked to do. I am very lucky.

And finally, the greatest thanks goes to Maria. She was always with me, especially during the hardest moments of my university studies, she supported me a lot, sometimes too much. She completes me. Love you.

6 REFERENCES

Armanini A., Dalrì C., Della Putta F., Larcher M., Rampanelli L., Righetti M. (2004) Design criteria of mudflow breakers – experimental and theoretical approach. 10th Congress INTERPRAEVENT 2004, Riva/Trient (Italy), 24-28 May 2004, Conference Proceedings, Vol. 3, Villach: Internationale Forchungsgesellschaft, pp. 1-11

Brighenti R., Segalini A., Ferrero A.M. (2013) Debris flow hazard mitigation: A simplified analytical model for the design of flexible barriers. Computers and Geotechnics, 54; 1-15

Bugnion L., McArdell B.W., Bartelt P., Wendeler C. (2012) Measurements of hillslope debris flow impact pressure on obstacles. Landslides, 9(2); 179-187

Bugnion L., von Boetticher A., Wendeler C. (2012) Large scale field testing of hillslope debris flows resulting in the design of flexible protection barriers. 12th Congress INTERPRAEVENT 2012, Grenoble (France), 23-23 April 2012, Conference Proceedings, Extended Abstracts, pp. 59-66

Canelli L., Ferrero A.M., Migliazza M., Segalini A. (2012) Debris flow risk mitigation by the means of rigid and flexible barriers – experimental tests and impact analysis. Natural Hazards & Earth System Sciences, 12(5); 1693–1699

Chanson H. (1999) Physical modelling of hydraulics. In: The Hydraulics of Open Channel Flow, Arnold, London, Chapter 14, pp. 261-283

Coussot P., Meunier M. (1996) Recognition, classification and mechanical description of debris flows. Earth-Science Reviews, 40; 209-227

Cruden D.M., Varnes D.J. (1996) Landslide types and processes. In: Landslides Investigation and Mitigation, Eds: Turner A.K. and Schuster R.L., Transportation and Road Research Board, Washington, D.C.: National Academy of Science, Special Report 247, pp. 36-75

D'Agostino (2008) Dimensionamento delle opere di protezione dalle colate detritiche. In: Sistemazione dei bacini montani e difesa del suolo, Ed. Ferro, Nuova Editoriale Bios, Castrolibero (CS), Chapter 22, pp. 605-623

DeNatale J.S., Iverson R.M., Major J.J., LaHusen R.G., Fiegel G.L., Duffy J.D. (1999) Experimental testing of flexible barriers for containment of debris flows. US Geological Survey Open-File Report 99-205, Vancouver, Washington, 38 pp.

Fattorelli S., D'Agostino V. (2008) Criteri di intervento per la difesa del territorio nei bacini montani. In: Tecniche per la difesa dall'inquinamento, Nuova Editoriale Bios, Castrolibero (CS), pp. 127-142

Geobrugg (2009) Flexible ring net barriers for debris flow protection: The economic solution. Available as pdf: http://www.geobrugg.com/contento/Portals/35/media/Download-Brochures/Geobrugg-AG_Debris-Flow_en.pdf, 16 pp.

Google Earth 7.1.2.204, 47°18'06.38''N and 12°59'38.40'' O, 1 August 2010, 8 May 2014.

Graham D.J., Midgley N.G. (2000) TECHNICAL COMMUNICATION - Graphical Representation of Particle Shape using Triangular Diagrams: An Excel Spreadsheet Method. Earth Surface Processes and Landforms, 25(13); 1473-1478

Hu K., Wei F., Li Y. (2011) Real-time measurement and preliminary analysis of debris-flow impact force at Jiangjia Ravine, China. Earth Surface Processes and Landforms, 36(9); 1268-1278

Hübl J., Fiebiger G. (2005) Debris-flow mitigation measures. In: Debris-flow Hazards and Related Phenomena, Eds: Jakob M and Hungr O., Springer, Berlin Heidelberg, Chapter 18, pp. 445-487

Hübl J., Strauss A., Holub M., Suda J. (2005) Structural mitigation measures. In: Proceedings zum 3rd Probabilistic Workshop: Technical Systems + Natural Hazards, 24-25 November 2005, Wien (Austria), 12 pp.

Hübl J. and Suda J. (2008) Debris flow mitigation measures in Austria. In: Debris Flows: Disasters, Risk, Forecast, Protection, Proceedings of the International Conference, Pyatigorsk (Russia), 22-29 September 2008, Ed: Chernomorets S.S., Part 1, pp. 27-30

Hübl J., Suda J., Proske D., Kaitna R., Scheidl C. (2009) Debris flow impact estimation. In: Eleventh International Symposium on Water Management and Hydraulic Engineering, Eds: Popovska C. and Jovanovski M., Vol 1, pp. 137-148

Hübl J., Wieser N., Falkensteiner M., Zott F., Scheidl C., Chiari M. (2014) Physikalische Modellierung zur Optimierung von flexiblen Murbarrieren am Beispiel Trattenbach, Institut für Alpine Naturgefahren, Universität für Bodenkultur - Wien (unveröffentlicht)

Hungr O. (1995) A model for the runout analysis of rapid flow slides, debris flows, and avalanches. Canadian Geotechnical Journal, 32(4); 610-623

Hungr O. (2005) Classification and terminology. In: Debris-flow Hazards and Related Phenomena, Eds: Jakob M. and Hungr O., Springer, Berlin, Chapter 2, pp. 9-23

Hungr O., Evans S.G., Bovis M.J., Hutchinson J.N. (2001) A review of the classification of landslides in the flow type. Environmental and Engineerin Geoscience, 7(3); 221-228

Hutchinson J.N. (1988) General Report: Morphological and Geotechnical Parameters of Landslides in Relation to Geology and Hydrogeology. In: Landslides, Proceedings of the Fifth International Symposium on Landslides, Lausanne (France), 10-15 July 1988, Eds: Bonnard C., Balkema, Rotterdam, Vol. 1, pp. 3-36

Itoh T., Horiuchi S., Mizuyama T., Kaitsuka K. (2013) Hydraulic model tests for evaluating sediment control function with a grid-type Sabo dam in mountainous torrents. International Journal of Sediment Research, 28(4), pp. 511-522

Iverson R.M. (1997) The physics of debris flows. Reviews of Geophysics 35(3); 245–296

Iverson R.M. (2003) The debris-flow rheology myth. Debris-flow hazards mitigation: mechanics, prediction, and assessment, Eds: Chen C.L., Rickenmann D., Millpress, Rotterdam, 1, 303-314

Iverson R.M., Logan M., LaHusen R.G., Berti M. (2010) The perfect debris flow? Aggregated results from 28 large scale experiments. Journal of Geophysical Research: Earth Surface (2003–2012), 115(F3), pp. 1-29

Iverson R.M., Reid M.E., Logan M., LaHusen R.G., Godt J.W., Griswold J.P (2011) Positive feedback and momentum growth during debris-flow entrainment of wet bed sediment. Nature Geoscience, 4(2), pp. 116-121

Kienholz H. (2003) Early warning systems related to mountain hazards. In: Early Warning Systems for Natural Disaster Reduction. Eds: Zschau J. and Kueppers A., Springer-Verlag Berlin Heidelberg, Chapter 5.24, pp. 555-564

Lien H.P. (2003) Design of slit dams for controlling stony debris flows. International Journal of Sediment Research, 18(1); 74-87

Pierson T.C., Costa J.E. (1987) A rheologic classification of subaerial sediment-water flows. In: Debris Flow/Avalanches: Process, Recognition, and Mitigation, Rev. Eng. Geol., Eds: Costa J.E. and Wieczoreck, Geolocical Society of America, Boulder, Colorado, Vol. 7, pp. 1-12

Rickenmann D. (1999) Empirical Relationships for Debris Flows. Natural Hazards 19; 47-77

Roth A., Kästli A., Frenez T. (2004) Debris flow mitigation by means of flexible barriers. Proc. 10th Congress INTERPRAEVENT 2004, Riva/Trient (Italy), 24-28 May 2004, Interpraevent, Klagenfurt, pp. 289-300

Saccomani C. (2009) Studio sperimentale, su modello fisico, dell'efficienza di frangiflutti galleggianti. Master Thesis, Facoltà di Scienze Matematiche, Fisiche e Naturali e Facoltà di Agraria, Università di Pisa, Italy; supervisor: Cappietti L., 89 pp.

Scheidl C., Chiari M., Kaitna R., Müllegger M., Krawtschuk A., Zimmermann T., Proske D. (2013) Analysing Debris-Flow Impact Models, Based on a Small Scale Modelling Approach. Surveys in Geophysics, 34(1); 121-140

Wehrmann H., Hübl J., Holzinger G. (2006) Classification of dams in torrential watersheds. In: Disaster Mitigation of Debris Flows, Slope Failures and Landslides, Proc. INTERPRAEVENT International Symposium, Niigata (Japan), 25-27 September 2006, Eds: Marui H., Marutan T., Watanabe N., Kawabe H., Gonda Y., Kimura M., Ochiai H., Ogawa K., Fiebiger G., Heumader J., Rudolf-Miklau F., Kienholz H., Mikos M., Universal Academy Press, Tokyo, Japan, Vol. 2, pp. 829-838

Wendeler C., Volkwein A., Roth A., Denk M., Wartmann S. (2007) Field measurements and numerical modelling of flexible debris flow barriers. Debris-Flow Hazards Mitig. Mech. Predict. Assess. Millpress, Rotterdam, pp. 681-687

Wendeler C., Volkwein A., Roth A., Herzog B., Hählen N., Wenger M. (2008). Hazard prevention using flexible multi-level debris flow barriers. Protection Against Debris Flows by Installation of 13 Flexible Barriers in The Milibach River (Canton Berne, Switzerland). In: Proceedings of the INTERPRAEVENT International Symposium, Dornbirn, Austria, 2008, Eds: Mikos, M.; Huebl, J.; Koboltschnig, G., Vol. 1, pp. 547-554

Zanuttigh B., Lamberti A. (2006) Experimental analysis of the impact of dry avalanches on structures and implication for debris flows. Journal of Hydraulic Research, 44(4); 522–534

Zhang S. (1993) A comprehensive approach to the observation and prevention of debris flows in China. Natural Hazards, 7(1); 1-23

APPENDICES

APPENDIX A: Technical net drawings

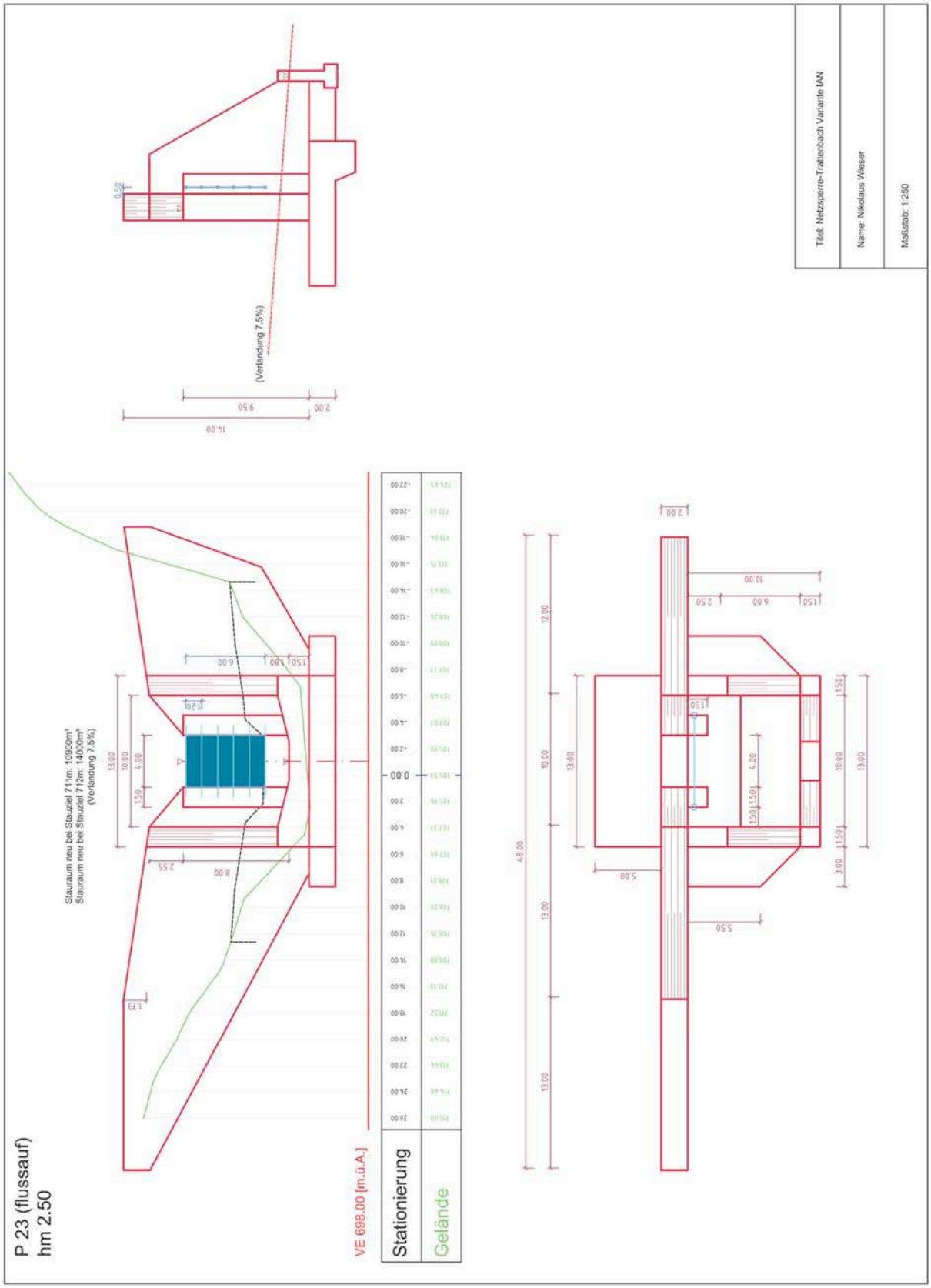

Figure 85. Technical drawing of the net slit dam (drawn by Nikolaus Wieser – IAN).

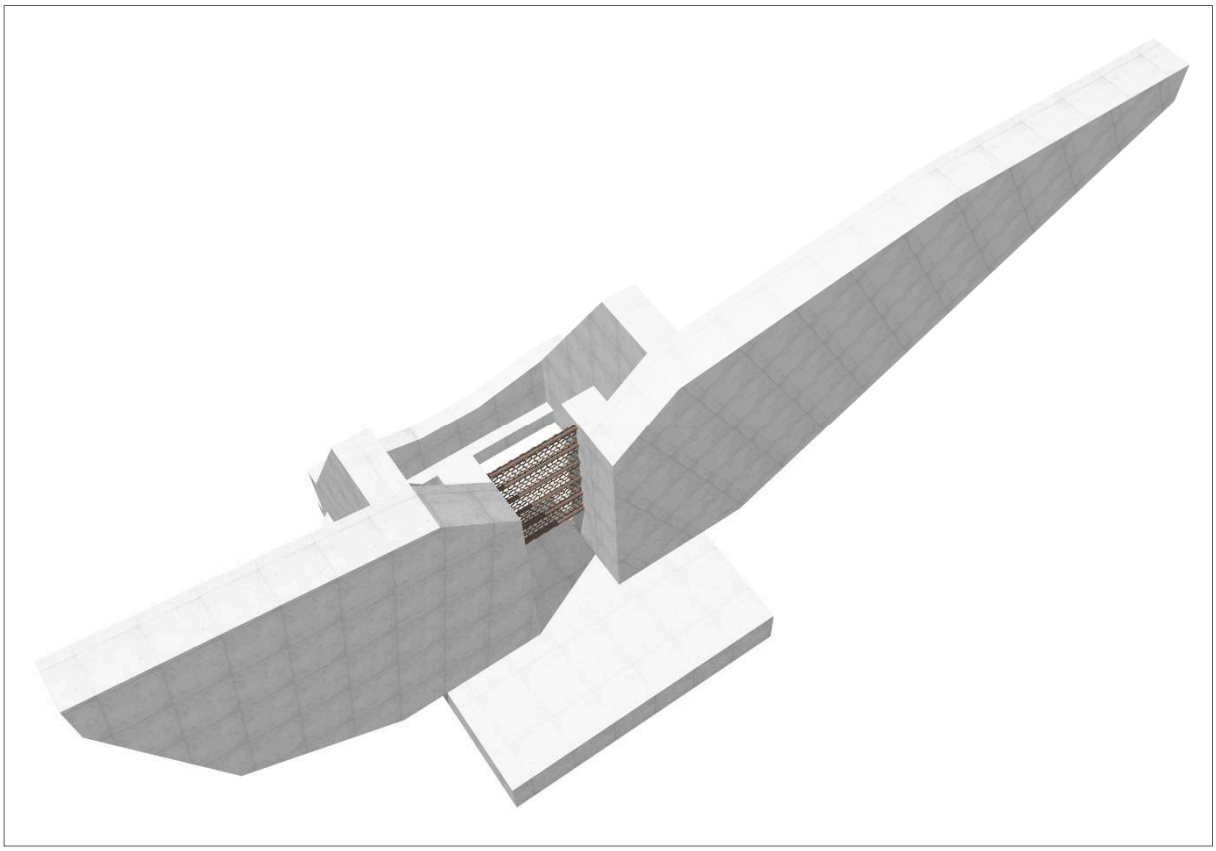

Figure 86. 3D model of the slit net dam, upstream view (drawn by M. Wagner).

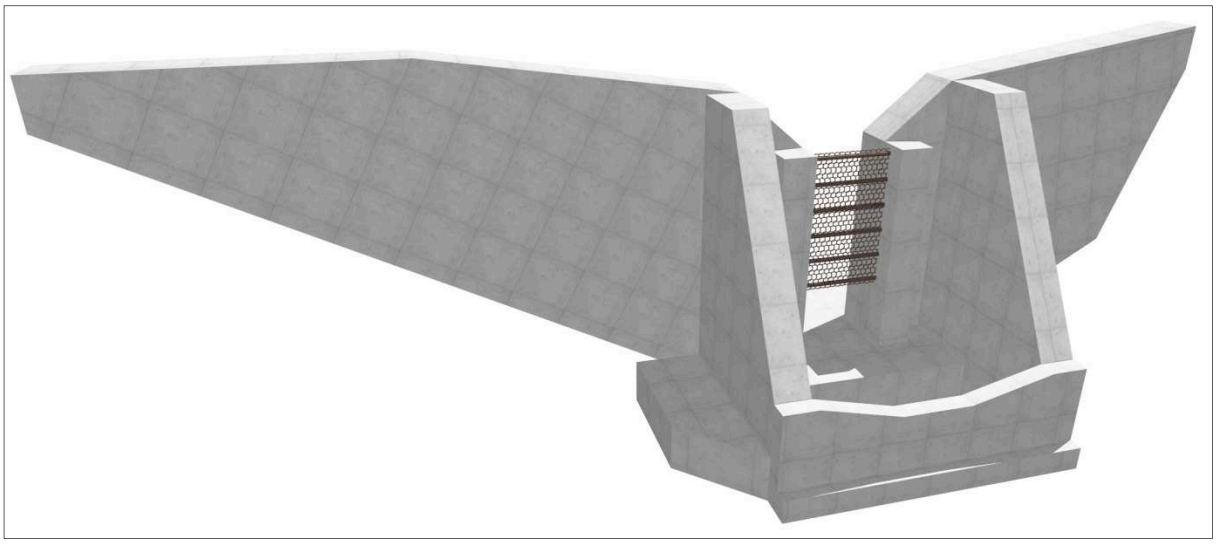

Figure 87. 3D model of the slit net dam, downstream view (drawn by M. Wagner).

APPENDIX B: Test sequences

The following Figures refer to the sequences of the sixteen experimental tests. The time steps are synchronized with the debris flow released. Time t=0 s relates to the passage of the flow at section L4 (end of the wood inlet channel) i.e. when the debris flow starts to flow into the model.

Test 1.1

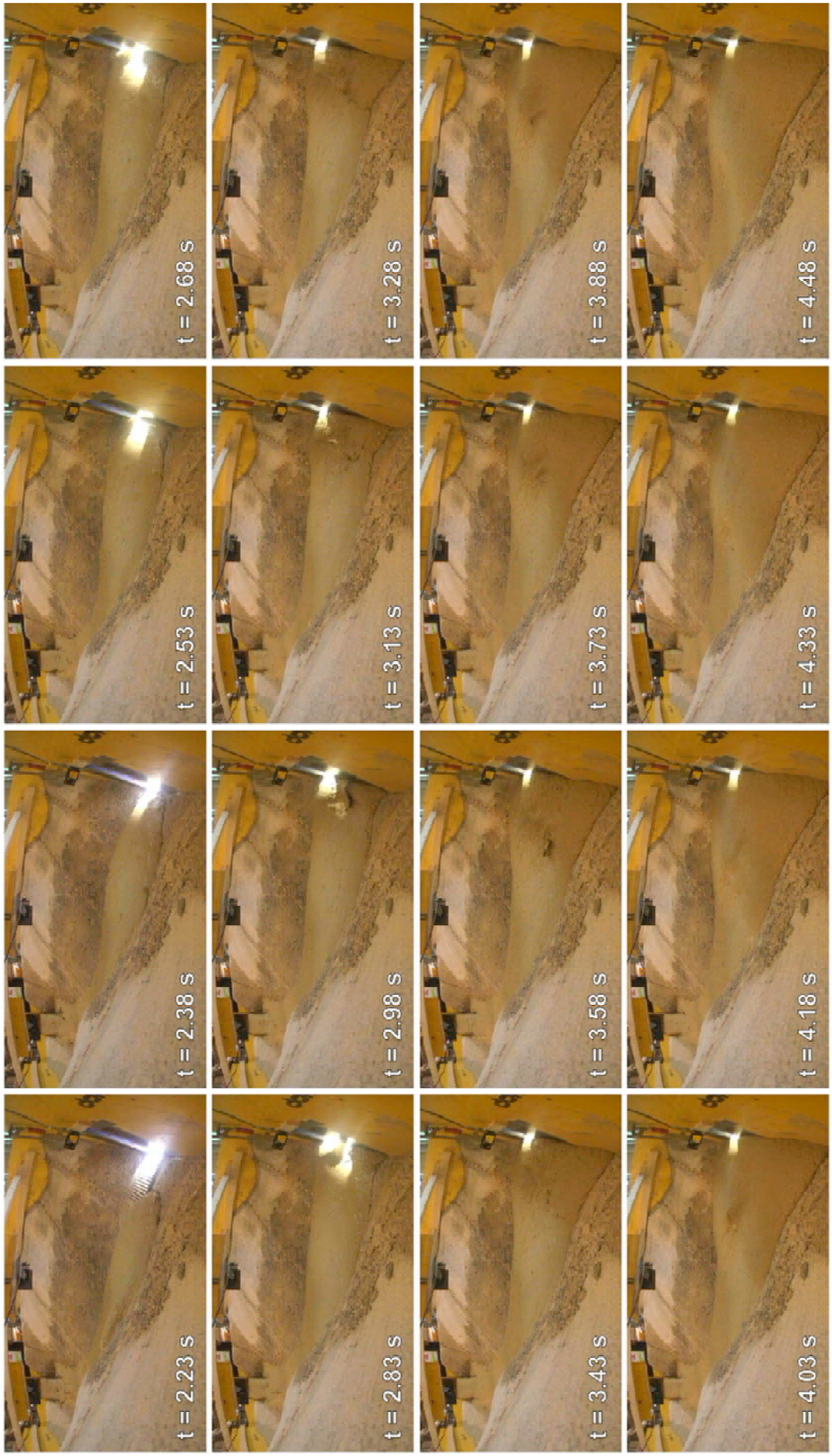
t = 2.23 s
t = 2.38 s
t = 2.53 s
t = 2.68 s
t = 2.83 s
t = 2.98 s
t = 3.13 s
t = 3.28 s
t = 3.43 s
t = 3.58 s
t = 3.73 s
t = 3.88 s
t = 4.03 s
t = 4.18 s
t = 4.33 s
t = 4.48 s

Test 1.2

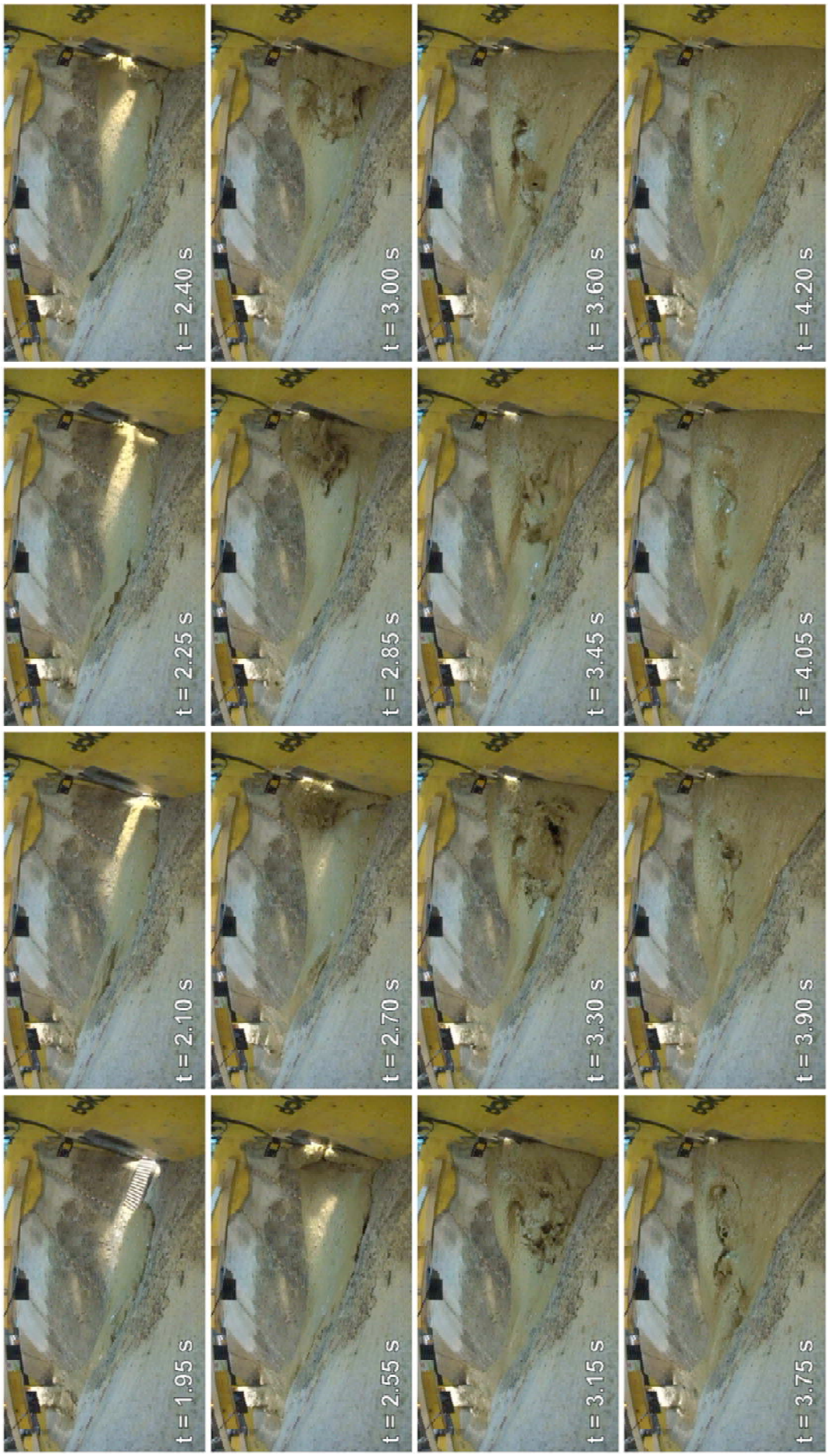
t = 1.95 s
t = 2.10 s
t = 2.25 s
t = 2.40 s
t = 2.55 s
t = 2.70 s
t = 2.85 s
t = 3.00 s
t = 3.15 s
t = 3.30 s
t = 3.45 s
t = 3.60 s
t = 3.75 s
t = 3.90 s
t = 4.05 s
t = 4.20 s

Test 1.3

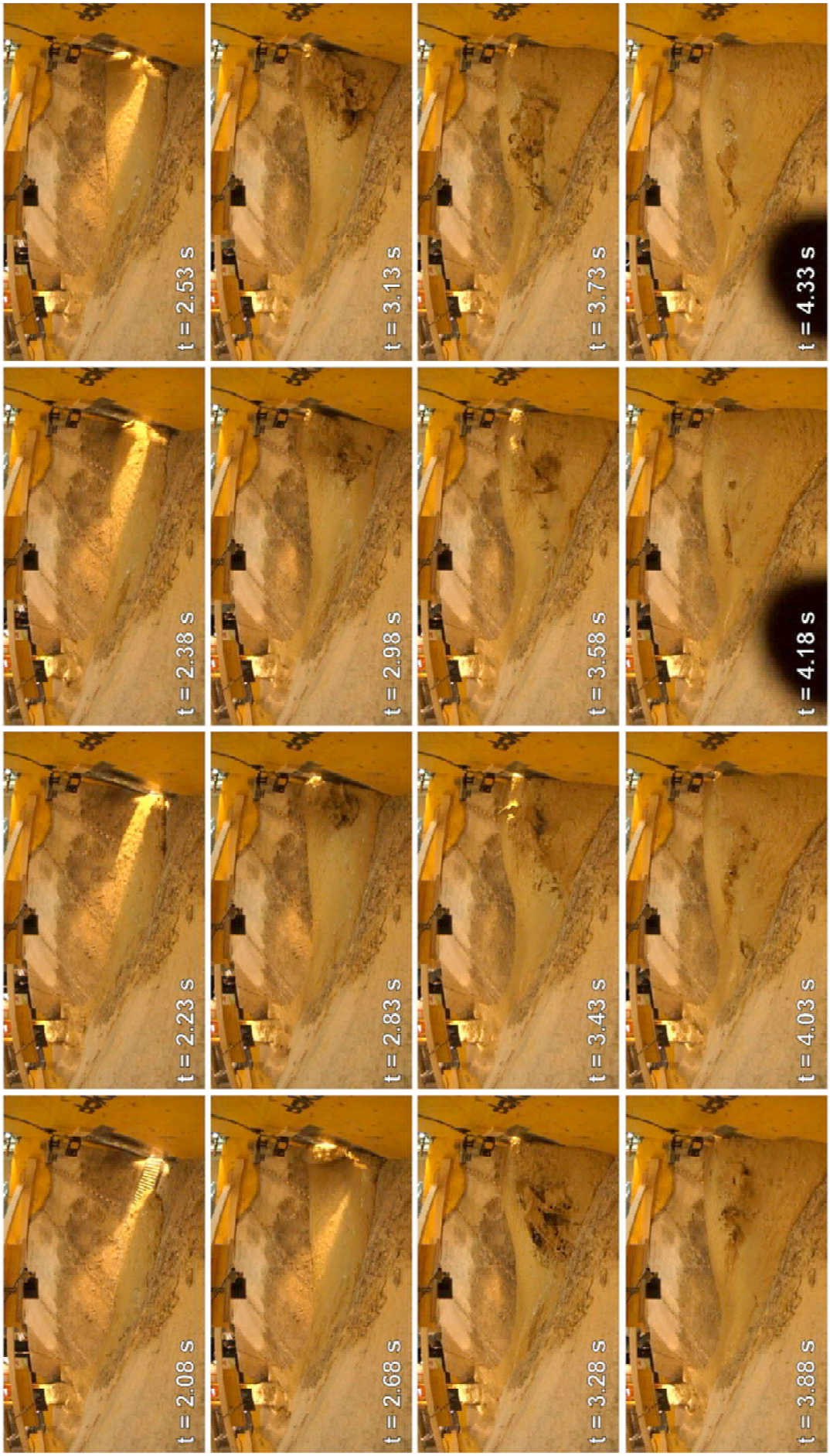
t = 2.08 s
t = 2.23 s
t = 2.38 s
t = 2.53 s
t = 2.68 s
t = 2.83 s
t = 2.98 s
t = 3.13 s
t = 3.28 s
t = 3.43 s
t = 3.58 s
t = 3.73 s
t = 3.88 s
t = 4.03 s
t = 4.18 s
t = 4.33 s

Test 1.4

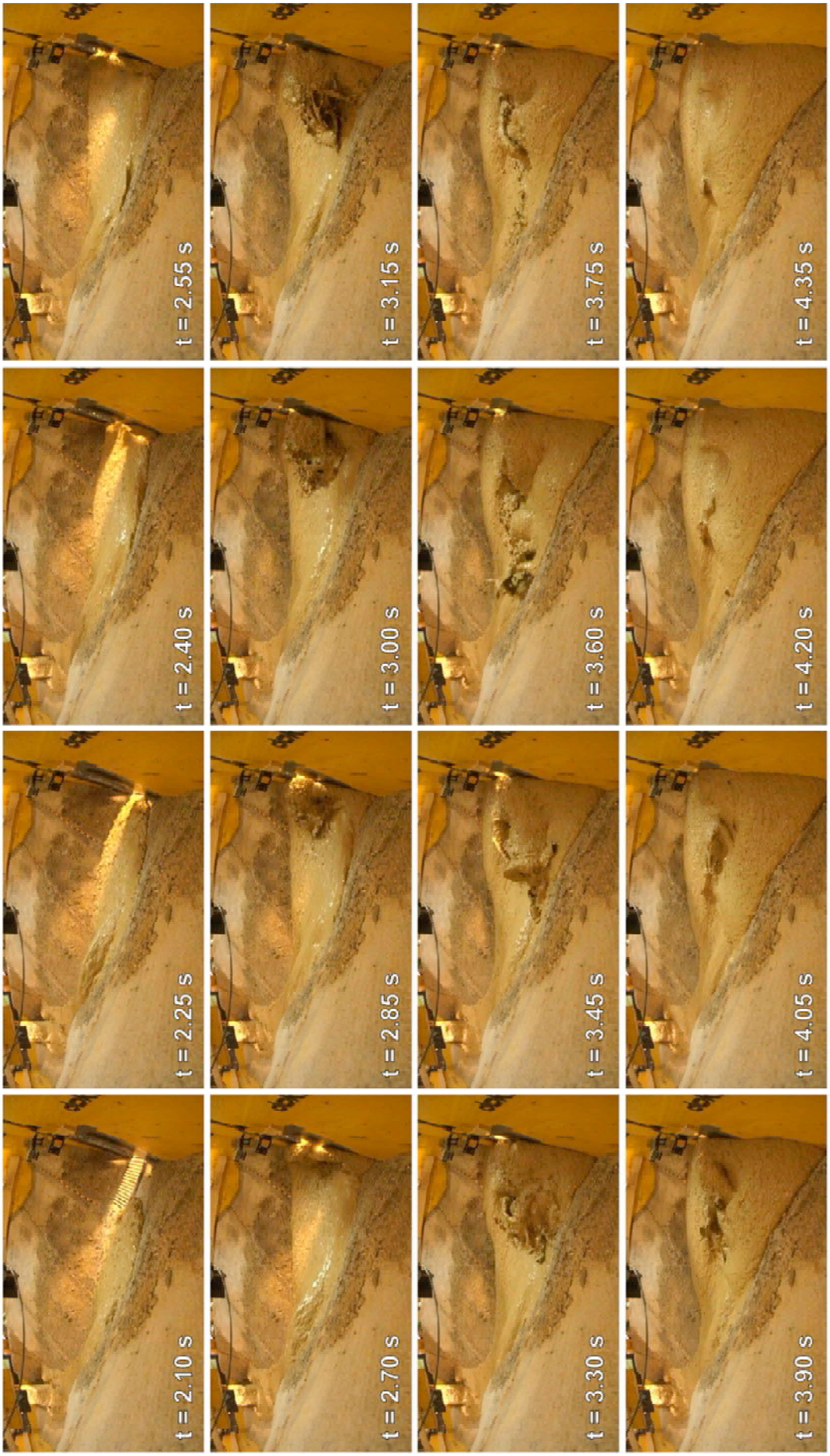
t = 2.10 s
t = 2.25 s
t = 2.40 s
t = 2.55 s
t = 2.70 s
t = 2.85 s
t = 3.00 s
t = 3.15 s
t = 3.30 s
t = 3.45 s
t = 3.60 s
t = 3.75 s
t = 3.90 s
t = 4.05 s
t = 4.20 s
t = 4.35 s

Test 2.1

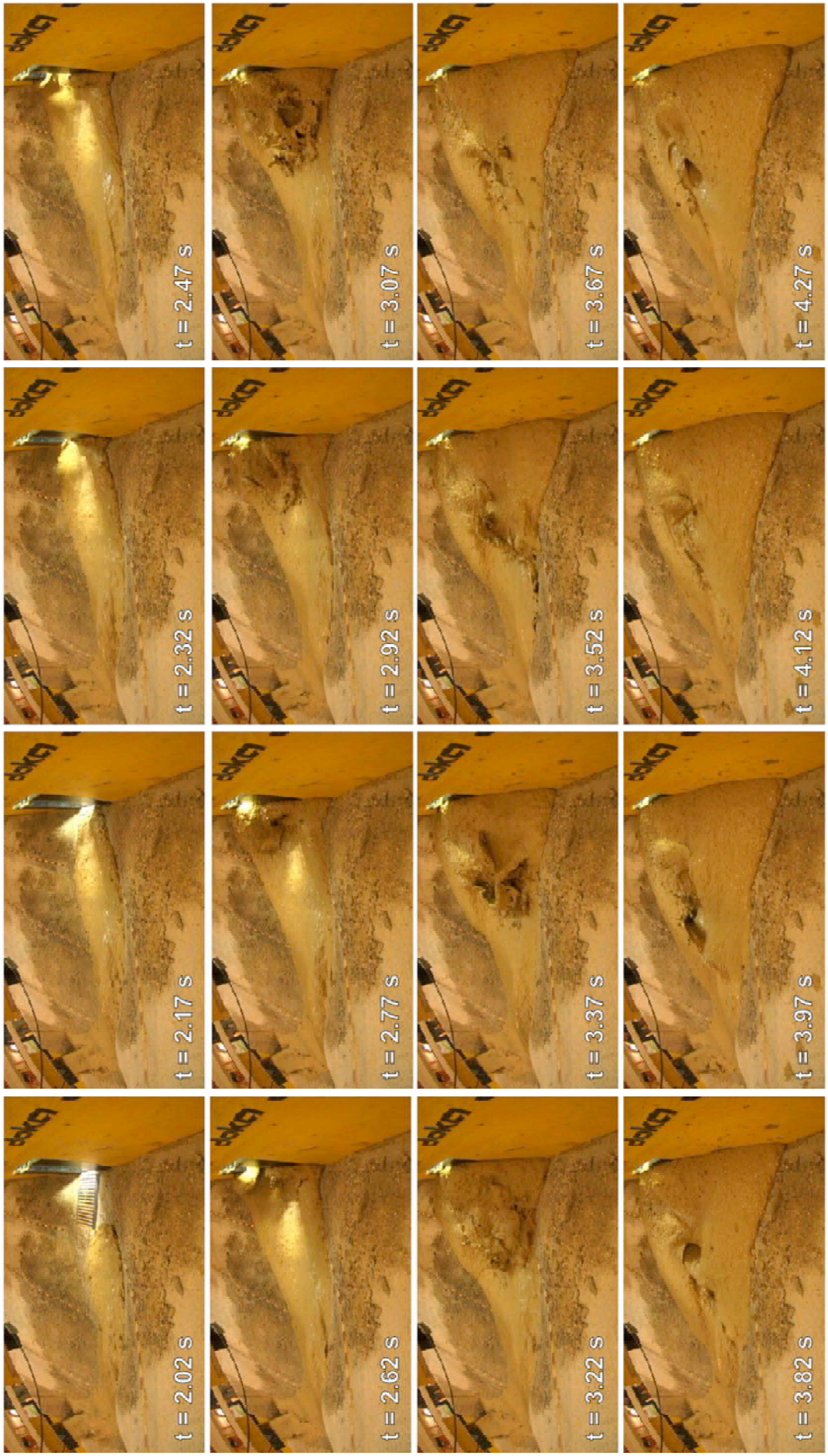
t = 2.02 s
t = 2.17 s
t = 2.32 s
t = 2.47 s
t = 2.62 s
t = 2.77 s
t = 2.92 s
t = 3.07 s
t = 3.22 s
t = 3.37 s
t = 3.52 s
t = 3.67 s
t = 3.82 s
t = 3.97 s
t = 4.12 s
t = 4.27 s

Test 2.2

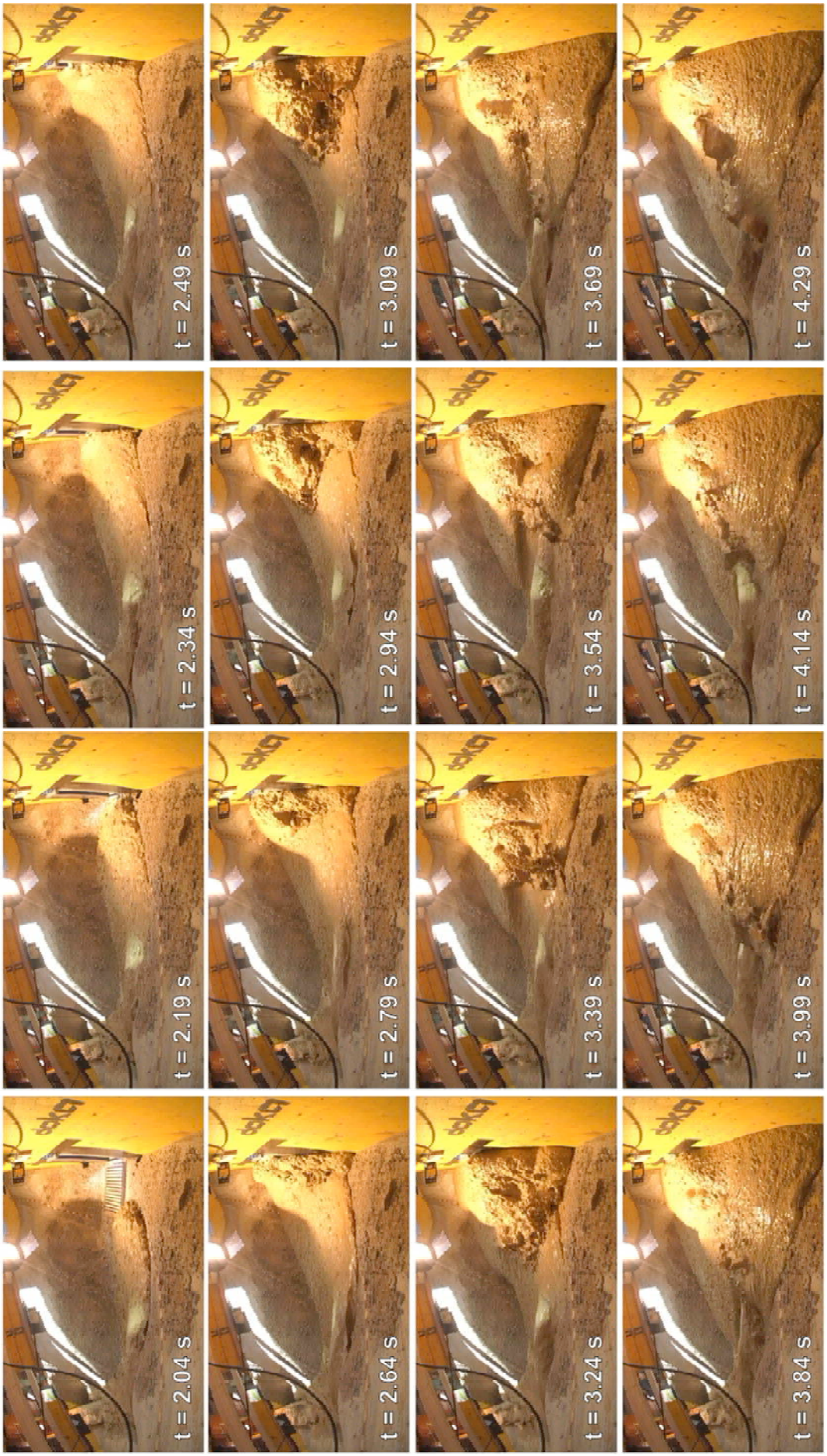
t = 2.04 s
t = 2.19 s
t = 2.34 s
t = 2.49 s
t = 2.64 s
t = 2.79 s
t = 2.94 s
t = 3.09 s
t = 3.24 s
t = 3.39 s
t = 3.54 s
t = 3.69 s
t = 3.84 s
t = 3.99 s
t = 4.14 s
t = 4.29 s

Test 2.3

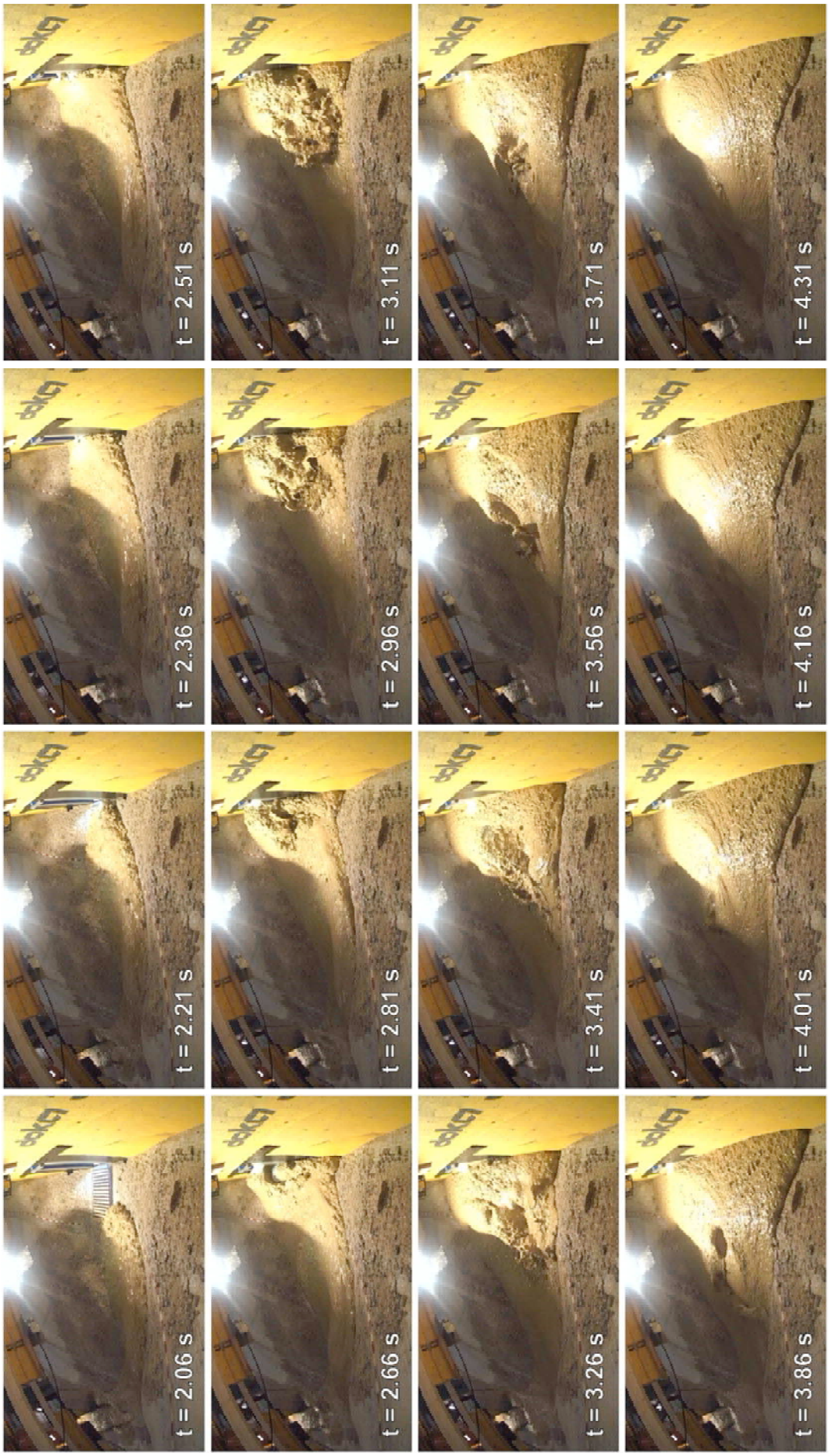
t = 2.06 s
t = 2.21 s
t = 2.36 s
t = 2.51 s
t = 2.66 s
t = 2.81 s
t = 2.96 s
t = 3.11 s
t = 3.26 s
t = 3.41 s
t = 3.56 s
t = 3.71 s
t = 3.86 s
t = 4.01 s
t = 4.16 s
t = 4.31 s

Test 2.4

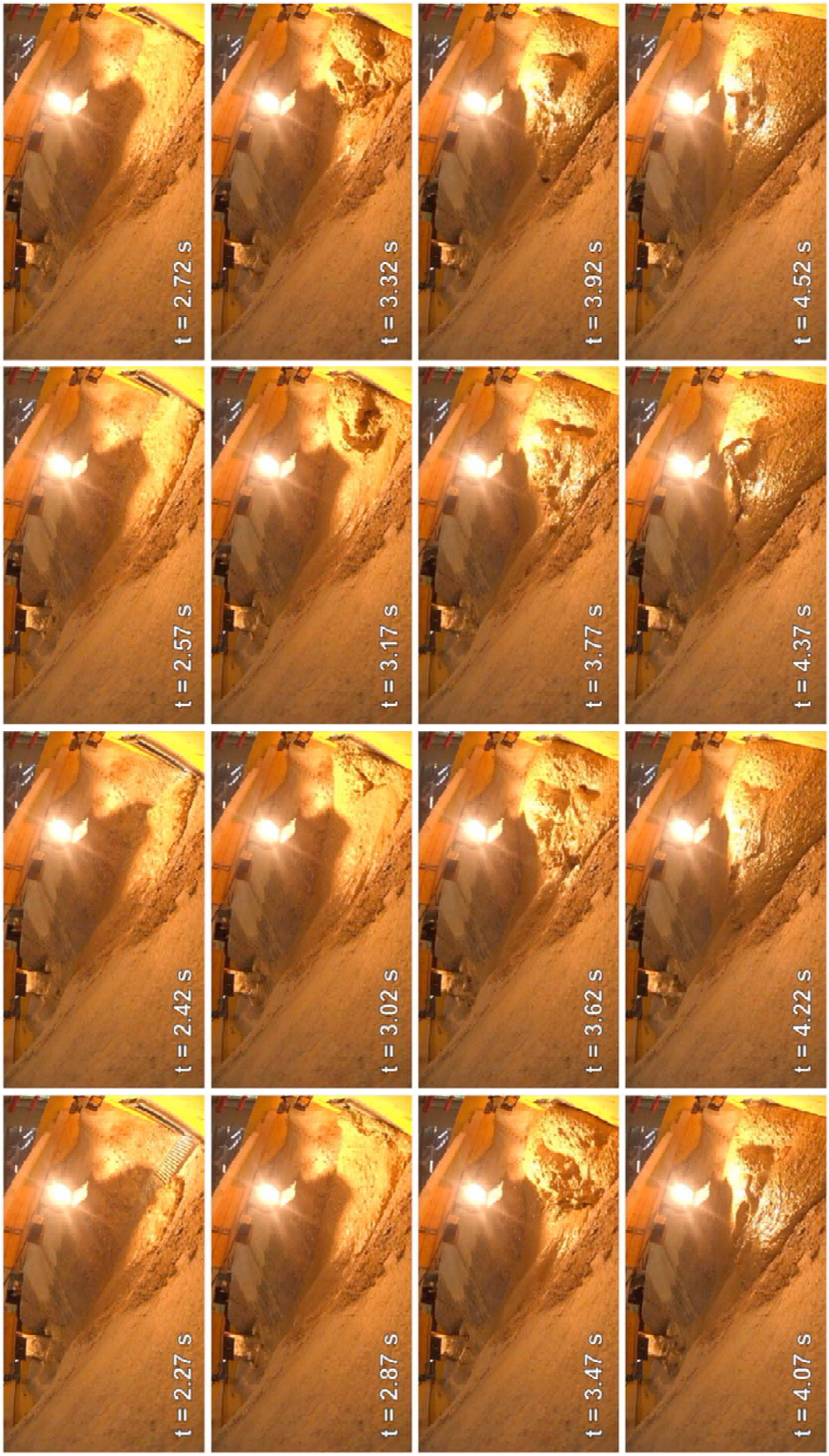
t = 2.27 s
t = 2.42 s
t = 2.57 s
t = 2.72 s
t = 2.87 s
t = 3.02 s
t = 3.17 s
t = 3.32 s
t = 3.47 s
t = 3.62 s
t = 3.77 s
t = 3.92 s
t = 4.07 s
t = 4.22 s
t = 4.37 s
t = 4.52 s

Test 3.1

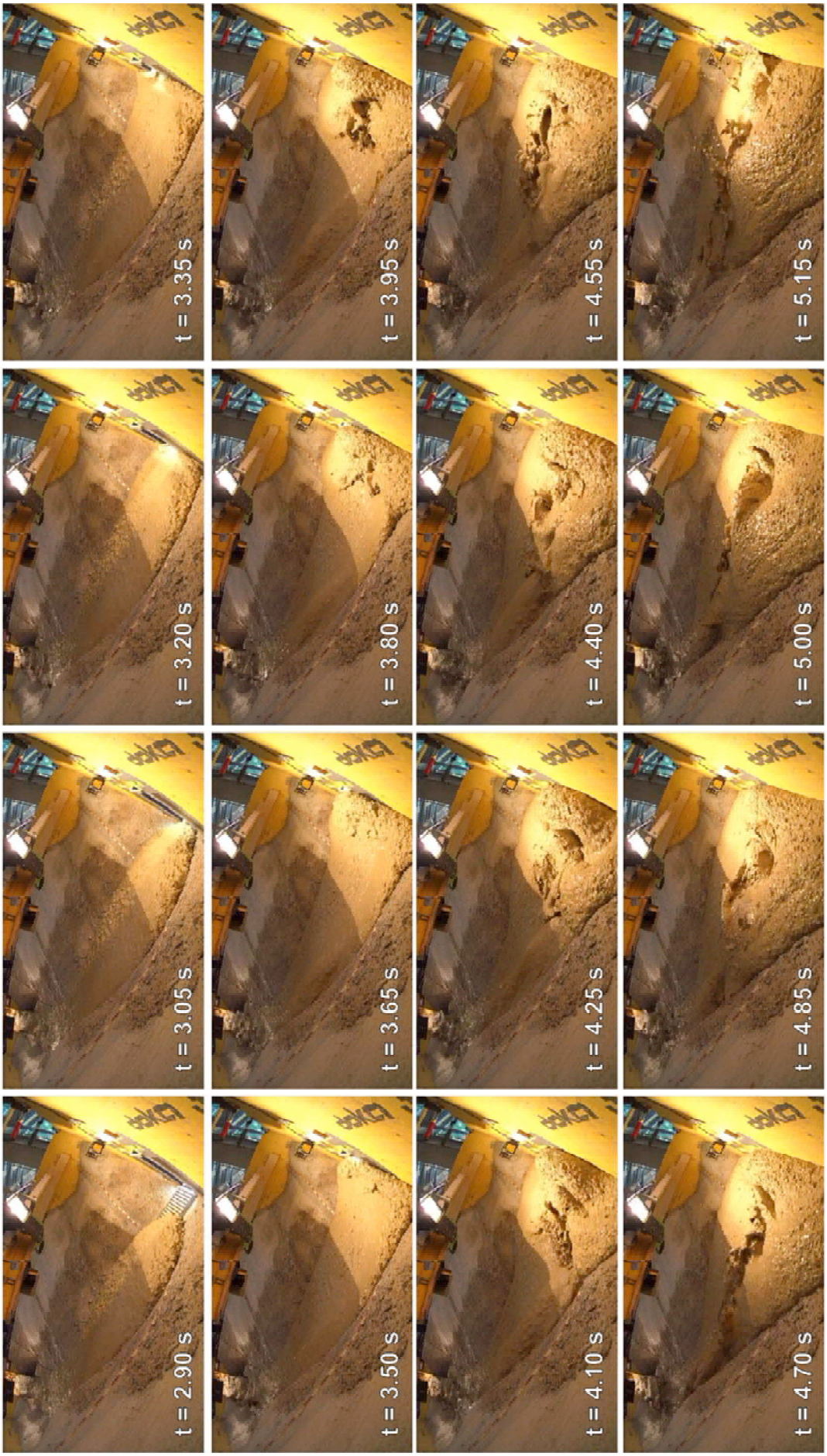
t = 2.90 s
t = 3.05 s
t = 3.20 s
t = 3.35 s
t = 3.50 s
t = 3.65 s
t = 3.80 s
t = 3.95 s
t = 4.10 s
t = 4.25 s
t = 4.40 s
t = 4.55 s
t = 4.70 s
t = 4.85 s
t = 5.00 s
t = 5.15 s

Test 3.2

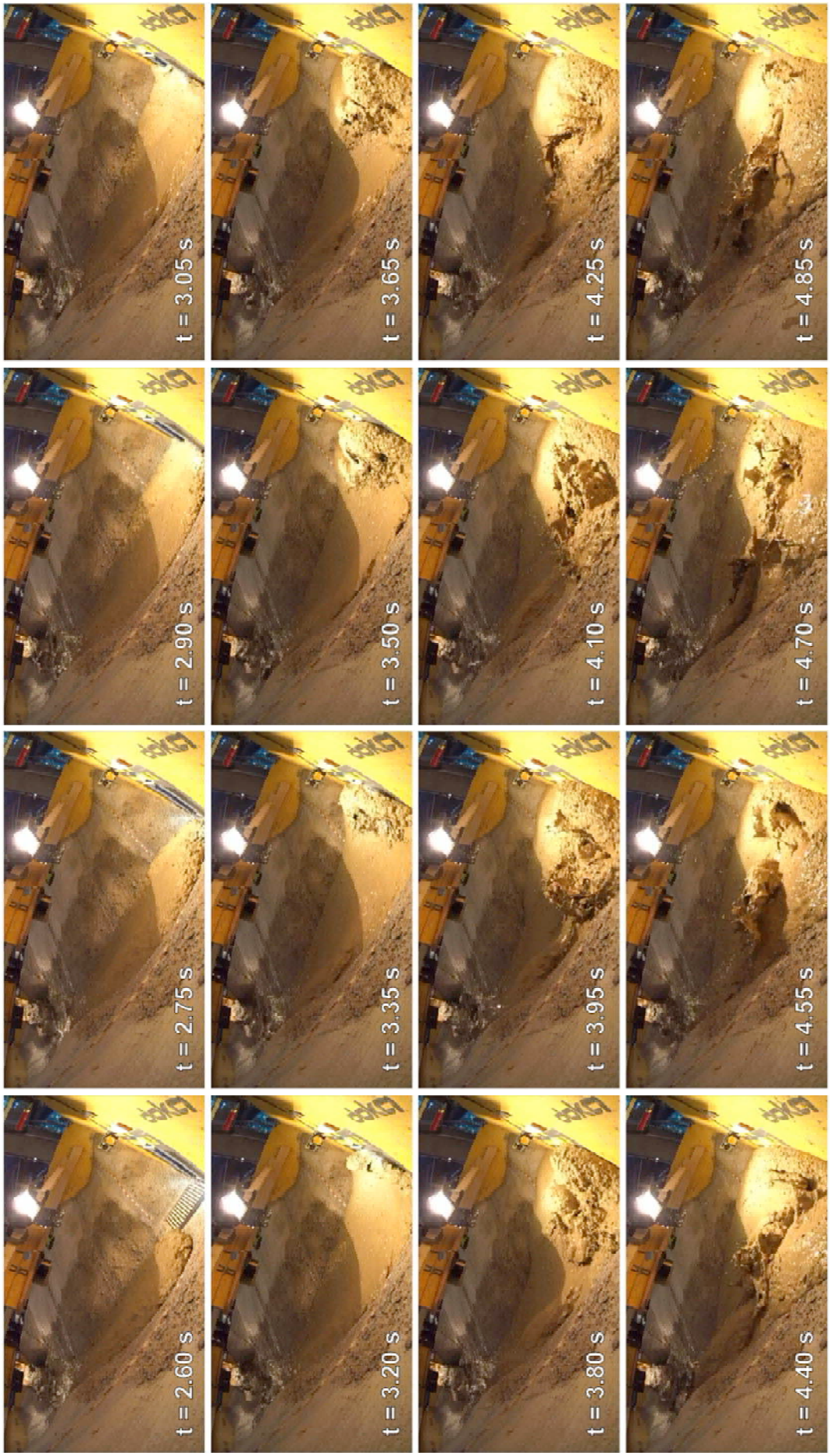
t = 2.60 s
t = 2.75 s
t = 2.90 s
t = 3.05 s
t = 3.20 s
t = 3.35 s
t = 3.50 s
t = 3.65 s
t = 3.80 s
t = 3.95 s
t = 4.10 s
t = 4.25 s
t = 4.40 s
t = 4.55 s
t = 4.70 s
t = 4.85 s

Test 3.3

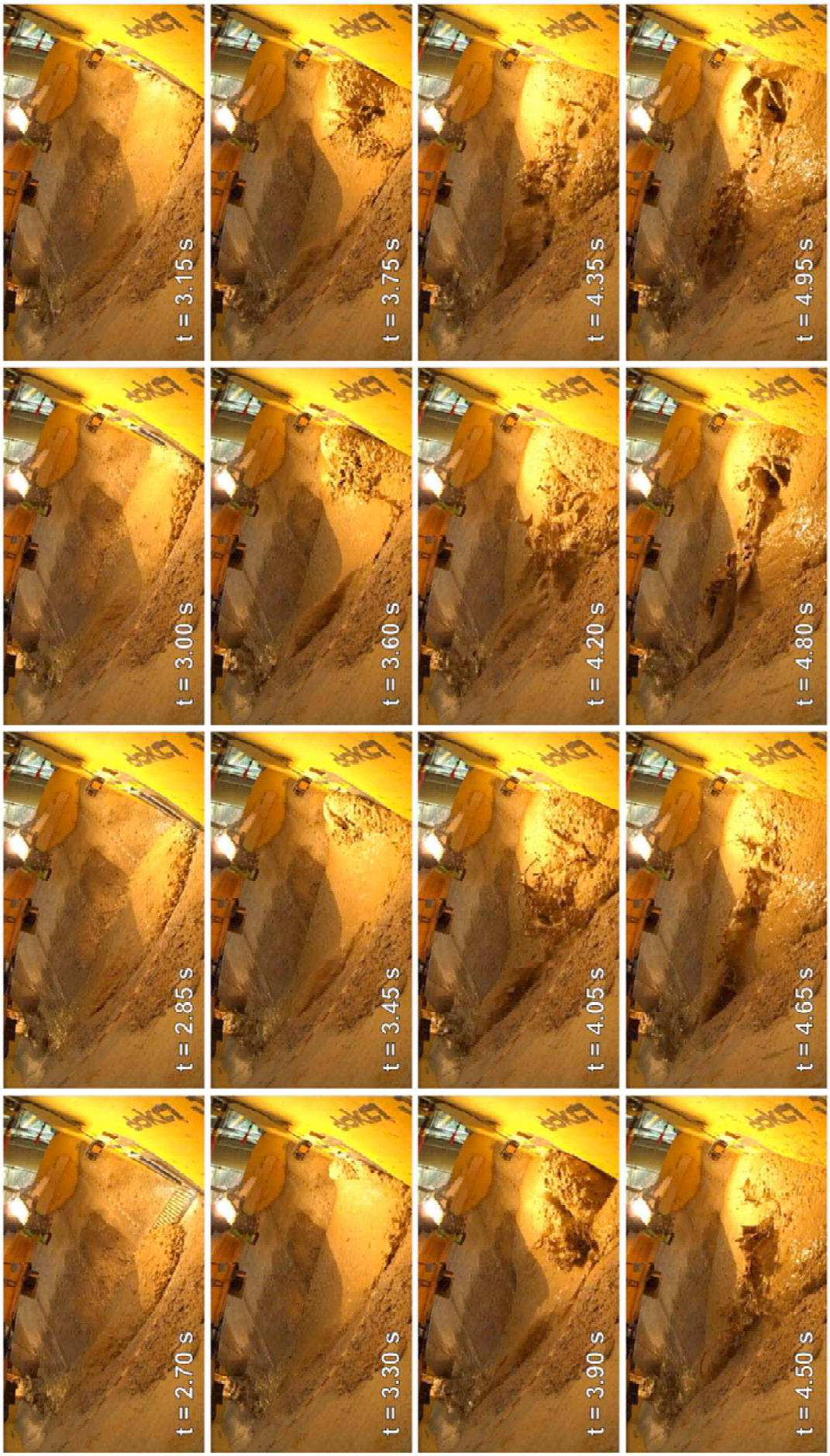
t = 2.70 s
t = 2.85 s
t = 3.00 s
t = 3.15 s
t = 3.30 s
t = 3.45 s
t = 3.60 s
t = 3.75 s
t = 3.90 s
t = 4.05 s
t = 4.20 s
t = 4.35 s
t = 4.50 s
t = 4.65 s
t = 4.80 s
t = 4.95 s

Test 3.4

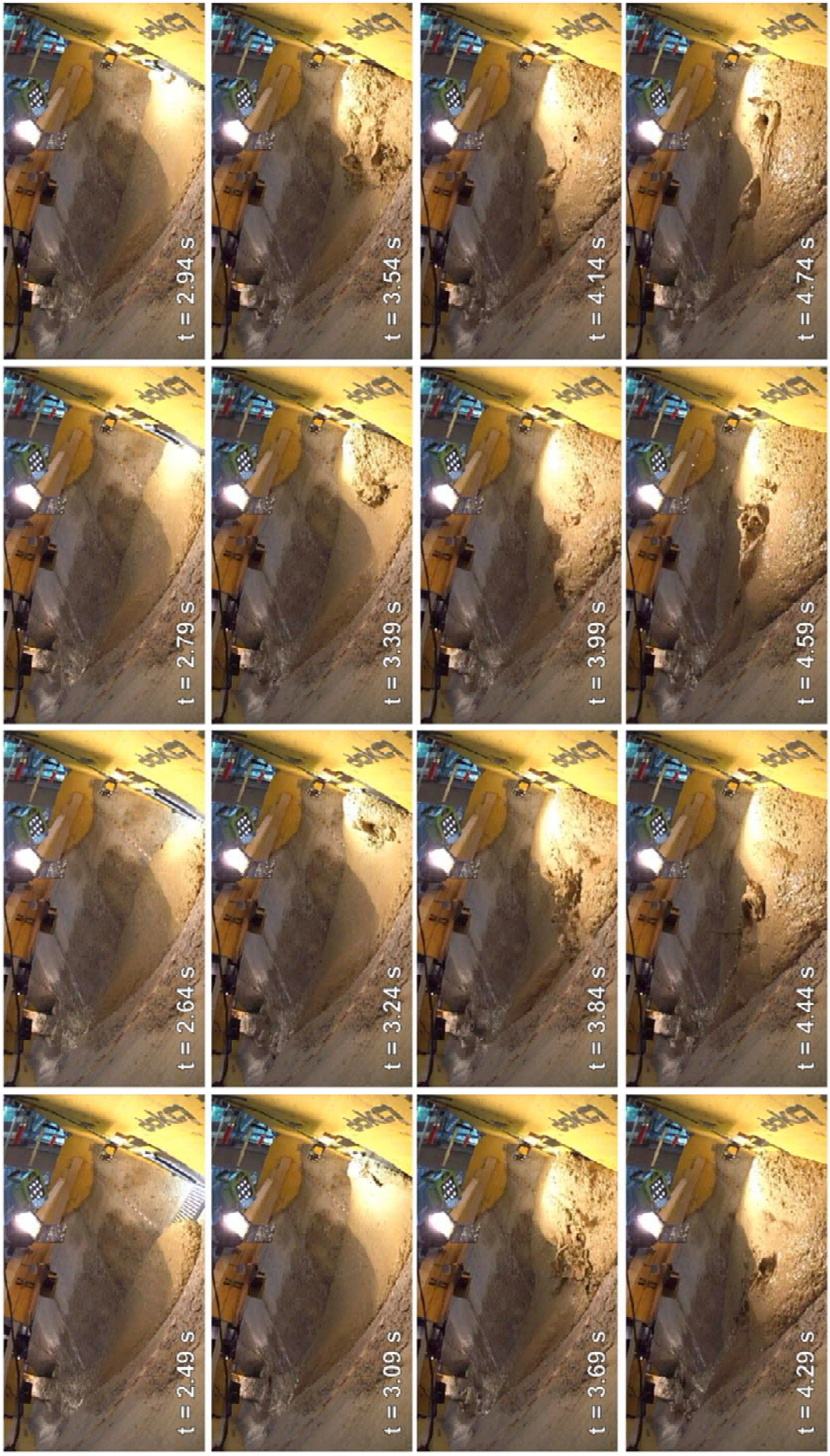
t = 2.49 s
t = 2.64 s
t = 2.79 s
t = 2.94 s
t = 3.09 s
t = 3.24 s
t = 3.39 s
t = 3.54 s
t = 3.69 s
t = 3.84 s
t = 3.99 s
t = 4.14 s
t = 4.29 s
t = 4.44 s
t = 4.59 s
t = 4.74 s

Test 4.1

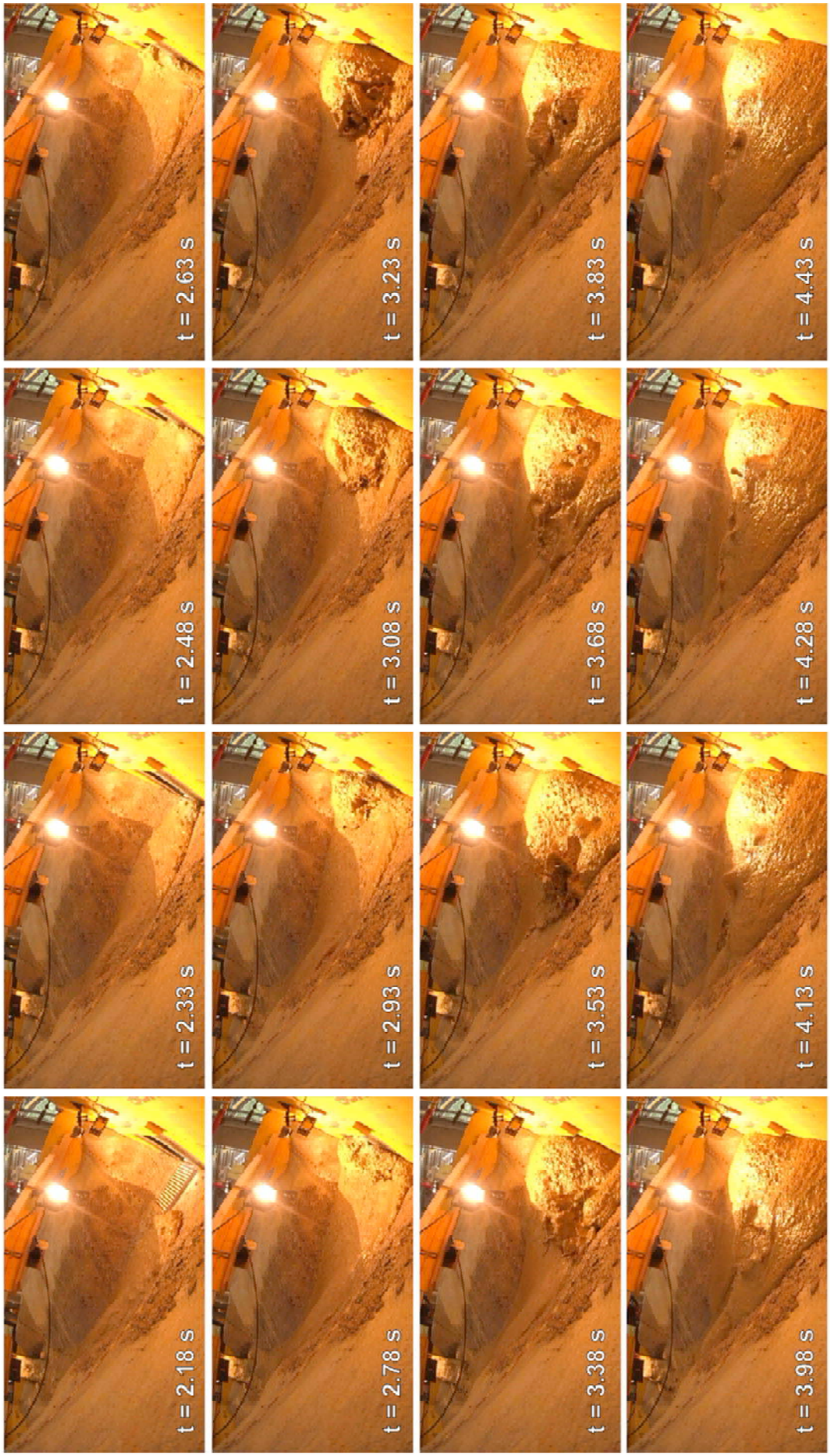
t = 2.18 s
t = 2.33 s
t = 2.48 s
t = 2.63 s
t = 2.78 s
t = 2.93 s
t = 3.08 s
t = 3.23 s
t = 3.38 s
t = 3.53 s
t = 3.68 s
t = 3.83 s
t = 3.98 s
t = 4.13 s
t = 4.28 s
t = 4.43 s

Test 4.2

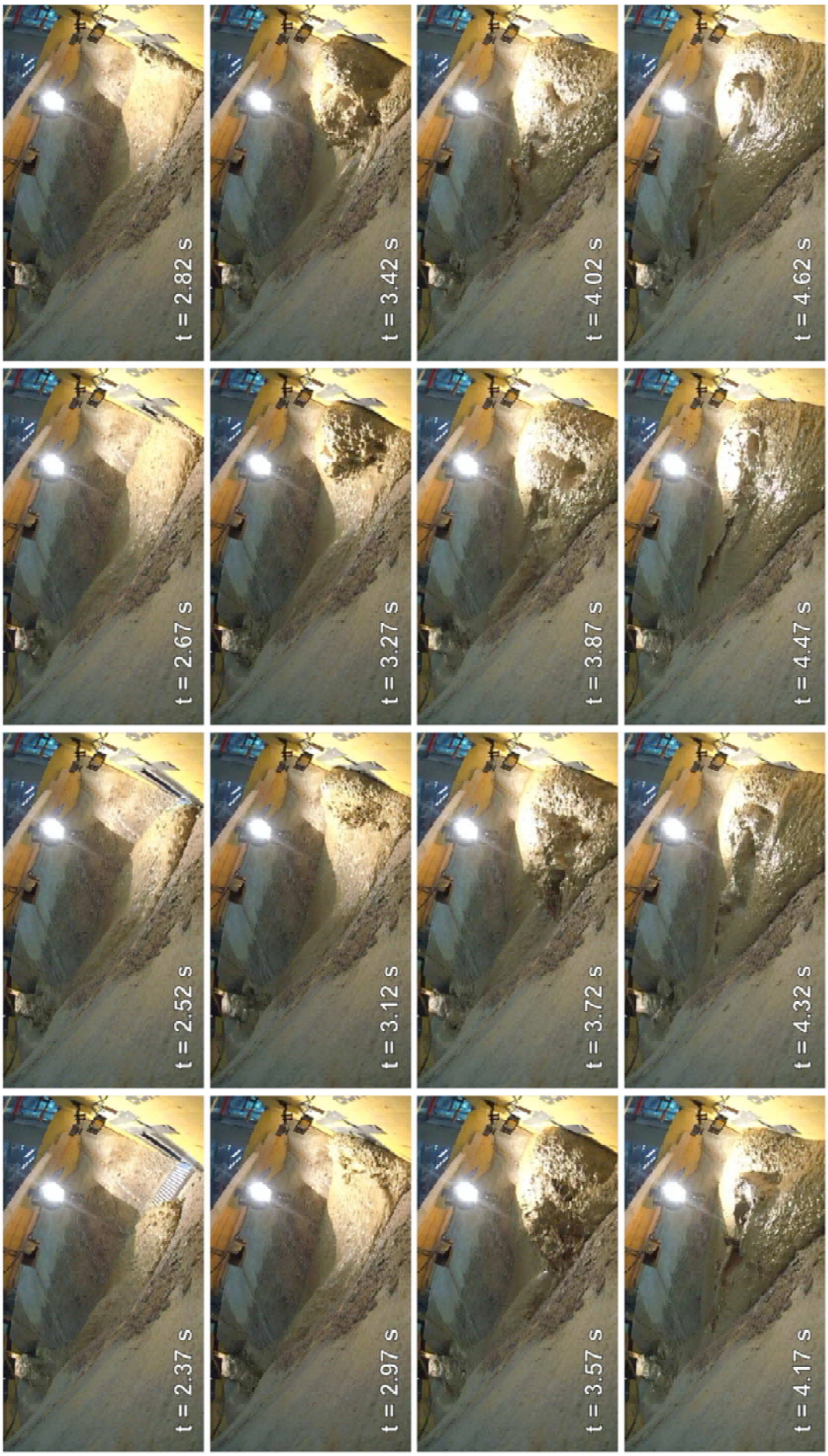
t = 2.37 s
t = 2.52 s
t = 2.67 s
t = 2.82 s
t = 2.97 s
t = 3.12 s
t = 3.27 s
t = 3.42 s
t = 3.57 s
t = 3.72 s
t = 3.87 s
t = 4.02 s
t = 4.17 s
t = 4.32 s
t = 4.47 s
t = 4.62 s

Test 4.3

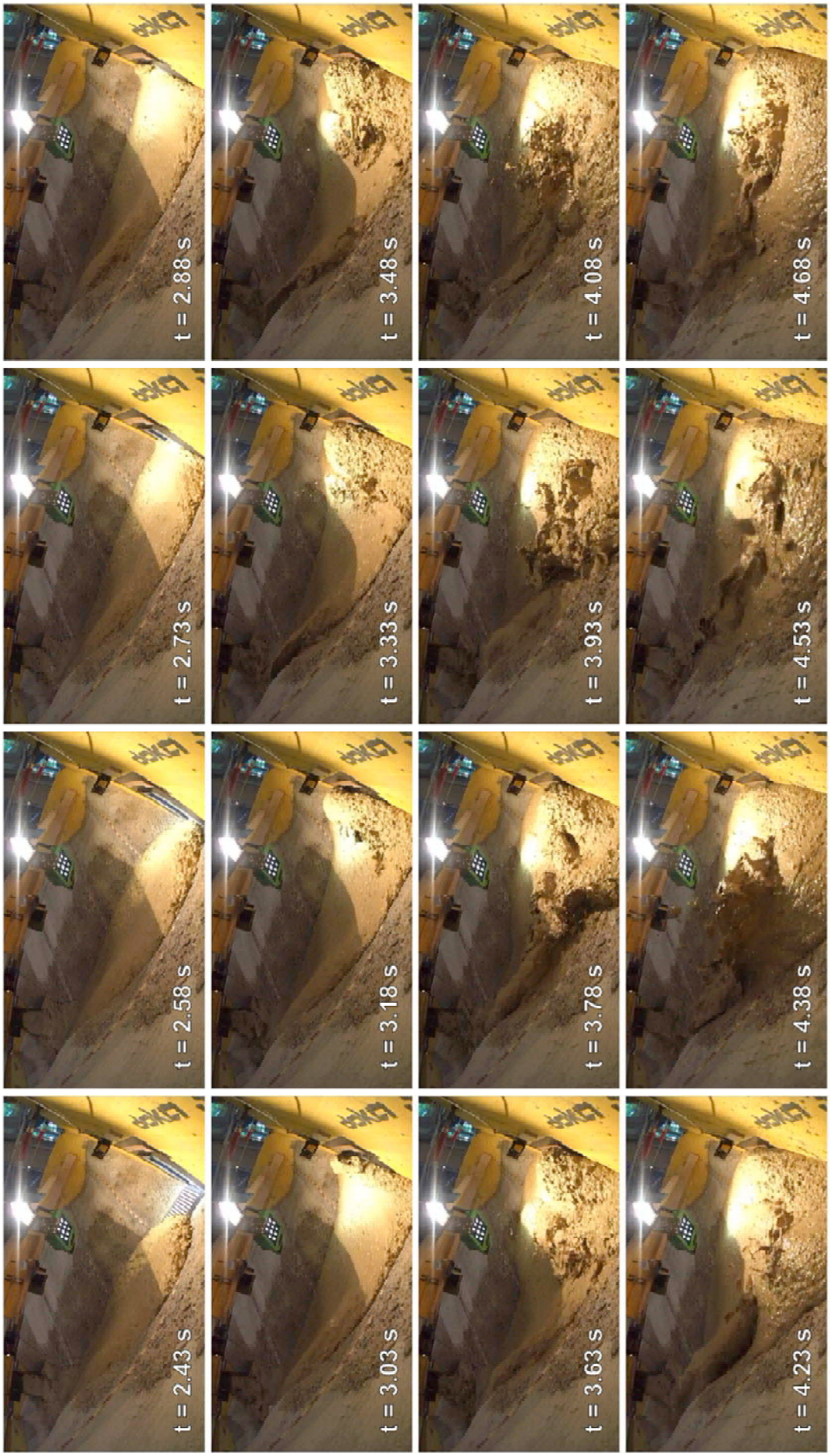
t = 2.43 s
t = 2.58 s
t = 2.73 s
t = 2.88 s
t = 3.03 s
t = 3.18 s
t = 3.33 s
t = 3.48 s
t = 3.63 s
t = 3.78 s
t = 3.93 s
t = 4.08 s
t = 4.23 s
t = 4.38 s
t = 4.53 s
t = 4.68 s

Test 5

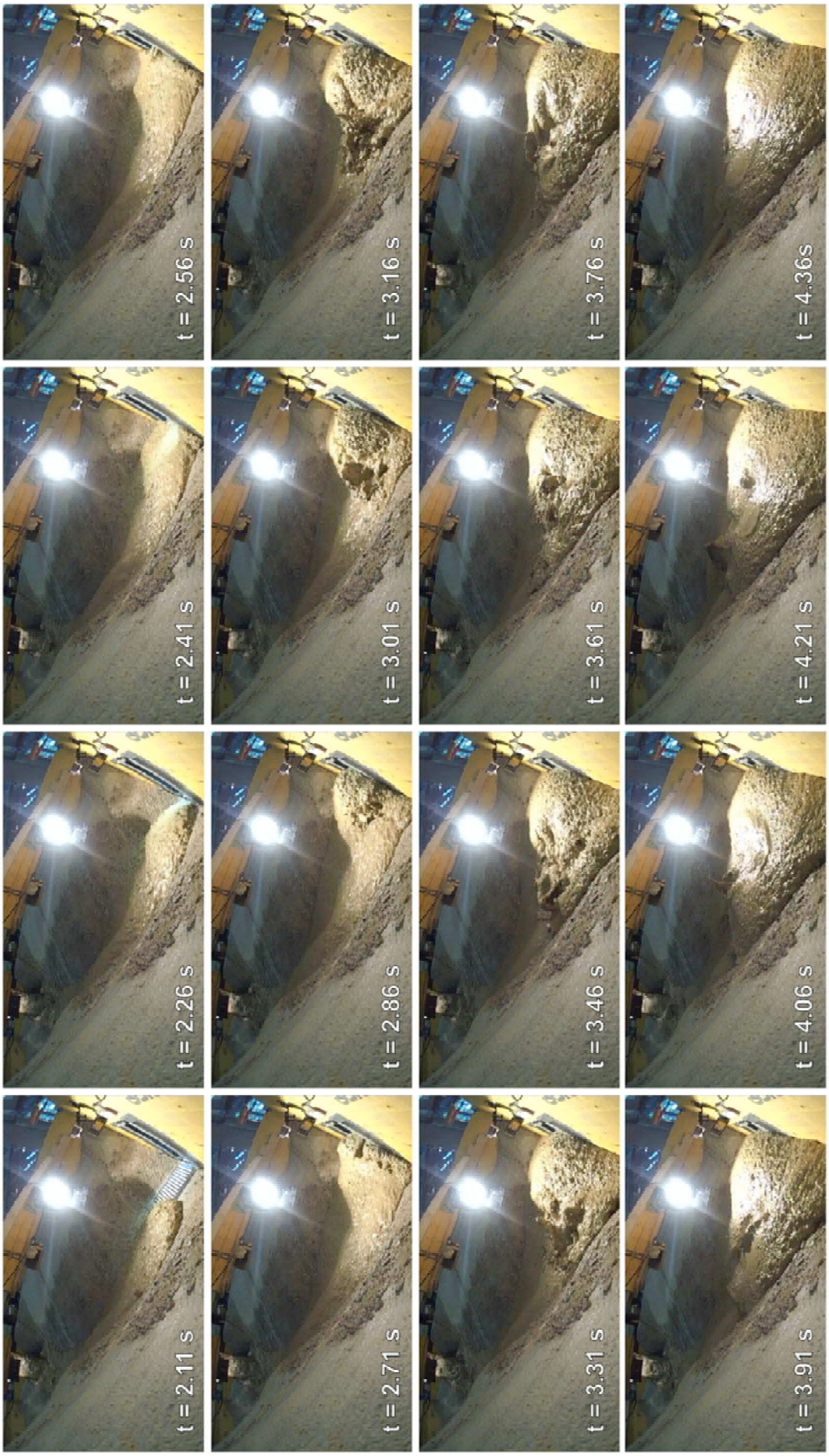
t = 2.11 s
t = 2.26 s
t = 2.41 s
t = 2.56 s
t = 2.71 s
t = 2.86 s
t = 3.01 s
t = 3.16 s
t = 3.31 s
t = 3.46 s
t = 3.61 s
t = 3.76 s
t = 3.91 s
t = 4.06 s
t = 4.21 s
t = 4.36s

APPENDIX C: 3D Surfaces

The following Figures report the 3D surface obtained with the software Surfer. They show the material deposited in the model at the end of the tests. The elaborations were obtained from the scans provided by the laser scanner.

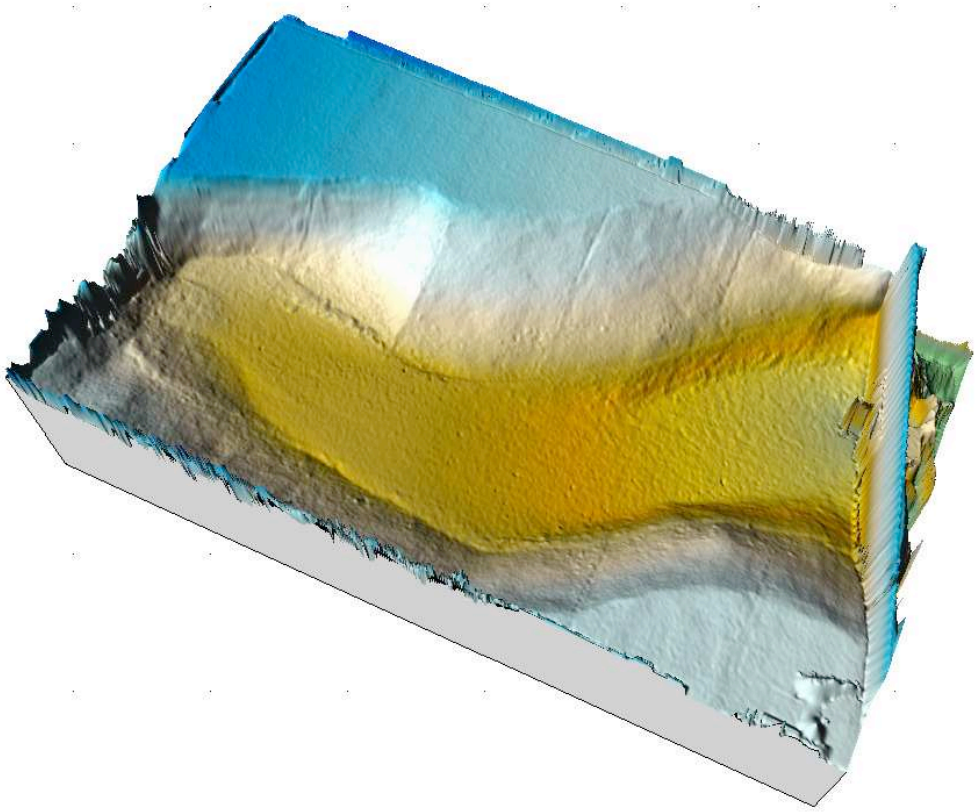

Figure 88. Deposited material for Test 1.1.

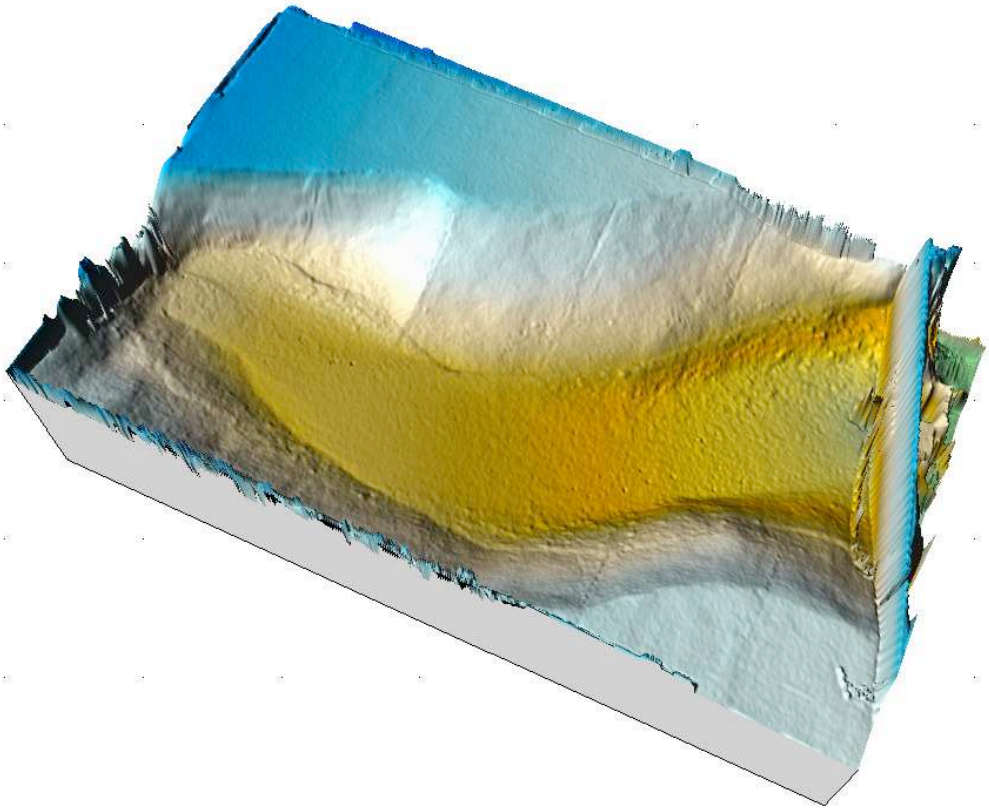

Figure 89. Deposited material for Test 1.2.

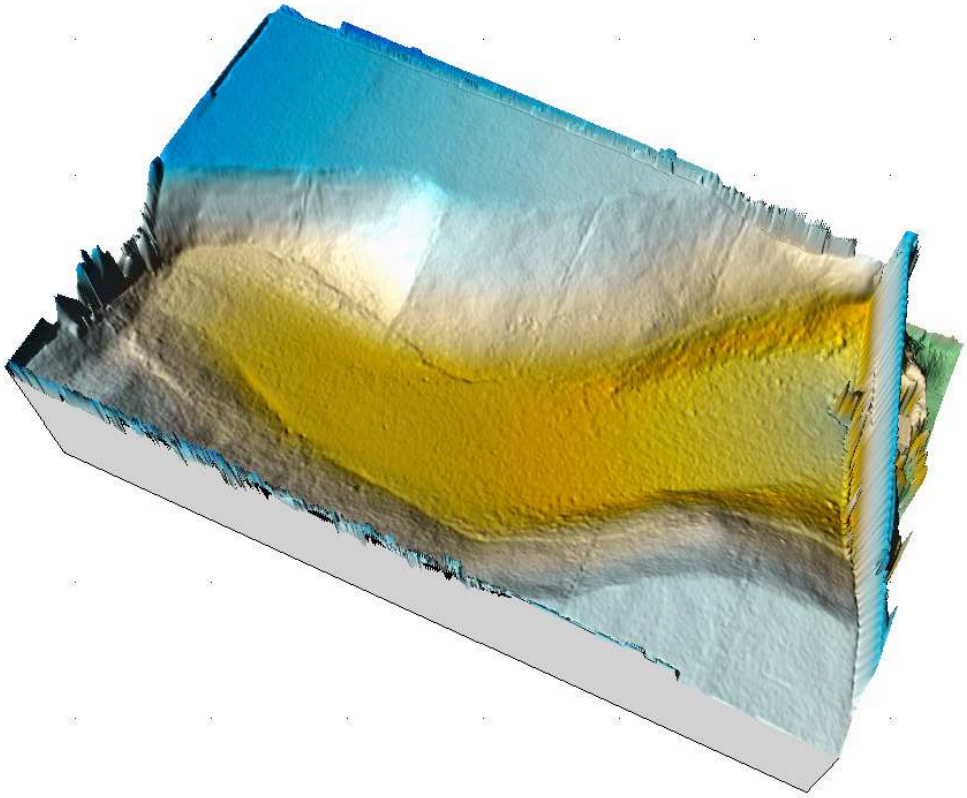

Figure 90. Deposited material for Test 1.3.

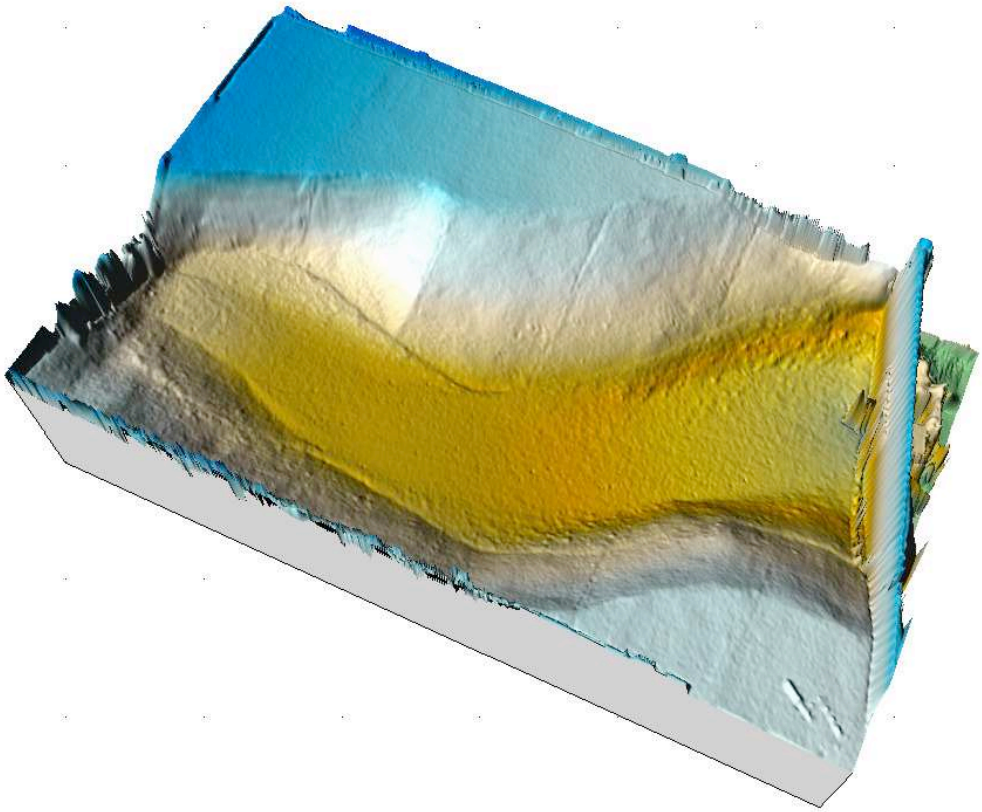

Figure 91. Deposited material for Test 1.4.

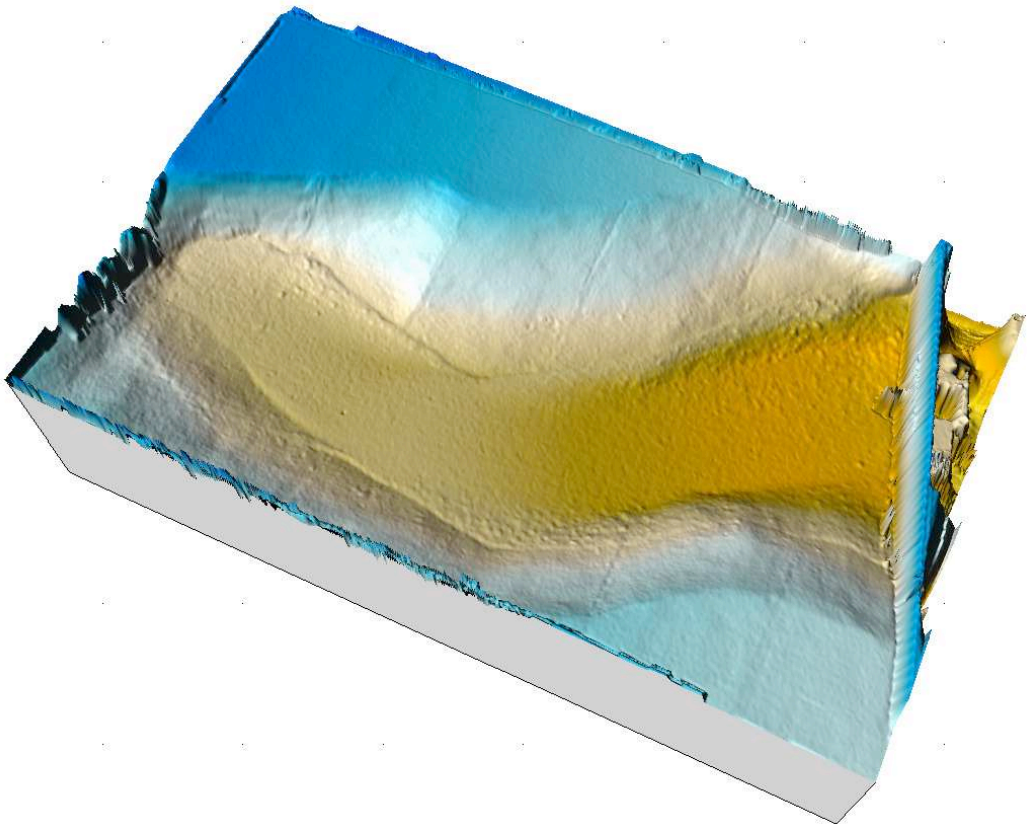

Figure 92. Deposited material for Test 2.1.

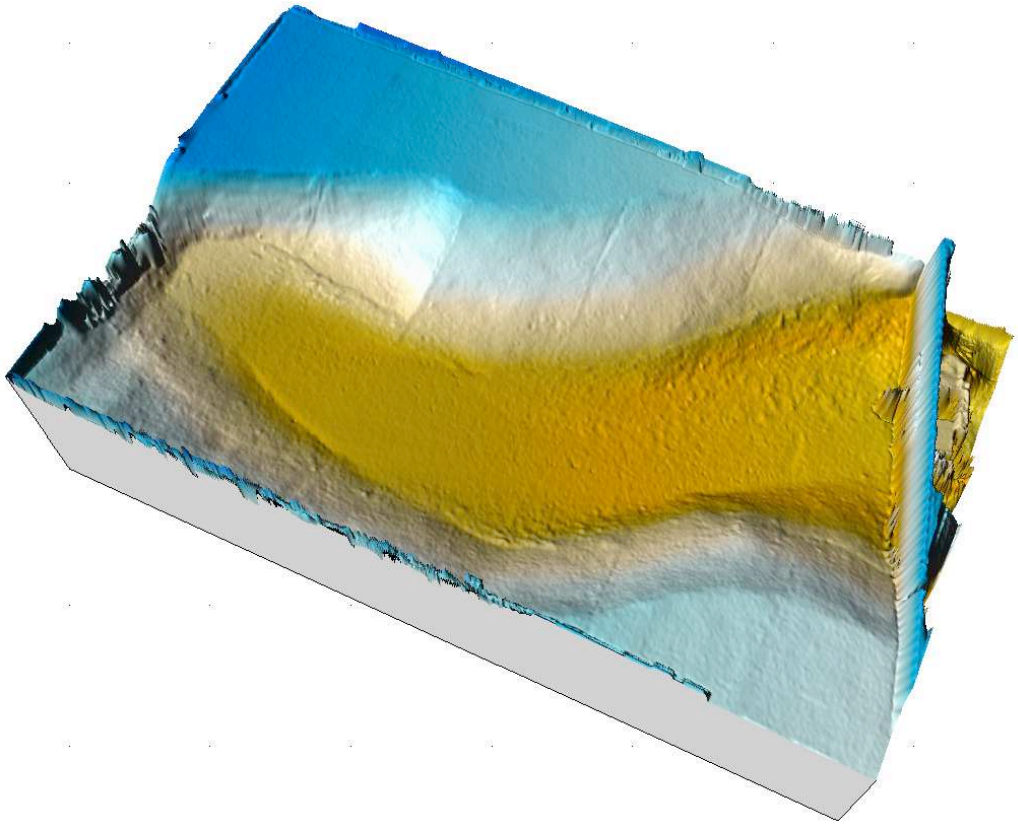

Figure 93. Deposited material for Test 2.2.

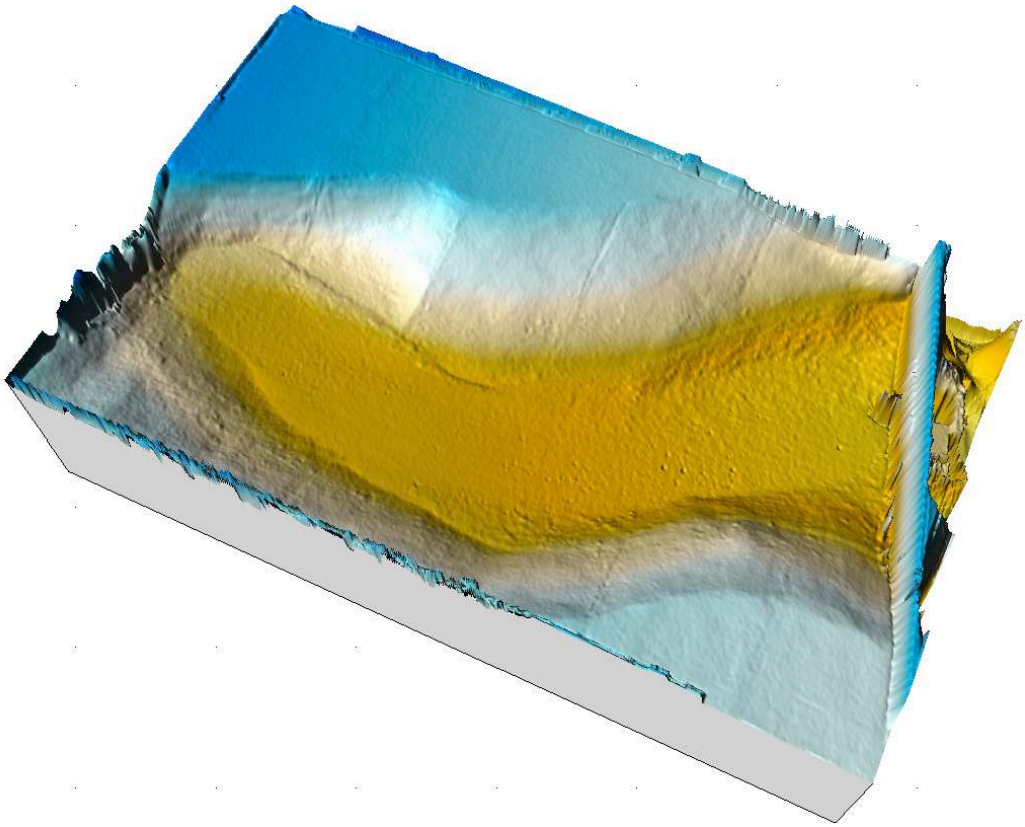

Figure 94. Deposited material for Test 2.3.

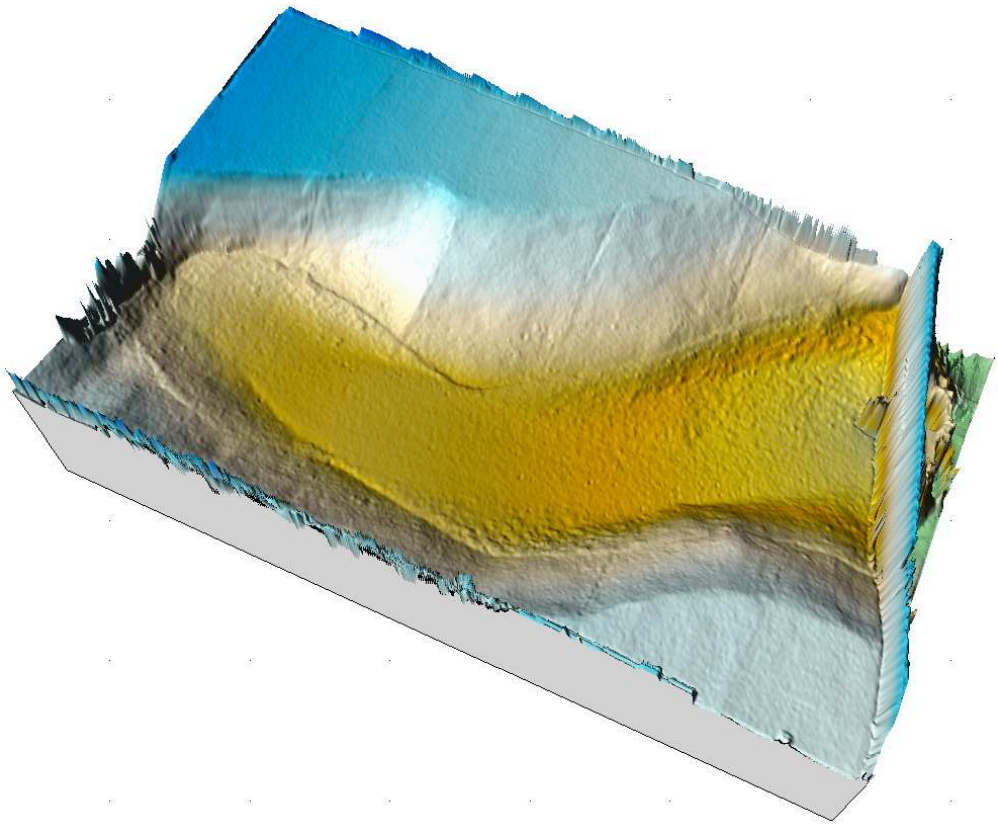

Figure 95. Deposited material for Test 2.4.

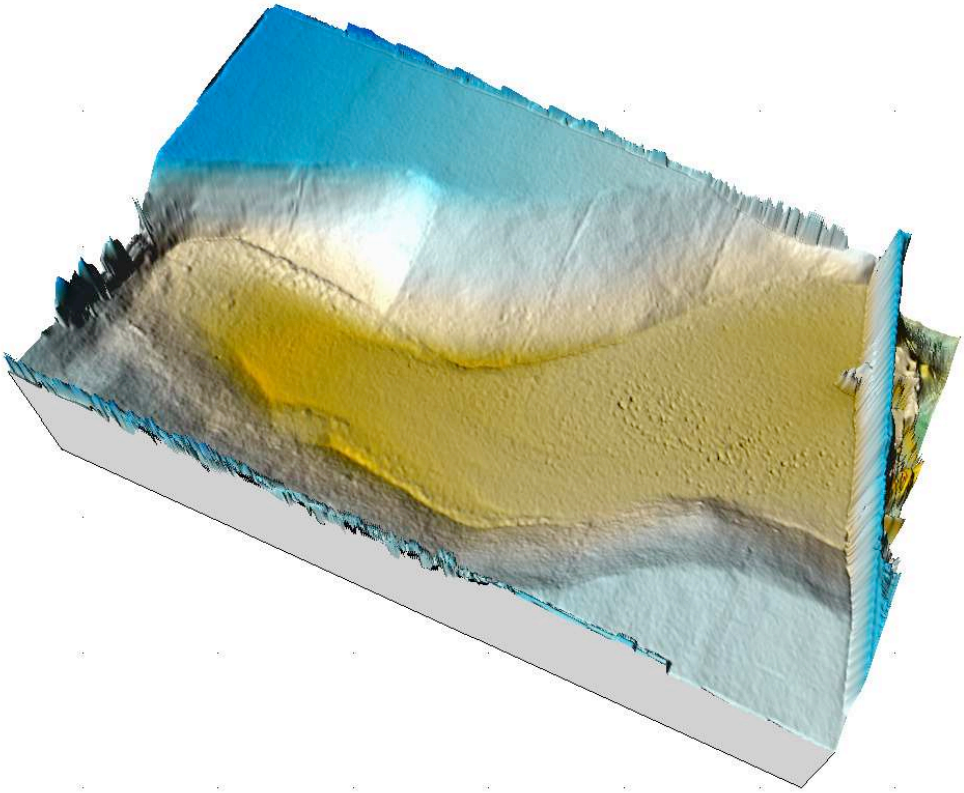

Figure 96. Deposited material for Test 3.1.

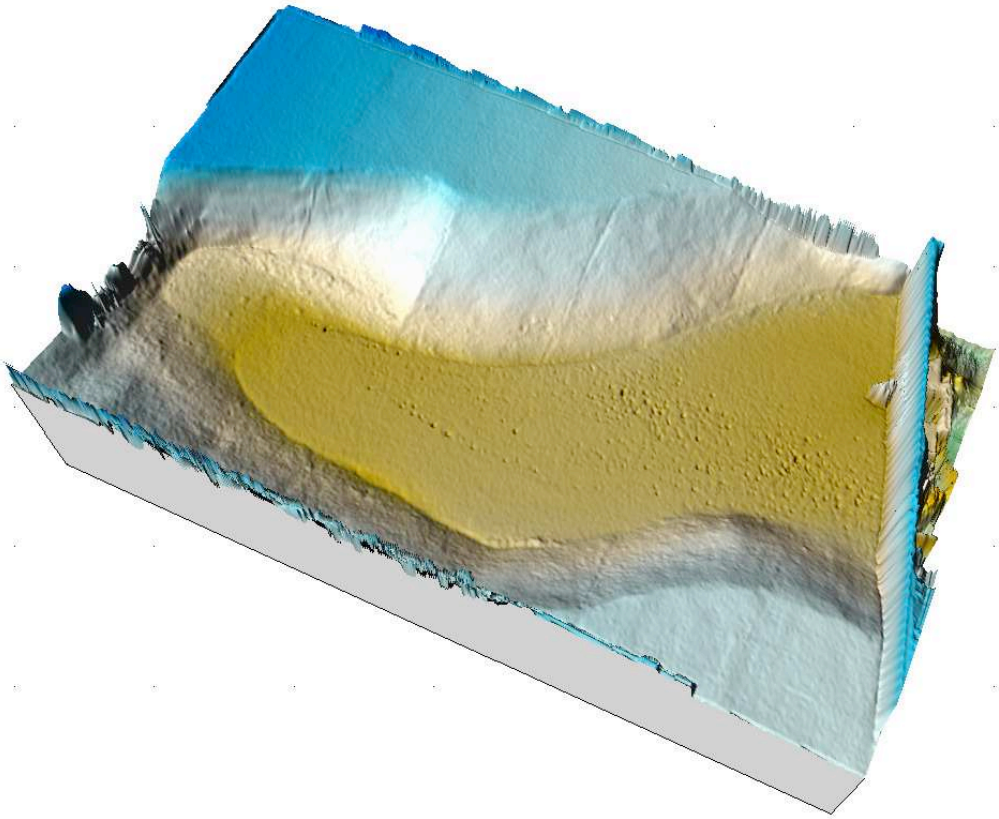

Figure 97. Deposited material for Test 3.2.

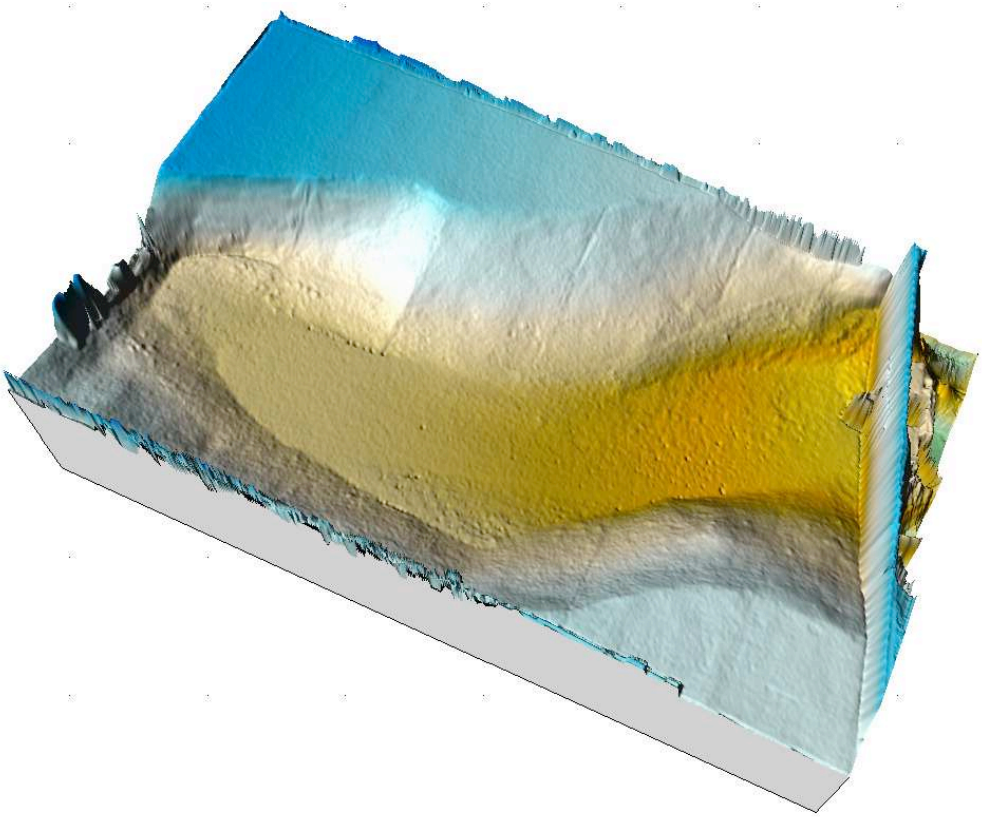

Figure 98 Deposited material for Test 3.3.

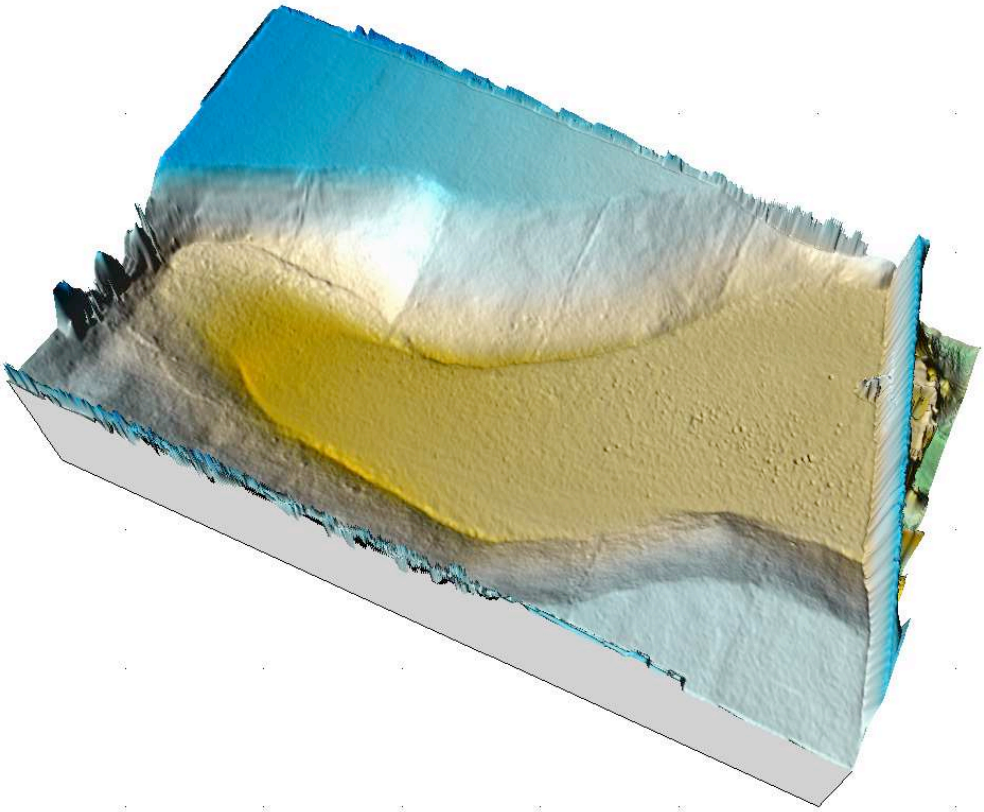

Figure 99. Deposited material for Test 3.4.

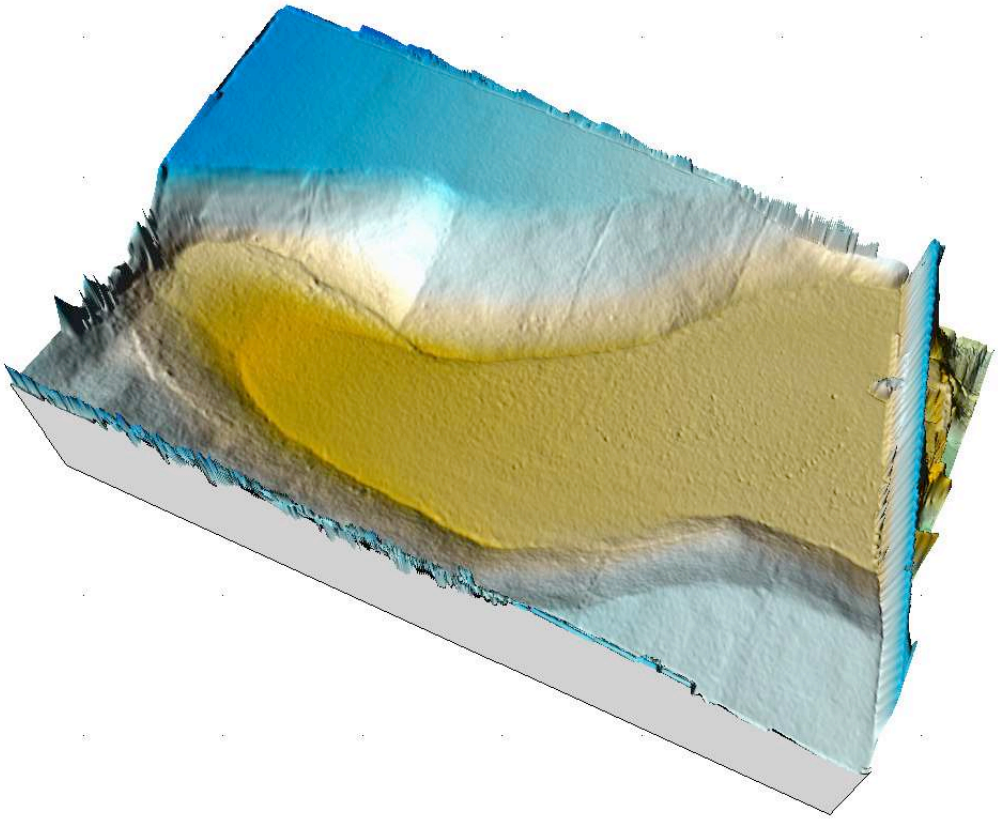

Figure 100. Deposited material for Test 4.1.

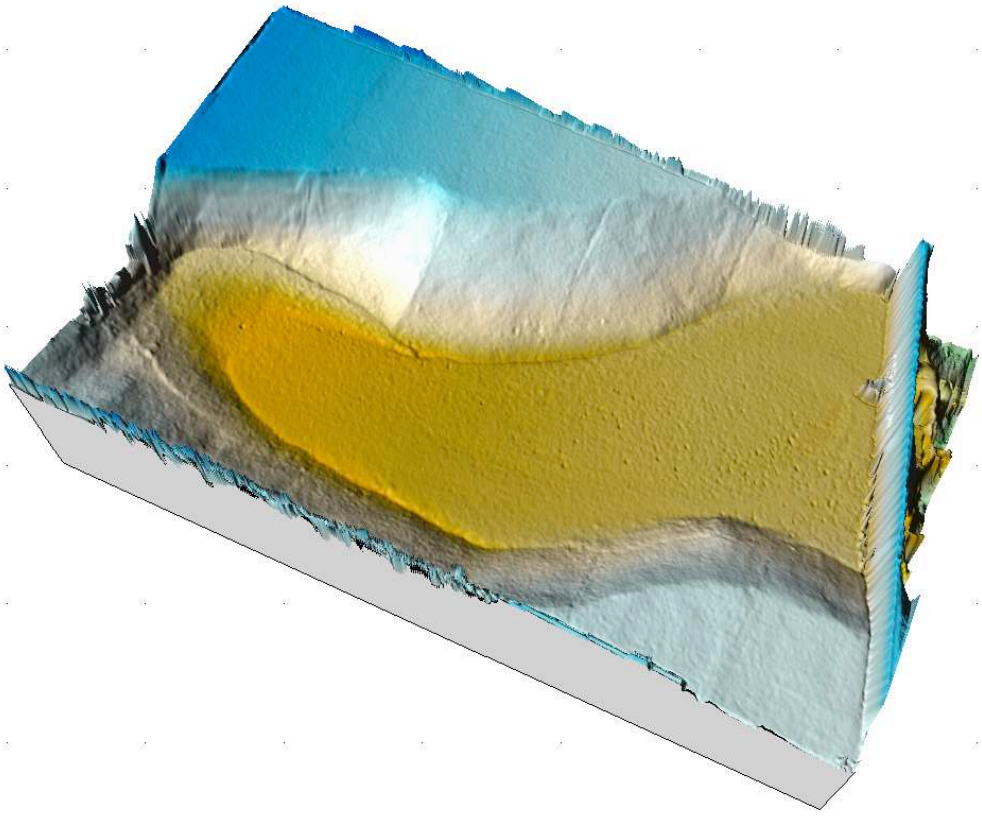

Figure 101. Deposited material for Test 4.2.

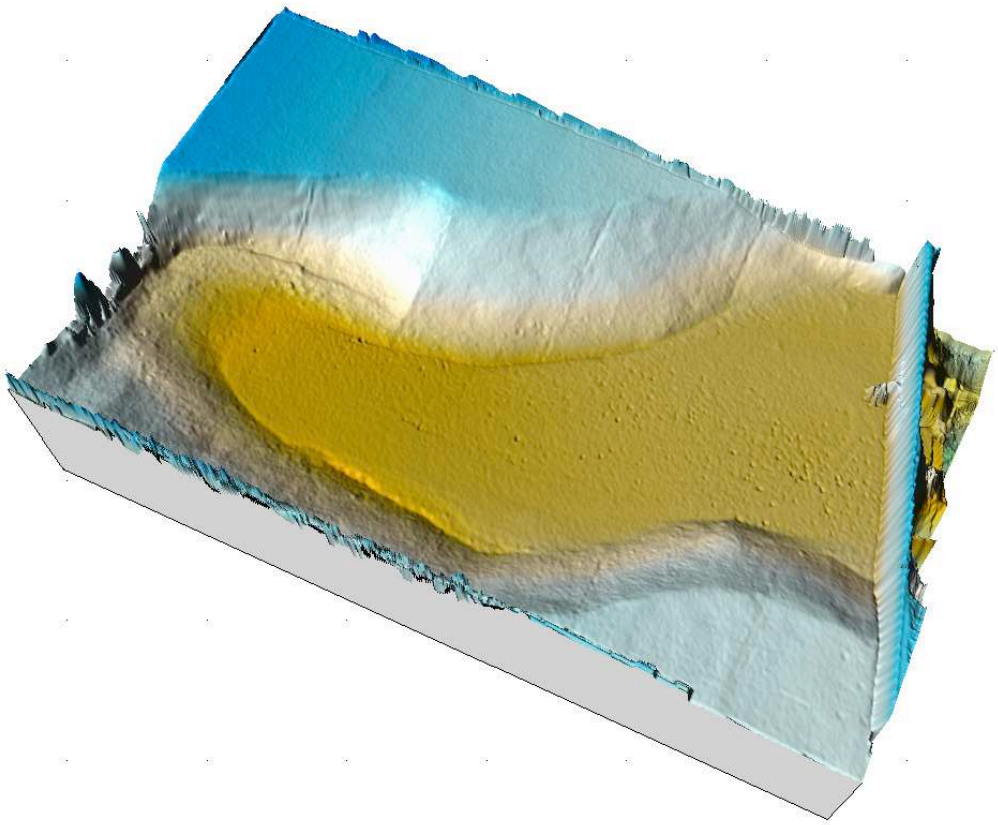

Figure 102. Deposited material for Test 4.3.

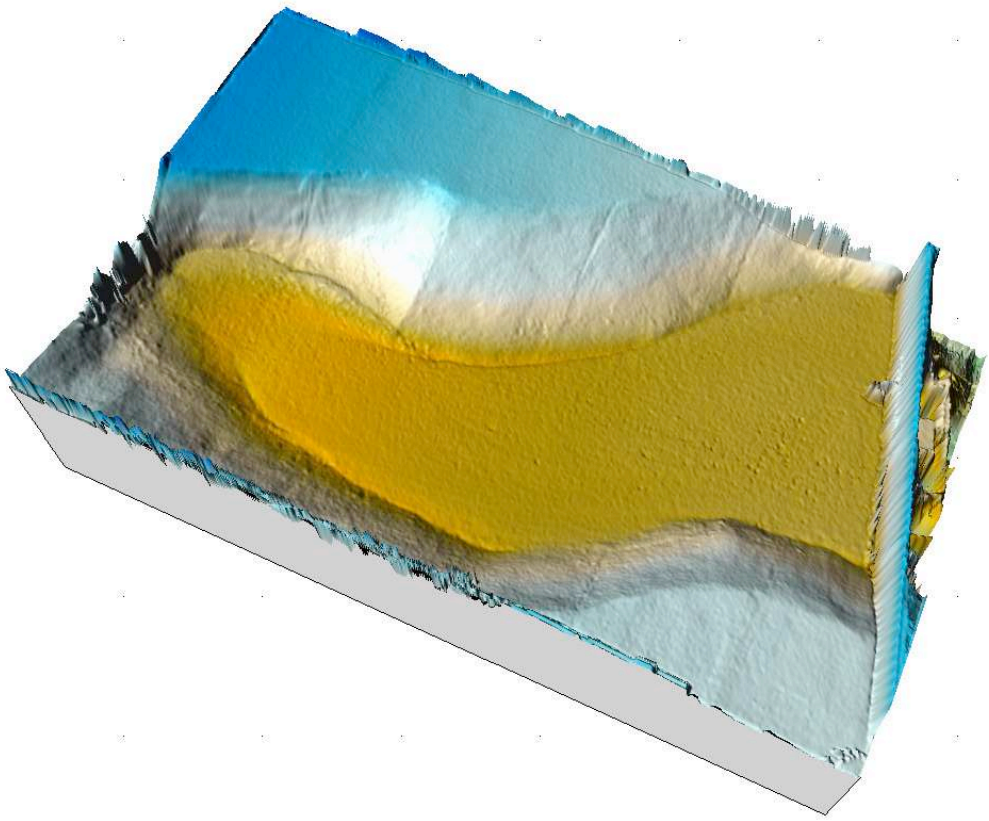

Figure 103. Deposited material for Test 5.

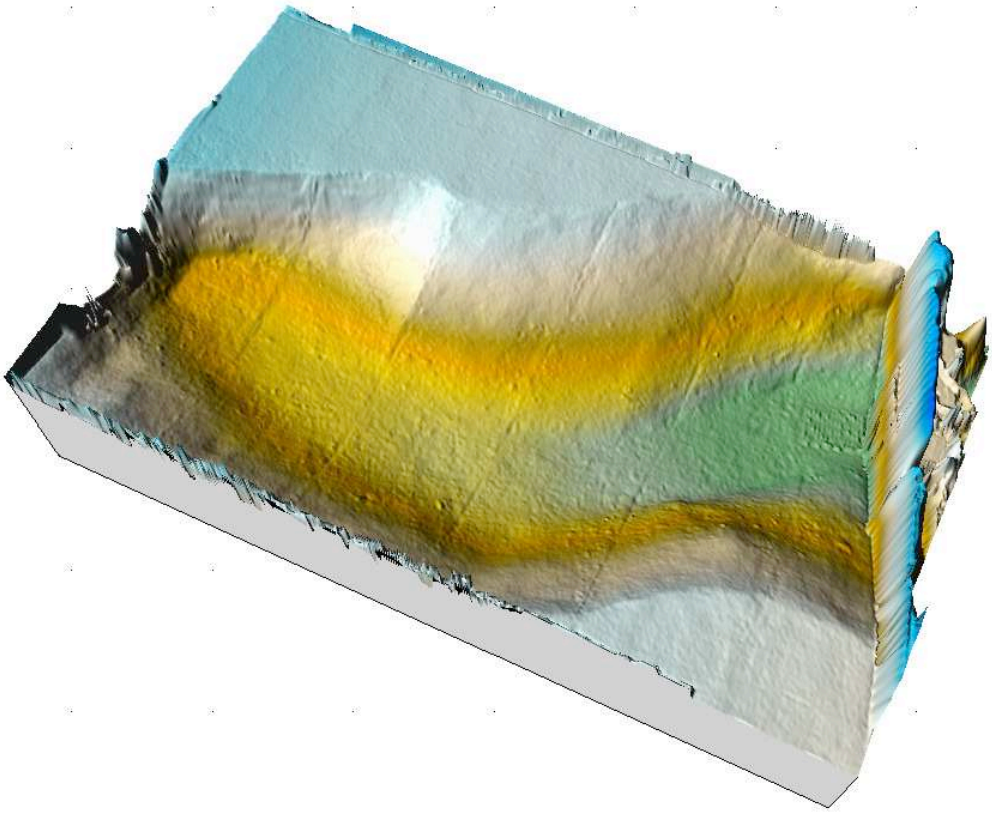

Figure 104. Model empty: without material deposited.